Report No.308

epaResearch
Climate - Water - Sustainability
Identifying pressures • Informing policy • Developing solutions

Al Source

Authors: Éva Ujaczki, Lisa O'Donoghue, Patricia Cusack, Mark Healy, Teresa Curtin and Ronan Courtney

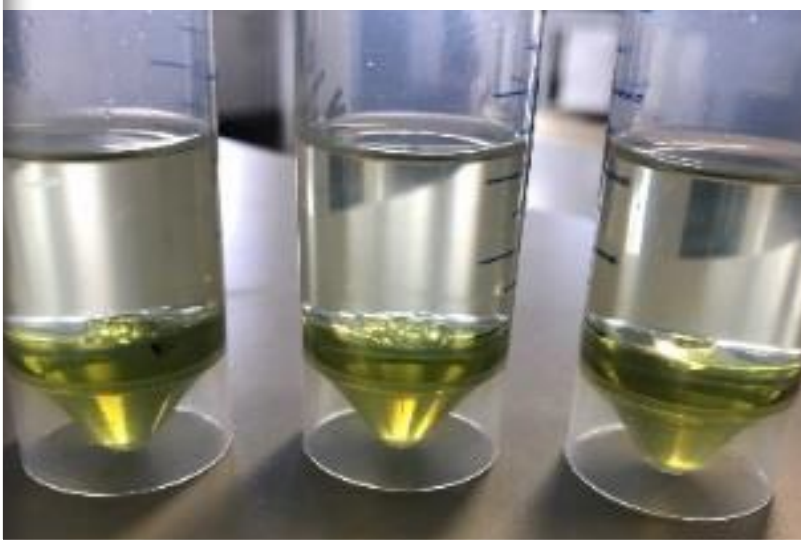

www.epa.ie

Rialtas na hÉireann
Government of Ireland

ENVIRONMENTAL PROTECTION AGENCY

The Environmental Protection Agency (EPA) is responsible for protecting and improving the environment as a valuable asset for the people of Ireland. We are committed to protecting people and the environment from the harmful effects of radiation and pollution.

The work of the EPA can be divided into three main areas:

Regulation: *We implement effective regulation and environmental compliance systems to deliver good environmental outcomes and target those who don't comply.*

Knowledge: *We provide high quality, targeted and timely environmental data, information and assessment to inform decision making at all levels.*

Advocacy: *We work with others to advocate for a clean, productive and well protected environment and for sustainable environmental behaviour.*

Our Responsibilities

Licensing

We regulate the following activities so that they do not endanger human health or harm the environment:

- waste facilities *(e.g. landfills, incinerators, waste transfer stations)*;
- large scale industrial activities (*e.g. pharmaceutical, cement manufacturing, power plants)*;
- intensive agriculture *(e.g. pigs, poultry)*;
- the contained use and controlled release of Genetically Modified Organisms *(GMOs)*;
- sources of ionising radiation *(e.g. x-ray and radiotherapy equipment, industrial sources)*;
- large petrol storage facilities;
- waste water discharges;
- dumping at sea activities.

National Environmental Enforcement

- Conducting an annual programme of audits and inspections of EPA licensed facilities.
- Overseeing local authorities' environmental protection responsibilities.
- Supervising the supply of drinking water by public water suppliers.
- Working with local authorities and other agencies to tackle environmental crime by co-ordinating a national enforcement network, targeting offenders and overseeing remediation.
- Enforcing Regulations such as Waste Electrical and Electronic Equipment (WEEE), Restriction of Hazardous Substances (RoHS) and substances that deplete the ozone layer.
- Prosecuting those who flout environmental law and damage the environment.

Water Management

- Monitoring and reporting on the quality of rivers, lakes, transitional and coastal waters of Ireland and groundwaters; measuring water levels and river flows.
- National coordination and oversight of the Water Framework Directive.
- Monitoring and reporting on Bathing Water Quality.

Monitoring, Analysing and Reporting on the Environment

- Monitoring air quality and implementing the EU Clean Air for Europe (CAFÉ) Directive.
- Independent reporting to inform decision making by national and local government *(e.g. periodic reporting on the State of Ireland's Environment and Indicator Reports)*.

Regulating Ireland's Greenhouse Gas Emissions

- Preparing Ireland's greenhouse gas inventories and projections.
- Implementing the Emissions Trading Directive, for over 100 of the largest producers of carbon dioxide in Ireland.

Environmental Research and Development

- Funding environmental research to identify pressures, inform policy and provide solutions in the areas of climate, water and sustainability.

Strategic Environmental Assessment

- Assessing the impact of proposed plans and programmes on the Irish environment *(e.g. major development plans)*.

Radiological Protection

- Monitoring radiation levels, assessing exposure of people in Ireland to ionising radiation.
- Assisting in developing national plans for emergencies arising from nuclear accidents.
- Monitoring developments abroad relating to nuclear installations and radiological safety.
- Providing, or overseeing the provision of, specialist radiation protection services.

Guidance, Accessible Information and Education

- Providing advice and guidance to industry and the public on environmental and radiological protection topics.
- Providing timely and easily accessible environmental information to encourage public participation in environmental decision-making *(e.g. My Local Environment, Radon Maps)*.
- Advising Government on matters relating to radiological safety and emergency response.
- Developing a National Hazardous Waste Management Plan to prevent and manage hazardous waste.

Awareness Raising and Behavioural Change

- Generating greater environmental awareness and influencing positive behavioural change by supporting businesses, communities and householders to become more resource efficient.
- Promoting radon testing in homes and workplaces and encouraging remediation where necessary.

Management and structure of the EPA

The EPA is managed by a full time Board, consisting of a Director General and five Directors. The work is carried out across five Offices:

- Office of Environmental Sustainability
- Office of Environmental Enforcement
- Office of Evidence and Assessment
- Office of Radiation Protection and Environmental Monitoring
- Office of Communications and Corporate Services

The EPA is assisted by an Advisory Committee of twelve members who meet regularly to discuss issues of concern and provide advice to the Board.

EPA RESEARCH PROGRAMME 2014–2020

Al Source

(2014-RE-MS-1)

EPA Research Project

Prepared for the Environmental Protection Agency

by

University of Limerick

Authors:

Éva Ujaczki, Lisa O'Donoghue, Patricia Cusack, Mark Healy, Teresa Curtin and Ronan Courtney

ENVIRONMENTAL PROTECTION AGENCY
An Ghníomhaireacht um Chaomhnú Comhshaoil
PO Box 3000, Johnstown Castle, Co. Wexford, Ireland

Telephone: +353 53 916 0600 Fax: +353 53 916 0699
Email: info@epa.ie Website: www.epa.ie

ACKNOWLEDGEMENTS

This report is published as part of the EPA Research Programme 2014–2020. The EPA Research Programme is a Government of Ireland initiative funded by the Department of Communications, Climate Action and Environment. It is administered by the Environmental Protection Agency, which has the statutory function of co-ordinating and promoting environmental research.

The authors would like to acknowledge the members of the project steering committee, namely Brian Donlon (EPA), Darren Byrne (Department of Communications, Climate Action and Environment) and Louise Clune (Aughinish Alumina Ltd), for their constructive input throughout the project, and Karen Roche (project manager on behalf of EPA Research).

Cover image: Investigation of the recovery of critical raw materials from bauxite residue.

DISCLAIMER

This report is based on research carried out/data from January 2015 to July 2018. More recent data may have become available since the research was completed.

The EPA Research Programme addresses the need for research in Ireland to inform policymakers and other stakeholders on a range of questions in relation to environmental protection. These reports are intended as contributions to the necessary debate on the protection of the environment.

EPA RESEARCH PROGRAMME 2014–2020
Published by the Environmental Protection Agency, Ireland

ISBN: 978-1-84095-869-0 March 2020

Price: Free Online version

Project Partners

Éva Ujaczki
Bernal Institute
Faculty of Science and Engineering
University of Limerick
Limerick
Ireland
Email: eva.ujaczki@ul.ie

Lisa O'Donoghue
Faculty of Science and Engineering
University of Limerick
Limerick
Ireland
Tel.: +353 (0)61 202910
Email: lisa.odonoghue@ul.ie

Patricia Cusack
Department of Biological Sciences and Bernal Institute
University of Limerick
Limerick
Ireland
Email: patricia.cusack@ul.ie

Mark Healy
Civil Engineering
College of Engineering and Informatics
NUI Galway
Galway
Ireland
Tel.: +353 91 495364
Email: mark.healy@nuigalway.ie

Teresa Curtin
Department of Chemical Sciences and Bernal Institute
University of Limerick
Limerick
Ireland
Tel.: +353 (0)61 202981
Email: teresa.curtin@ul.ie

Ronan Courtney
Department of Biological Sciences and Bernal Institute
University of Limerick
Limerick
Ireland
Tel.: +353 (0)61 202427
Email: ronan.courtney@ul.ie

Contents

Acknowledgements ii

Disclaimer ii

Project Partners iii

List of Figures vii

List of Tables ix

Executive Summary xi

1 Introduction 1

2 Literature Review 3

2.1 Bauxite Ore Occurrence 3

2.2 Bauxite Residues from Alumina Production 3

2.3 Bauxite Residue Composition 3

2.4 Traditional Bauxite Residue Treatment and Disposal 4

2.5 Current Bauxite Residue Reuse Options for Metal/Critical Raw Material Recovery 4

2.6 Current Bauxite Residue Reuse Options for Phosphorus Recovery 7

3 Gallium Recovery from Bauxite Residue 10

3.1 Materials and Methods 10

3.2 Results 11

3.3 Discussion 19

4 Phosphorus Recovery from Wastewater Using Bauxite Residue 22

4.1 Enhancement of Bauxite Residue As a Low-cost Adsorbent for Phosphorus in Aqueous Solution, Using Seawater and Gypsum Treatments 22

4.2 Efficiency of Bauxite Residue As a Low-cost Adsorbent in the Removal of Dissolved Reactive Phosphorus from Agricultural Wastewaters 28

5 Further Development of Results 38

5.1 Evaluation of Techniques for Gallium Recovery from Bauxite Residue 38

5.2 Evaluation of the Technique for Phosphorus Recovery from Wastewater Using Bauxite Residue 40

6 Conclusions **42**

6.1 Gallium Recovery 42

6.2 Phosphorus Recovery 42

References **43**

Abbreviations **53**

List of Figures

Figure 3.1.	The XRD pattern collected from the dried and sieved bauxite residue sample, annotated with major phase peaks detected	12
Figure 3.2.	Morphology and chemical composition of the bauxite residue detected by SEM-EDS.	12
Figure 3.3.	Effect of leaching parameters on extraction efficiency and pH of Al, Fe and Ga	14
Figure 3.4.	Two-factor interaction effects on the extracted Ga	15
Figure 3.5.	Effect of adsorption parameters on Ga removal efficiency and pH from synthetic Ga solution by the zeolite CBV 500	16
Figure 3.6.	Two-factor interactions effects on the extracted Ga: adsorbent dosage and contact time	17
Figure 3.7.	Bauxite residue leachate compounds partitioning into supernatant and adsorbent during adsorption on the zeolite CBV 500 under the following conditions: 5 mg/mL absorbent dosage, 1 h contact time and temperature of 20°C	18
Figure 3.8.	Bauxite residue leachate compounds partitioning into organic solvent and leachate during LLE under the following conditions: 1 M D2EHPA in kerosene, 1 h contact time, temperature of 20°C and O/A ratio of 3:1	18
Figure 3.9.	Morphology and chemical composition of the by-product of leaching detected by SEM-EDS	19
Figure 3.10.	The XRD pattern obtained from the dried and sieved by-product of the leaching sample annotated with the major phase peaks detected	19
Figure 4.1.	The XRD pattern as determined for the column media before and after the loading period with dairy soiled water or forest run-off	30
Figure 4.2.	(a) The breakthrough curves showing the effluent dissolved reactive P content versus loading time for dairy soiled water using experimental and modelled data and (b) the predicted modelled retention behaviour of P for the bauxite residue media	31
Figure 4.3.	(a) The breakthrough curves showing the effluent dissolved reactive P content versus loading time for forest run-off using experimental and modelled data and (b) the modelled predicted P retention of the bauxite residue media	32
Figure 4.4.	The mean pH values of (a) the dairy soiled water and (b) the forest run-off effluent from the columns over the 24–36 h loading period	32
Figure 4.5.	FT-IR analysis of the bauxite residue media (a) before and (b) after use in the column treating dairy soiled water	33

Figure 4.6. FT-IR analysis of the bauxite residue media before (a) and after (b) use in the column treating forest run-off 34

Figure 4.7. Comparison of the composition of (a) Al, (b) Cu, (c) Fe and (d) Mn in influent and effluent in the columns treating dairy soiled water over the 24–36 h loading period 35

Figure 4.8. Comparison of the composition of (a) Al, (b) Cu, (c) Fe and (d) Mn in influent and effluent in the columns treating forest run-off over the 24–36 h loading period 36

Figure 5.1. Mass balance calculation for the LLE process. Values and costs are also indicated. Leaching parameters: 2.5 M $H_2C_2O_4$, 21.7 h contact time, 80°C 10 g/L slurry concentration. LLE parameters: 1 M D2EHPA in kerosene, 1 h contact time, 20°C, O/A ratio 3:1 39

Figure 5.2. Mass balance calculation for the adsorption process. Values and benefits are also indicated. Leaching parameters: 2.5 M $H_2C_2O_4$, 21.7 h contact time, 80°C, 10 g/L slurry concentration. Adsorption parameters: 5 g/cm^3, 1 h contact time, 20°C 39

Figure 5.3. Mass balance calculation for P recovery from wastewater using gypsum-neutralised bauxite residue. This is based on the use of a synthetic P water using batch studies. The corresponding P value is based on the current price of phosphate rock from USGS (2017) and the price of gypsum as supplied by Lennox Ireland 40

Figure 5.4. Mass balance calculation for P recovery from wastewater using the Callery mix and bauxite residue. This is based on the use of columns treating forest run-off and dairy soiled water. The corresponding P value is based on the current price of phosphate rock from USGS (2017) 41

List of Tables

Table 2.1.	Concentrations and maximally recoverable financial values of CRMs and elements of high economic importance in bauxite residues from different origins	5
Table 2.2.	Summary of CRM extraction techniques from bauxite residues	6
Table 2.3.	Examples of concentration/purification of CRMs from bauxite residue	7
Table 2.4.	Phosphorus adsorption studies that have been carried out using untreated and treated bauxite residue and their recovery efficiencies	8
Table 3.1.	Characteristic of zeolites in the comparative adsorption study	11
Table 3.2.	Major elemental composition of the bauxite residue as determined by XRF	12
Table 3.3.	Extraction efficiencies for leaching bauxite residue with HCl, H_2SO_4, HNO_3 and $H_2C_2O_4$[a]	13
Table 3.4.	Removal efficiencies for adsorption of Ga with the zeolites CBV 500, CP 811E-75 and CBV 2314[a]	16
Table 3.5.	Aqua regia-accessible composition of bauxite residue and partitioning of metal(loid)s during leaching, LLE and adsorption	18
Table 4.1.	Mineralogical composition of the bauxite residues (untreated and treated)	23
Table 4.2.	Elemental composition of the bauxite residues (untreated and treated) (mg/kg)	24
Table 4.3.	Physical and chemical characterisation of the bauxite residues (untreated and treated)	25
Table 4.4.	Maximum adsorbency (mg P/g media) of P using each of the bauxite residue samples (untreated and treated)[a]	26
Table 4.5.	Main mineralogical composition (%) of the bauxite residue used, as determined by XRF analysis	30
Table 4.6.	Soil and plant analysis following the RHIZOtest	36
Table 5.1.	The list of by-products formed per 1 kg of bauxite residue column media used	41
Table 5.2.	The list of by-products formed per 1 kg of bauxite residue column media used	41

Executive Summary

The scope of the Al Source project is to determine the optimisation of state-of-the-art technologies that could offer potential in the reuse of bauxite residue to recover valuable elements.

Bauxite residue is the slurry by-product generated during the treatment of bauxite ores using the Bayer process to produce alumina. Because of the high volumes generated (~150 million tonnes per annum), the management of bauxite residue continues to be a global concern. Consequently, there is an immediate need for re-utilisation and storage of these residues.

In this project two utilisation techniques were evaluated for bauxite residue to highlight its value when being utilised. In the first part of the research and development work, a state-of-the-art technology was evaluated for recovery of metal gallium (Ga) from bauxite residue. In the other part, a process for recovering phosphorus (P) from agricultural wastewater using bauxite residue was developed.

Linked to the valuable metal recovery study, bauxite residue was extracted using oxalic acid and, for the first time, studies were conducted to adsorb the Ga in the solution onto a zeolite at the laboratory scale. Optimisation was achieved with the help of a design of experiments (DOE) software calculation, which was validated with laboratory experiments. The efficiency of Ga adsorption onto the zeolite was compared with conventional liquid–liquid extraction by di-(2-ethylhexyl)phosphoric acid (D2EHPA) dissolved in kerosene. The residue left after the processing was characterised to understand the influence of the extraction process on pH change, morphology and chemical change.

Consequently, the general composition and valuable metal content of bauxite residue was evaluated to establish a baseline for Irish bauxite residue from a characterisation and composition aspect.

The developed optimal conditions allowed extraction of 85.8 mg of Ga from 1 kg of bauxite residue, corresponding to 71% of the total (aqua regia-accessible) Ga content present in bauxite residue. There are future challenges related to separation techniques (adsorption, liquid/liquid extraction), e.g. the concentration of Ga or improving the selectivity of Ga against major components. There is also a challenge related to the utilisation of the reprocessed residue produced during Ga extraction from bauxite residue.

For the recovery of P from wastewater using bauxite residue, gypsum and seawater treatments were applied to the various bauxite residue samples obtained and the effects on its mineral, elemental and physiochemical properties were examined, as well as the effect on its P adsorption capacity. Bauxite residue was then packed into rapid small-scale columns and used to treat dairy soiled water and forest run-off to investigate the removal rate and retention capacity for dissolved reactive P.

The evaluation of the recovery of P from wastewater using bauxite residue demonstrated that the maximum adsorption capacity was estimated to range from 0.345 to 2.73 mg P/g bauxite residue. When bauxite residue medium was packed into rapid small-scale columns it had a high potential for the treatment of both low and high P-concentrated agricultural wastewaters, dairy soiled water and forest run-off. Short-term laboratory-based investigations using the P-saturated medium showed no detrimental impact on plant growth or soil properties. Further characterisation of the P-saturated bauxite residue medium is warranted to determine the potential for P recovery or its potential as a substitute for P fertiliser. Upscaling of these trials to land application should involve consultation with regulators to consider the potential for metal leaching and impacts on soil.

1 Introduction

> Critical raw materials (CRMs) are fundamental to Europe's economy, growth and jobs and they are essential for maintaining and improving our quality of life. (EC, 2014a)

This statement by the European Union's (EU) Raw Materials Initiative recognises factual issues of insecure future raw materials within the EU and is reflected by many major economies (e.g. Kawamoto, 2008; MineralsUK, 2017; Natural Resources Canada, 2017; US National Research Council, 2008). Within the framework of the European Innovation Partnership on Raw Materials, a list of 27 critical raw materials (CRMs) was derived, including platinum group metals (PGMs) and rare earth elements (REEs) (EC, 2017). REEs are divided into light REEs (La, Ce, Pr, Nd, Sm) and heavy REEs (Eu, Gd, Tb, Dy, Ho, Er, Tm, Yb, Lu, Y), plus Sc (Rollat *et al*., 2016; Wall, 2014). The new 2017 list includes nine additional materials (e.g. V and Sc) compared with the 2014 list, making V economically more interesting in bauxite residue. Sc has been included on the list individually since 2017, as heavy REEs, light REEs and PGMs are assessed individually; however, they remain as groups on the critical list to ensure comparability with the previous assessment (EC, 2017). Many industrial sectors rely on CRMs as functional materials in their products. REEs are used, for instance, in such diverse applications as phosphors (lightning, displays), magnets, catalysts, metallurgical applications and alloys, ceramics and glass and glass polishing (EC, 2014b).

The challenges related to safeguarding the CRM supply can be addressed in a variety of ways, depending on the particular material. Demand for materials can be reduced through the development of new products and processes that substitute for CRMs (Ku and Hung, 2014). In some cases, additional supply might be available through new/improved mining of primary ores and production processes (minimising losses). Further, CRM supply risk can be reduced by exploitation of secondary (i.e. not ore-related) sources (i.e. in the frame of so-called urban mining) at the end of a product's life. Prominent secondary sources are, for instance, incineration slags and ashes, demolition wastes or e-wastes (Hennebel *et al*., 2015). One little-tapped CRM secondary source to date may be bauxite residues (Binnemans *et al*., 2015; Deady *et al*., 2014; Liu *et al*., 2014; Paramguru *et al*., 2005). Depending on the origin of the residues, they may contain considerable amounts of CRMs, in particular REEs and Sc (Abdulvaliyev *et al*., 2015; Borra *et al*., 2015a; Laskou and Economou-Eliopoulos, 2013; Mohapatra *et al*., 2012; Qu *et al*., 2013; Ujaczki *et al*., 2017a).

Bauxite residues (or "red mud", "Bayer process tailings", "bauxite process tailings") are generated from alumina production, in which bauxite is digested in hot NaOH solution via the Bayer process (Evans, 2015). The production of 1 tonne of alumina generates between 1 and 1.5 tonnes of bauxite residue (Zhang *et al*., 2011). Currently, the yearly global production of bauxite residue is 150 million tonnes (Evans, 2016) and the total inventory is estimated to exceed 2.7 billion tonnes to date (Binnemans *et al*., 2015).

Some strategies (e.g. direct magnetic separation, pyro- and hydrometallurgical processes) have been investigated to recover the main elements present in the residues (Al, Fe and Ti). These were mainly driven by waste reduction considerations (Agatzini-Leonardou *et al*. 2008; Çengeloglu *et al*., 2001; Deep *et al*., 2001; Erçağ and Apak, 1997; Ghorbani and Fakhariyan, 2013; Guo *et al*., 2013; Jamieson *et al*., 2006; Jayasankar *et al*., 2012; Kasliwal and Sai, 1999; Kumar and Premchand, 1998; Li *et al*., 2009, 2011; Liu *et al*., 2009, 2012; Urík *et al*., 2015; Uzun and Gulfen, 2007; Vachon *et al*., 1994; Yang *et al*., 2015; Zhang *et al*., 2011; Zhong *et al*., 2009; Zhu *et al*., 2012). Fewer attempts have been made to use the residues as a secondary source of CRMs (Abhilash *et al*., 2014; Borra *et al*., 2015a, 2016a,b; Davris *et al*., 2016; Ochsenkühn-Petropoulou *et al*., 1996; Qu *et al*., 2015; Roosen *et al*., 2016; Ujaczki *et al*., 2017a,b; Wang *et al*., 2013).

Some other reuse options for bauxite residue have included polymers (Hertel *et al*., 2016), ceramics (Pontikes *et al*., 2009) and catalysts (Wang *et al*., 2008) and adsorbents for wastewater treatment (Bhatnagar *et al*., 2011), particularly for the removal of As (Arco-Lázaro *et al*., 2018; Castaldi *et al*.,

2011; Sahu *et al*., 2010), Cr (Dursun *et al*., 2008), Ni (Hannachi *et al*., 2010; Smiljanić *et al*., 2010), Cu (Atasoy and Bilgic, 2018; Nadaroglu *et al*., 2010), Cd (Ha *et al*., 2017) and P (Cusack *et al*., 2018; Yue *et al*., 2010), as well as applications as potential soil ameliorants (Ujaczki *et al*., 2015).

2 Literature Review

2.1 Bauxite Ore Occurrence

Bauxite ore is formed from the intense lateritic weathering of residual clays, which accumulate in topographic lows on continental surfaces (Deady *et al*., 2014). Bauxite deposits can be classified according to their geological formation into lateritic (89%), karst (10%) and Tikhvin-type (< 1% of the world's resources) deposits (Bárdossy, 1982; Meyer, 2004). Trace elements, including REEs, Ga, Ti, Cr, Zr, etc., can be adsorbed onto the surface of residual clays. During lateritic weathering the adsorbed elements become concentrated with depth in the resulting bauxite deposits (Maksimović, 1976; Maksimović and Roaldset, 1976). There are estimated to be 55–75 billion tonnes of bauxite resources worldwide, with the following distribution: 32% in Africa, 23% in Oceania, 21% in South America and the Caribbean, 18% in Asia and 6% elsewhere (Senyuta *et al*., 2013; Vassiliadou, 2014). The 1970s saw a major expansion of the alumina industry in response to growth in primary Al demand, accompanied by rapid production growth (Power *et al*., 2011). In 2016, the quantity of bauxite consumed was estimated to be 6.8 million tonnes, with more than 90% of the bauxite converted to alumina and the remainder used for non-metallurgical products (USGS, 2017).

2.2 Bauxite Residues from Alumina Production

Aluminium production consists of two key stages: first, alumina refining ("Bayer process"), which involves the generation of alumina from bauxite ore, and, second, Al smelting (Hall–Héroult process), the process of transforming alumina into Al (Lumley, 2010). Most of the world's alumina is produced using the Bayer process, although minor volumes are obtained from non-bauxite sources such as kaolin, anorthosite, alunite and dawsonite in some refineries (particularly in China and Russia) (Murray, 1981; Patel and Pal, 2015). The Bayer process is often referred to as the "red side" and affects the properties of the residue produced. It includes the steps of bauxite milling, pre-desilication, digestion, cooling, clarification, washing and disposal of residues. The steps associated with the obtained pregnant liquor are precipitation/ crystallisation, classification and calcination (IAI, 2012).

Depending on the requirements of the residue storage facility, further filtration steps and amendments (e.g. seawater, CO_2, SO_2, gypsum, mineral acids) are added prior to disposal (Power *et al*., 2011). Various size fractions can be distinguished within bauxite residues (from 100 nm to coarse fraction process sand of > 150–200 µm) (Pradhan *et al*., 1996; Roach *et al*., 2001). The majority (~80%) of the particles in red mud may be of a size of < 100 µm (Jones *et al*., 2011). The amount of process sand is typically around 5%, but may vary from < 1% to as high as 50%. In several cases the process sand is separated before clarification and is transferred to a separate system for washing (Bánvölgyi and Huan, 2010).

2.3 Bauxite Residue Composition

Bauxite residues are solid–solution mixtures ranging in initial solid content from 20% to 80% by weight (depending on the disposal method of the refinery). They can exhibit a high pH (*c*.13) when no further treatment is carried out and have a high Na^+ content and electrical conductivity (EC) (Gräfe *et al*., 2011; Wang *et al*., 2008). Roughly 70% of the solid bauxite residue is in a crystalline phase (Gräfe *et al*., 2011), including primary mineral phases, which are those that are already present in bauxite, e.g. haematite, diaspore, boehmite and goethite, and secondary mineral phases, which are formed in the Bayer process, such as hydrogarnet, cancrinite, perovskite and gibbsite (Vind *et al*., 2018). The bauxite parent material, climate, age and topography influence bauxite residue composition (Bárdossy and Aleva, 1990). Haematite is the most prevalent of the minerals found in bauxite residue, ranging from 7% to 29% (Gräfe *et al*., 2011). Aluminous goethite is generally found in residues from bauxite from Jamaica and Australia (Gräfe *et al*., 2011), which shows a low substitution of Al within the goethite structure (Lawson *et al*., 2014). Further factors influencing bauxite residue composition are NaOH and heat and pressure conditions used during digestion, as well

as the chemical additives used (Cablik, 2007). For instance, residues produced from “low-grade”, high-silicon bauxite differ because of the amount of caustic lime that is added in the Bayer process. Here, the major minerals present are calcite, perovskite, illite, haematite and magnetite (Liu *et al*., 2007a).

The order of elemental abundance within the bauxite residue would typically be Fe > Al > Si ~ Ti > Ca > Na (Gräfe *et al*., 2011), with these elements being present as oxides (Fe_2O_3, Al_2O_3, SiO_2, TiO_2, CaO and Na_2O) (for a review see Binnemans *et al*., 2015). However, comparatively few data are available on the content of CRMs in bauxite residues (Table 2.1). Some studies have indicated that bauxite residues may be rich in CRMs (Sc, Cr, Ga, REEs) and other valuable elements (Ni, V, Zn, Zr) (Deady *et al*., 2014; Liu and Naidu, 2014; Mohapatra *et al*., 2012). Mohapatra *et al*. (2012) reported that the amount of Sc, Ni and Cr increased in the order bauxite ore < process sand < red mud, whereas the amount of Ga was depleted in the order bauxite ore > process sand > red mud. Moreover, it was observed that the concentration of other valuable elements such as Co, Y, Zr, V, Zn and Nb was highest in process sand (Mohapatra *et al*., 2012).

2.4 Traditional Bauxite Residue Treatment and Disposal

Up until the 1970s, marine discharge and lagooning were primarily used to dispose of bauxite residue. Now, so-called “dry stacking” (although residues are not entirely dry; ~70% solid) and dry cake disposal have become the industry norm. Dry stacking involves thickening the bauxite residue to 48–55% solids, which subsequently is pumped through a sloped pipeline. Then, de-watering/air drying occurs before the next thin layer is released at the disposal area (Power *et al*., 2011). The bauxite residues are deposited as a slurry-type paste of pH 11–13, with a high fine silt to clay size proportion and a high sodium content. This leads to a preference for particle dispersion (Dodoo-Arhin *et al*., 2013) and results in difficulties in handling and storing residues (Mayes *et al*., 2016; Palmer and Frost, 2009). Dry cake disposal involves thickening and pressure filtration, before using dump trucks to transfer residues to the storage area (Power *et al*., 2011). Pressure filtration not only results in a residue with a lower water content but also reduces losses of entrapped NaOH. This makes thickened/filtered residue more suitable for safer storage, but also for transport and utilisation in other industries (cement, iron, etc.).

The current best practice in the industry is disposal in engineered bauxite residue disposal areas (BRDAs), using dry stacking and “mud farming” (amphirolling) to aid residue de-watering and increase compactation/consolidation, thereby reducing alkalinity (pH < 11.5) (Evans, 2016; Gomes *et al*., 2016; Higgins *et al*., 2016).

2.5 Current Bauxite Residue Reuse Options for Metal/Critical Raw Material Recovery

Efforts to reuse bauxite residue have long been proposed but no more than 2–3% of the 150 million tonnes of bauxite residue produced annually is used in a productive way (Evans, 2016). Currently, these minor uses include cement and ceramic production (see, for example, Binnemans *et al*., 2015; Klauber *et al*., 2011; Kumar *et al*., 2006; Liu and Zhang, 2011; Pontikes and Angelopoulos, 2013). Further, technologies have been proposed for major metal (Al, Fe, Ti) recovery, such as direct magnetic separation, smelting in a blast furnace and pyrometallurgical and hydrometallurgical recovery (Liu and Naidu, 2014). For example, Fe recovery by direct magnetic separation was found to reduce energy costs compared with pyrometallurgical recovery (Xiang *et al*., 2001). The magnetic fraction can be used for Fe production, whereas the non-magnetic fraction can be used in building materials or added back into the Bayer process (Hammond *et al*., 2013). Al has been extracted by both organic and inorganic acids (including acids produced by bacteria; Liu and Naidu, 2014). Pyrometallurgical (and hydrometallurgical) routes have been proposed to recover Ti from bauxite residues (Agatzini-Leonardou *et al*., 2008).

Because of the high costs of disposal some attempts to completely reuse bauxite residues (towards the “zero waste” objective) have been made. For instance, Erçağ and Apak (1997) developed a procedure for the recovery of TiO_2, Al_2O_3 and pig iron from Turkish bauxite residues. Here, bauxite residue was mixed with dolomite and coke, pelletised, sintered and smelted. The slag was leached and solvent extraction applied. Ultimately, silica and Al_2O_3 were recovered from the raffinate, whereas Ti was stripped, hydrolysed and calcined to produce pigment-grade TiO_2.

Table 2.1. Concentrations and maximally recoverable financial values of CRMs and elements of high economic importance in bauxite residues from different origins

Elements	Market price[a] (US$/t)	Price basis	Australia		China		Greece		Hungary		India		Russia		Turkey	
			Content[b] (mg/kg)	Financial value (US$/t)	Content[c] (mg/kg)	Financial value (US$/t)	Content[d] (mg/kg)	Financial value (US$/t)	Content[e] (mg/kg)	Financial value (US$/t)	Content[f] (mg/kg)	Financial value (US$/t)	Content[g] (mg/kg)	Financial value (US$/t)	Content[h] (mg/kg)	Financial value (US$/t)
Ce	2000	Oxide	NA		842	1.7	368	0.8	430	0.9	191	0.4	NA		NA	
Co	26,444	Metal	NA		NA		NA		59	1.6	24	0.6	NA		NA	
Cr	11,000	Metal	497	5.5	848	9.3	NA		646	7.1	740	8.1	NA		NA	
Dy	184,500	Oxide	NA		48	8.9	17	3.1	21	3.9	4	0.7	NA		NA	
Er	5500	Mischmetal	NA		28	0.1	14	0.1	12	0.1	1	0.0	NA		NA	
Eu	66,000	Oxide	NA		110	7.3	5	0.3	6	0.4	2	0.1	NA		NA	
Ga	400,000	Metal	89	35.6	570	228.0	NA		27	10.6	91	36.4	NA		25	10.0
Gd	5500	Mischmetal	NA		56	0.3	22	0.1	27	0.1	7	0.0	NA		NA	
Ho	5500	Mischmetal	NA		25	0.1	4	0.0	4	0.0	NA		NA		NA	
In	240,000	Metal	NA		NA		NA		1	0.1	NA		NA		NA	
La	2000	Oxide	NA		416	0.8	114	0.2	166	0.3	112	0.2	NA		NA	
Lu	5500	Mischmetal	NA		14	0.1	2	0.0	2	0.0	NA		NA		NA	
Nd	39,500	Oxide	NA		341	13.5	99	3.9	151	6.0	48	1.9	NA		NA	
Ni	9298	Metal	31	0.3	169	1.6	NA		307	2.8	53	0.5	NA		NA	
Pr	5500	Mischmetal	NA		95	0.5	28	0.1	39	0.2	18	0.1	NA		NA	
Sc	4,600,000	Oxide	54	248.4	158	726.8	121	556.6	80	368.0	58	266.8	90	414.0	NA	
Sm	5500	Mischmetal	NA		64	0.3	21	0.1	28	0.1	9	0.1	NA		NA	
Tb	417,500	Oxide	NA		184	76.8	4	1.7	4	1.5	NA		NA		NA	
Tm	5500	Mischmetal	NA		14	0.1	2	0.0	2	0.0	NA		NA		NA	
V	6889	Oxide	730	5.0	4220	29.1	NA		337	2.3	517	3.6	NA		112	0.8
Y	35,000	Metal	68	2.4	266	9.3	76	2.7	100	3.5	13	0.5	NA		NA	
Yb	5500	Mischmetal	NA		28	0.1	14	0.1	11	0.1	2	0.0	NA		NA	
Zr	918	Metal	NA		2,070	1.9	NA		NA		279	0.3	650	0.6	NA	
Sum over all elements			1469	297.2	10,566	1116.6	911	569.8	2460	410.4	2169	320.3	740	414.6	137	10.8
Reference			Wang *et al.* (2013)		Qu *et al.* (2013)		Borra *et al.* (2015a)		Ujaczki *et al.* (2017a)		Mohapatra *et al.* (2012)		Petrakova *et al.* (2015)		Abdulvaliyev *et al.* (2015)	
Alumina production in 2016 (TMT)[i]			20,900		60,900		821		NA		6030		2680		NA	

[a]Prices USGS (2016). For Er, Gd, Ho, Lu, Pr, Sm, Tm and Yb, no market price is available; the mischmetal price was used, probably underestimating actual prices.

[b]The metal concentrations in all aqueous samples were determined by inductively coupled plasma atomic emission spectroscopy (ICP-AES).

[c]Chemical analysis was performed after total digestion according to the US EPA SW 846 Method 3050B (HNO_3 and H_2O_2; US EPA, 1996) by inductively coupled plasma mass spectroscopy (ICP-MS).

[d]Chemical analysis was performed after complete dissolution by alkali fusion and acid digestion in a 1:1 (v/v) HCl solution by ICP-MS.

[e]Chemical analysis was performed after aqua regia-assisted microwave digestion by ICP-MS.

[f]Chemical analysis was performed after acid digestion (HNO_3 and HF 1:1) based on the Balram *et al.* (1990) method by ICP-MS.

[g]Information on metal analysis was not available.

[h]Chemical analysis was performed by X-ray fluorescence (XRF).

[i]Data in thousands of metric dry tons (TMT) (USGS, 2016). Producing 1 tonne of alumina generates 1−2 tonnes of bauxite residue (Bray *et al.*, 2018).

NA, not available.

CRM recovery strategies can be categorised as direct leaching, leaching following pyrometallurgical/mechanical operations (reductive smelting, roasting) and combinations thereof. In direct hydrometallurgical leaching, mostly mineral acids (H_2SO_4, HCl or HNO_3) have been used to recover CRMs from bauxite residues (Table 2.2). Leaching following pyrometallurgical treatment may result in more efficient/more selective extraction, yet at the expense of higher energy investments. For instance, Fe removal by smelting reduction was shown to be beneficial for selective leaching of REEs from the resulting slag phase (Binnemans *et al*., 2015; Borra *et al*., 2016b; Logomerac, 1979; Sargic and Logomerac, 1974). Borra *et al*. (2016a) investigated a combined sulfation–roasting–leaching process to selectively leach REEs while leaving Fe undissolved in the residue. They reported extraction rates of about 60% Sc and 80% other REEs, while the dissolution of other major elements was minor (< 1% Fe, Ti; < 20% Al).

Similar procedures were developed for the selective extraction of Ni and Co from Fe-rich lateritic ores and were also applied for selective extraction of Nd from Nd–Fe–B magnets (Önal *et al*., 2015).

After extraction, dissolved metals are mostly purified/concentrated using either solvent extraction and/or ion exchange. Further proposed techniques, such as carbon adsorption, precipitation, use of ionic liquids or ultra/nanofiltration, have found minor use only (Table 2.3). Solvent extraction (liquid–liquid extraction, LLE) is based on the partitioning of the dissolved metal into a non-miscible organic phase (extract), followed by regeneration (stripping) of the solvent phase (Free, 2013). Dissolved impurities such as Fe pose a challenge to solvent extraction and are usually removed by precipitation before proceeding (Xie *et al*., 2014). A limited number of studies are available regarding extraction/concentration of CRMs from bauxite residue (reviewed in Liu and Naidu, 2014). Non-aqueous solvents (i.e. ionic liquids, salts

Table 2.2. Summary of CRM extraction techniques from bauxite residues

Bauxite residue source	Target metals	Technique	Recovery efficiency	Fe co-extracted	Scale of the study	Reference
Greece	REEs	Extraction using HCl	68% Sc, 33–70% REEs	11% Fe	Laboratory scale in 0.5 L reactor	Ochsenkühn-Petropoulou *et al*. (1996)
Greece	REEs	Extraction using HCl	63% Sc, 70–85% REEs	80% Fe	Laboratory scale in 0.5 L reactor	Borra *et al*. (2015a)
Greece	REEs	Extraction using HNO_3	80% Sc, 29–96% REEs	3% Fe	Laboratory scale in 0.5 L reactor	Ochsenkühn-Petropoulou *et al*. (1996)
Greece	REEs	Extraction using H_2SO_4	21–77% REEs		Laboratory scale in 0.5 L reactor	Ochsenkühn-Petropoulou *et al*. (1996)
Greece	REEs	Extraction using HbetTf2N	45% Sc, 60–80% REEs	3% Fe	Laboratory scale ~0.5 L reactor	Davris *et al*. (2016)
Hungary	REEs, Co, Cr, Ga	Extraction using HCl	64% of the total CRMs	67% Fe	Laboratory scale in 0.05 mL tubes	Ujaczki *et al*. (2017a)
India	La	Extraction using H_2SO_4	100%		Laboratory scale ~0.1 mL vessel	Abhilash *et al*. (2014)
India	Ce	Extraction using H_2SO_4	100%		Laboratory scale ~0.1 mL vessel	Abhilash *et al*. (2014)
Turkey	Ga, V	High-temperature leaching using a high-modulus solution	56% Ga, 66% V_2O_5		Laboratory scale ~0.1 mL vessel	Abdulvaliyev *et al*. (2015)
China	REEs, Ga, V	Bioleaching by filamentous fungi (*Aspergillus niger*)	47% Ga, 40% Sc, 25–55% REEs		Laboratory scale in 12 L reactor	Qu *et al*. (2015)
China	Cr, Ni, Zn, Zr	Bioleaching by filamentous fungi (*A. niger*)	25% Cr, 50% Ni, 80% Zn, 11% Zr		Laboratory scale in 12 L reactor	Qu *et al*. (2015)
China	REEs	Bioleaching by filamentous fungi (*Penicillium tricolor*)	73% Sc, 28–80% REEs		Laboratory scale in 12 L reactor	Qu *et al*. (2015)

HbetTf2N, betainium bis(trifluoromethylsulfonyl)imide.

Table 2.3. Examples of concentration/purification of CRMs from bauxite residue

Bauxite residue source	Target CRM	Technique	Efficiency	Fe co-extracted	Reference
Australia	Sc	Combined LLE with D2EHPA/TBP in Shellsol D70	99% Sc transfer from leachate to solvent	1% Fe	Wang *et al.* (2013)
Hungary	REEs	Combined LLE with D2EHPA in kerosene	62% Sc transfer from leachate to concentrate	13% Fe	Ujaczki *et al.* (2017b)
Hungary	V	Anion exchange by Amberlite® IRA-400	76% V eluted from resin		Gomes *et al.* (2016)
Greece	Sc	Ion exchange with functionalised hybrid materials	100% Sc transfer from leachate to ion exchange material		Roosen *et al.* (2016)
Greece	Sc	Solvent extraction using ionic liquids	>90% Sc transfer from leachate to solvent		Hoogerstraete *et al.* (2013)

D2EHPA/TBP, di-(2-ethylhexyl)phosphoric acid/tributyl phosphate; LLE, liquid–liquid extraction.

in the liquid state) can be used as an alternative to conventional water/organic solvent systems. In ion exchange, a charged solid phase applied as a packed column or in direct contact is used to electrostatically attract the metal of interest (Alexandratos, 2009). Anion exchange resin (Amberlite® IRA-400) was investigated for V removal from synthetic bauxite residue leachate solution (Gomes *et al.*, 2016). It should be noted that the concentrating of CRMs from BRDA leachates does not require extraction as a precursor step. Next to commercial ion exchange resins (Ochsenkühn-Petropoulou *et al.*, 1996), some further (hybrid) materials have been applied [e.g. functionalised chitosan-silica particles with ethyleneglycol tetraacetic acid (EGTA) and diethylenetriamine pentaacetic acid (DTPA) groups; Qu *et al.*, 2015]. Nanofiltration is a pressure-driven process that makes use of both fixed charges in and on a membrane material and steric effects (i.e. size of ions or molecules) (Pontalier *et al.*, 1997; Yaroshchuk *et al.*, 2009). Acid-resistant nanofiltration may prove to be a suitable approach in the future (Zimmermann *et al.*, 2014), but to date has not been applied to bauxite residue leachates.

Further refining is required to get the dissolved metals in the refined solution to the end uses. Various techniques have been used for the recovery of elemental metal or suitable compounds from the concentrate: metal compounds by crystallisation or ionic precipitation, metals/metal compounds by reduction with gas, metals by electrochemical reduction and metals by electrolytic reduction (Gupta, 2017).

2.6 Current Bauxite Residue Reuse Options for Phosphorus Recovery

Phosphorus, a non-metal of the N group, is an essential component of all plant and animal life (Desmidt *et al.*, 2015) and critical in the production and maintenance of the food supply (Cordell and White, 2011). As of 2017, P has been listed as a CRM, in addition to phosphate rock, which was on the original CRM list issued in 2011 (EC, 2017). P is also identified as one of the key nutrients that leads to the eutrophication of water bodies, in which there is an excess production of algal blooms, resulting in detrimental effects on aquatic life present in the water bodies (Schindler *et al.*, 2016). Common sources of P that makes its way into water bodies include the effects of erosion and surface run-off (Bolster *et al.*, 2017) and agricultural practices such as the over-application of slurry and fertiliser (Smith *et al.*, 2015).

The movement of P from soil to water bodies is predominantly in the form of particulate or dissolved P (Penn *et al.*, 2014), with the latter being 100% available for aquatic biota and therefore having an immediate effect on the surrounding ecosystems (Penn *et al.*, 2014). Conventional methods of P removal from water have involved the use of enhanced biological removal systems (Ge *et al.*, 2015; Sukačová *et al.*, 2015), precipitation methods (Hauduc *et al.*, 2015; Zhou *et al.*, 2015), adsorbents (Callery *et al.*, 2016; Callery and Healy 2017; Grace *et al.*, 2015), ion exchange (Acelas *et al.*, 2015; Nur *et al.*, 2014) and electrodialysis and reverse osmosis (Wang Z. *et al.*, 2016). Although these methods are effective, they are often expensive (Bhatnagar and Sillanpää,

2010). In recent years, emphasis has been placed on the potential utilisation of industrial wastes to form low-cost adsorbents (Grace *et al*., 2016), such as fly ash (Nowak *et al*., 2013; Vohla *et al*., 2011), steel slags (Barca *et al*., 2012; Claveau-Mallet *et al*., 2013) and bauxite residue (Cusack *et al*., 2018; Grace *et al*., 2015, 2016; Taneez *et al*., 2017).

Fine-fraction bauxite residue comprises Fe oxides (20–45%) and Al oxides (10–22%) (IAI, 2015), which makes it suitable as a medium to adsorb P. In comparison to standard P removal by sand, bauxite residue has a high P retention capacity (Vohla *et al*., 2007). However, its P removal potential is enhanced following treatment by heat, acid or gypsum (Table 2.4). Of the methods employed, acid and heat treatment have proved most successful in increasing the P adsorption capacity of the bauxite residue, with maximum adsorption capacities of up to 203 mg P/g bauxite being achieved (Liu *et al*., 2007b) compared with an adsorption capacity of 0.20 mg P/g for untreated residue (Grace *et al*., 2015) (see Table 2.4). However, although acid and heat treatments have proven to be very successful in increasing the adsorption capacity of bauxite residue, they are expensive, are energy consuming (using high temperatures of up to 700°C) and, without further treatment, do not allow for the easy reuse of the bauxite residue (e.g. as a possible medium for plant growth) (Xue *et al*., 2016).

The main mechanism of phosphate adsorption onto the surface of Fe and Al oxides dominant in the bauxite residue may be separated into two processes: specific and non-specific adsorption (Cornell and Schwertmann, 2003; Stumm, 1992). Specific adsorption takes place through the process of ligand exchange (Jacukowicz-Sobala *et al*., 2015). A phosphate ion exchanges with one or more hydroxyl groups, with the release of OH_2 and/or OH^- back into the surrounding solution, contributing to the alkalisation of the surrounding environment (Cornell and Schwertmann, 2003), as shown in the following equations:

Table 2.4. Phosphorus adsorption studies that have been carried out using untreated and treated bauxite residue and their recovery efficiencies

Residue	P recovery technique	Factors investigated	Type of water	Initial P concentration of the water (mg P/L)	P recovered (mg P/g)	Reference
Untreated bauxite residue	Batch adsorption experiment	Kinetics, pH, temperature	Synthetic water	5–100	0.20	Grace *et al*. (2015)
Untreated bauxite residue	Column study	Initial concentration, particle size	Synthetic water	60–1000	25[a]	Herron *et al*. (2016)
Gypsum-treated bauxite residue	Batch adsorption experiment	Contact time	Synthetic water	20–400	7.03	Lopez *et al*. (1998)
Brine-treated bauxite residue (Bauxsol™)[b]	Batch adsorption experiment	pH, ionic strength, time	Synthetic water	0.5–2	6.5–14.9	Akhurst *et al*. (2006)
Brine-treated bauxite residue (Bauxsol™)[b]	Column study	Kinetics, particle size	Secondary treated effluent	3–9.2	2.85–8.74	Despland *et al*. (2011)
Acid- and brine-treated bauxite residue (Bauxsol™)[b]	Batch adsorption experiment	Kinetics, isotherms	Synthetic water	200	55.72	Ye *et al*. (2014)
Heat-treated bauxite residue	Batch adsorption experiment	Time, pH, initial concentration	Synthetic water	155	155.2	Liu *et al*. (2007b)
Acid- and heat-treated bauxite residue	Batch adsorption experiment	Time, pH, initial concentration	Synthetic water	155	202.9	Liu *et al*. (2007b)
Acid-treated bauxite residue	Batch adsorption experiment	Acid type, pH	Synthetic water	1	1.1	Huang *et al*. (2008)

Source: amended from Cusack *et al*. (2018).

[a]P_{max} value given, i.e. maximum amount of P adsorbed per g of bauxite residue media, as determined using the Langmuir adsorption isotherm.

[b]Bauxsol™ = neutralised bauxite residue produced using the Basecon™ procedure, which uses brines that are high in Ca^{2+} and Mg^{2+} (McConchie *et al*., 2001).

$$\equiv FeOH + An^- \leftrightarrow \equiv FeAn + OH^- \quad (2.1)$$

$$Fe(OH)_2 + An^- \leftrightarrow \equiv Fe_2 + An^+ + 2OH^- \quad (2.2)$$

Non-specific adsorption is inclusive of electrostatic interactions between the surface of the adsorbent and the phosphate ion (Jacukowicz-Sobala *et al*., 2015). Depending on the pH of the solution, the species of P found in aqueous solution are H_3PO_4, $H_2PO_4^-$, HPO_4^{2-} and PO_4^{3-} (Zhang *et al*., 2016).

The adsorption of P onto media is influenced by many factors, including particle size, pH and surface characteristics (Wang X. *et al*., 2016). Numerous studies have investigated the effect of parameters such as kinetics (Akhurst *et al*., 2006; Grace *et al*., 2015; Liu *et al*., 2007b; Ye *et al*., 2014), the ionic solution (Akhurst *et al*., 2006), pH (Grace *et al*., 2015; Huang *et al*., 2008; Liu *et al*., 2007b) and various enhancement treatments (see Table 2.4) on the adsorption of P from aqueous solution.

Enhancement treatments such as seawater or gypsum provide relatively inexpensive, alternative treatments, which may not only enhance the P adsorption capacity of the bauxite residue medium but also help to improve its physicochemical characteristics. Seawater treatment improves bauxite's physical structure because of the addition of Mg and Ca, which behave as flocculating agents, allowing many of the fine particles in bauxite residue to form more stable aggregates (Jones and Haynes, 2011), and a partial decrease in Na, as a result of ion exchange with Mg, Ca and K (Hanahan *et al*., 2004). Seawater-treated bauxite residues also allow adsorbed P to become bioavailable, unlike the metal cations, which are unavailable, highlighting the P and metal retention capabilities (Fergusson, 2009). Revegetation of bauxite residue using gypsum has also improved plant growth by reducing its alkalinity and salinity and improving the structure of the residue (Courtney *et al*., 2009; Courtney and Kirwan, 2012). In addition to this, modern alumina refineries are often located close to deep water ports, to allow for the bulk shipment of incoming bauxite (sometimes from multiple sources) to the refinery and/or the bulk shipment of alumina to Al smelters situated elsewhere. Therefore, there is potential scope for the increasing use of seawater neutralisation technology for pre-treatment of residues in refineries not already employing treatments previously mentioned, prior to their deposition in the BRDA, reducing the alkalinity limitation relating to the reuse of bauxite residue. However, such a practice would require significant capital investment.

In addition to this, there is ample scope for investigation of the use of bauxite residue as an adsorbent for P and, following the adsorption process, investigating the potential to strip P from the spent bauxite residue media. Similarly, there is potential to use the spent bauxite residue media as a potential source of P.

3 Gallium Recovery from Bauxite Residue

In the current study, bauxite residue was extracted using low-molecular-weight organic acid ($H_2C_2O_4$) and, for the first time, experiments were conducted to adsorb Ga in the solution onto a zeolite. Optimisation was achieved with the help of design of experiments (DOE) software calculations, which were validated with experiments. The efficiency of Ga adsorption onto the zeolite was compared with conventional LLE by di-(2-ethylhexyl)phosphoric acid (D2EHPA) dissolved in kerosene. The residue left after processing was characterised to understand the influence of the extraction process on pH change, morphology and chemical change.

3.1 Materials and Methods

3.1.1 Physicochemical and mineralogical characterisation

The bauxite residue used in this study (pH 10.9, EC = 0.9 mS and 28% moisture content) is produced by the Bayer process and stored after de-watering by vacuum filtration and mud farming at the disposal area. Samples were dried at 105°C for 24 h, pulverised using a mortar and pestle and sieved to a particle size of < 2 mm. The pH and EC were measured using 5 g samples in aqueous extract at a 1:5 ratio (solid:liquid) using an Aqualytic AL15 multimeter (Courtney and Harrington, 2010). X-ray fluorescence (XRF) analysis was carried out onsite at the refinery using a Panalytical Axios XRF system. X-ray diffraction (XRD) analysis was carried out on 1 g powdered samples using a Philips X'Pert PRO MPD® (Kα-radiation) and the patterns were collected in the angular range from 5° to 80° (2ɵ), with a step size of 0.008° (2ɵ) (Castaldi *et al*., 2011). Scanning electron microscopy (SEM) and energy-dispersive X-ray spectroscopy (EDS) were performed on a Hitachi SU-70 microscope.

3.1.2 Elemental analyses

Elemental analysis was performed after aqua regia digestion at a 1:10 ratio (solid:liquid) using a Multiwave 3000 (Rotor 8XF100) microwave digestion system at 200°C and 1.25 MPa. The solutions after digestion were filtered with a 0.45 µm polyvinyl difluoride (PVDF) syringe filter and diluted in 1 M HNO_3 before analysis (Ujaczki *et al*., 2017a). An Agilent Technologies 5100 inductively coupled plasma optical emission spectrometer (ICP-OES) was used for metal analysis. Standard solution and samples were diluted with 1 M HNO_3. The following analytical lines (in nm) were used for calculations: Al 308.215, 394.401, 396.152; Ca 396.847, 422.673; Fe 234.350; Ga 294.363; Na 589.592; Si 250.690, 251.611, 288.158; Ti 334.188, 336.122, 368.520; and V 268.796 (Bridger and Knowles, 2010).

3.1.3 Leaching study

The comparative metal leaching tests were performed with equivalent normality acids (1 M H_2SO_4, 2 M HNO_3, 2 M HCl, 1 M $H_2C_2O_4$) under the following conditions: 60°C, 24 h, 100 g/L slurry concentration in triplicate (Ujaczki *et al*., 2017a). All tests were carried out in 100 mL conical flasks. These were shaken on an IKA KS 4000i control incubation shaker at 250 rpm. Further leaching tests were carried out with $H_2C_2O_4$ by varying several parameters, i.e. acid concentration (0.05–3 M), contact time (1–24 h) temperature (20–80°C) and slurry concentration (10–200 g/L). The contact time was extended to 24 h for every extraction step to ensure that the leaching was complete. The bauxite residue leachate solutions were centrifuged for 5 min at 3500 rpm and 20°C (Sorvall TC-6), filtered, diluted in 1 M HNO_3 and analysed using an ICP-OES, as described above. The extraction efficiencies were determined by the ratio of metal extracted to the aqua regia-accessible metal content.

3.1.4 Adsorption study

Comparative experiments on Ga adsorption were conducted with three types of zeolite (Table 3.1).

A stock solution of 50 mg/L of Ga was prepared by diluting 1000 mg/L of Ga standard solution. All tests were carried out in 100 mL conical flasks with constant shaking at 250 rpm. Further adsorption tests were carried out with the zeolite CBV 500 by varying several

Table 3.1. Characteristic of zeolites in the comparative adsorption study

Zeolite products	SiO_2/Al_2O_3 mole ratio	Nominal cation form	Pore size (Å)	Type
CBV 500	5.1	NH_4^+	7.4	Y
CP 811E-75	75	NH_4^+	6.8	Beta
CBV 2314	23	NH_4^+	5.5	ZSM-5

parameters, i.e. adsorbent dosage (0.4–25.0 mg/mL), contact time (0–24 h) and temperature (20–80°C). Adsorption of Ga on zeolite CBV 500 was also investigated from bauxite residue $H_2C_2O_4$ leachate. The adsorbent was separated from the solution using a 0.45 µm PVDF syringe filter and diluted in 1 M HNO_3 before analysis using an ICP-OES, as described above. The adsorption efficiencies were determined by the ratio of metal extracted to the stock solution metal content and to the $H_2C_2O_4$ leachate metal content

3.1.5 Liquid–liquid extraction study

Liquid–liquid extraction was performed according to Ujaczki *et al*. (2017b) as follows: 6 mL of bauxite residue $H_2C_2O_4$ leachate was extracted using an organic solvent phase composed of 13.5 mL of kerosene and 4.5 mL of D2EHPA. D2EHPA was chosen as the organophosphorus reagent as it is commonly used as an attractant (Chen *et al*., 2014; Mihaylov and Distin, 1993; Tsai and Tsai, 2013). All of the experiments were carried out in 100 mL conical flasks at room temperature with constant shaking at 250 rpm for 60 min. Subsequently, phase separation was allowed for 24 h. After extraction, the concentration of metals in the organic phase was calculated from the difference in $H_2C_2O_4$ leachate concentration and the concentration in the aqueous phase analysed using an ICP-OES, as described above.

3.1.6 Experimental design and statistical analysis

Minitab 17 software was used for the development and analysis of experimental designs using the response surface methodology. In the leaching study, a linear model was fitted to the maximal extracted Ga concentration that was recovered by extraction with $H_2C_2O_4$ under varied parameters. The effects of four factors were considered, i.e. $H_2C_2O_4$ concentration, contact time, temperature and slurry concentration. In the adsorption study, a linear model was fitted to the removal of maximal Ga concentration from solution under varied parameters. The effects of three factors were considered, i.e. adsorbent dosage, contact time and temperature. Both models were subsequently reduced to only contain potentially significant factors ($p \leq 0.05$) and factors necessary to maintain model hierarchy using the stepwise automatic model regression of the software. The proposed optimal parameters were then tested experimentally.

3.2 Results

3.2.1 Bauxite residue composition

The elemental composition of the bauxite residue was dominated by Fe (~43.3%), Al (~16.5%), Si (~9.4%), Ti (~8.9%), Ca (~6.2%) and Na (~6.0%) oxides, as detected by XRF (Table 3.2); the Ga concentration was 114.5 ± 5.2 mg/kg, as analysed using an ICP-OES (see Table 3.5).

The XRD analysis showed that bauxite residue contained cancrinite [sodium aluminium silicate carbonate; $Na_6(Al_6Si_6O_{24})\cdot 2(CaCO_3).0(H_2O)$], gibbsite [aluminium hydroxide; $Al(OH)_3$], goethite (iron oxide hydroxide; FeOOH), haematite (iron oxide; Fe_2O_3), perovskite (calcium titanate; $CaTiO_3$), rutile (titanium dioxide; TiO_2) and sodalite [sodium aluminium silicon oxide hydroxide hydrate; $Na_6(Al_6Si_6O_{24})\cdot(2NaOH, Na_2SO_4)$] (Figure 3.1).

3.2.2 SEM microanalysis

The SEM analysis shows the bauxite residue powder as fine particles that form agglomerates (Figure 3.2). EDS mapping showed that the composition of the particles is homogeneous, with the presence of Al, Fe, Na and Si, along with traces of Ca and Ti. Measuring the composition of the residue using EDS data could lead to misinterpretation, but with EDS of secondary raw materials it is possible to determine the presence of only dominating elements. The detected dominance

Table 3.2. Major elemental composition of the bauxite residue as determined by XRF

Element	Content (g/kg)[a]	Oxide	Content (%)[a]	Associated minerals[b]	Unit cell formula
Al	87.4±3.2	Al_2O_3	16.5±0.6	Gibbsite	$Al(OH)_3$
Ca	44.2±2.1	CaO	6.2±0.3	Perovskite	$CaTiO_3$
Fe	302.8±8.4	Fe_2O_3	43.3±1.2	Haematite	Fe_2O_3
				Goethite	FeOOH
Na	44.4±8.8[c]	Na_2O	6.0±0.3[c]	Sodalite	$Na_6(Al_6Si_6O_{24})\cdot(2NaOH, Na_2SO_4)$
				Cancrinite	$Na_6(Al_6Si_6O_{24})\cdot2(CaCO_3)\cdot0(H_2O)$
Si	43.8±2.3	SiO_2	9.4±0.5	Sodalite	$Na_6(Al_6Si_6O_{24})\cdot(2NaOH, Na_2SO_4)$
				Cancrinite	$Na_6(Al_6Si_6O_{24})\cdot2(CaCO_3)\cdot0(H_2O)$
Ti	53.3±3.0	TiO_2	8.9±0.5	Rutile	TiO_2
				Perovskite	$CaTiO_3$

[a]Determined by XRF.
[b]Determined by XRD.
[c]Determined by ICP-OES.

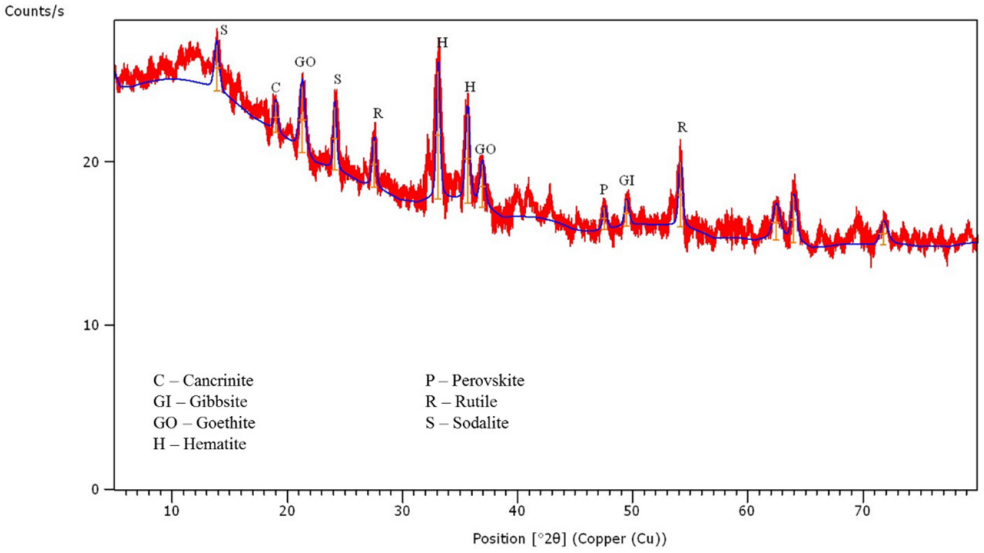

Figure 3.1. The XRD pattern collected from the dried and sieved bauxite residue sample, annotated with major phase peaks detected.

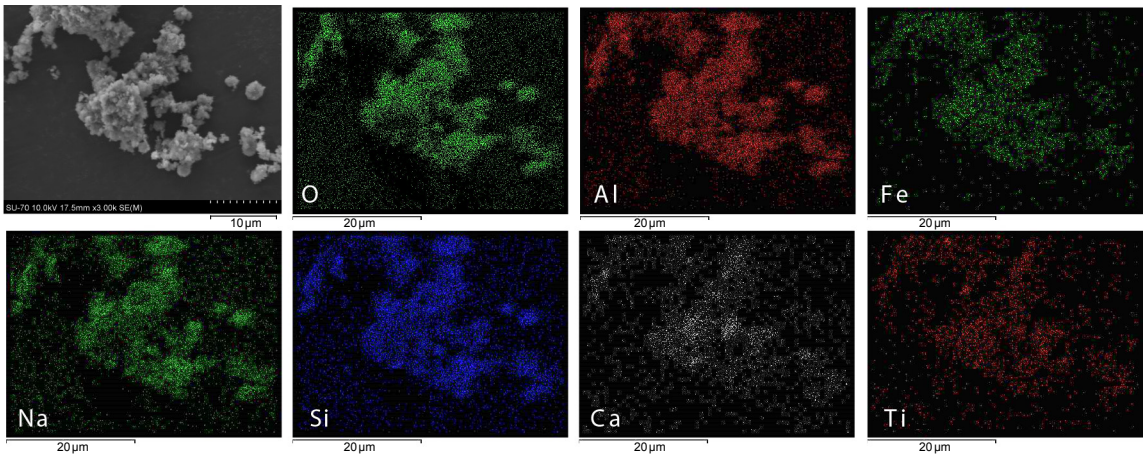

Figure 3.2. Morphology and chemical composition of the bauxite residue detected by SEM-EDS (10.0 kV, 17.5 mm, ×3.00k).

of elements by EDS – Fe, Al, Na, Si, Ca, and Ti oxides – corresponds to the composition detected by XRF and ICP-OES. Phases related to minor elements, such as Ga, V, La and Sc, were not detectable by EDS.

3.2.3 Comparative metal acid leaching study

Three mineral acids (HCl, HNO_3, H_2SO_4) and a small-molecular-weight organic acid ($H_2C_2O_4$) were used for the extraction of Ga from bauxite residue. The comparative extraction study showed that the most efficient extraction method for Ga used $H_2C_2O_4$ (39%, ~44.8 mg/kg), followed by HCl (32%, ~37.2 mg/kg), H_2SO_4 (27%, ~30.6 mg/kg) and HNO_3 (26%, ~29.8 mg/kg) under the following conditions: normality = 2 N, contact time 24 h, 60°C, 100 g/L slurry concentration and shaking at 250 rpm (Table 3.3).

Therefore, $H_2C_2O_4$ was chosen for further investigation of leaching parameters. Al and Fe were also investigated as they are major elements in bauxite residue and their selectivity is an important factor. Using 2 N $H_2C_2O_4$, Al (54% extraction efficiency, ~49,802 mg/kg) and Fe (23% extraction efficiency, ~81,563 mg/kg) were also extracted under the conditions above.

3.2.4 Effects of leaching parameters

The effects of acid concentration, temperature, contact time and slurry concentration on the extraction of Al, Fe and Ga from bauxite residue were studied (Figure 3.3). Increasing the $H_2C_2O_4$ concentration from 0.05 M to 3 M increased the extraction efficiency of Ga from 3% (~3.6 mg/kg) to 44% (~50.9 mg/kg) under the following conditions: contact time 24 h, 60°C, 100 g/L slurry concentration and shaking at 250 rpm. An extraction efficiency of 41% (~44.1 mg/kg) was already achieved using 1 M $H_2C_2O_4$; therefore, 1 M $H_2C_2O_4$ was chosen for the following leaching experiments. Increasing the contact time from 1 to 24 h increased the extraction efficiency of Ga from 12% (~13.8 mg/kg) to 38% (~44.1 mg/kg) using 1 M $H_2C_2O_4$, 60°C, 100 g/L slurry concentration and shaking at 250 rpm. In addition, elevating the temperature from 22°C to 80°C resulted in a large increase in extraction efficiency of Ga from 18% (~19.5 mg/kg) to 40% (~42.7 mg/kg) using 1 M $H_2C_2O_4$, a contact time of 24 h, 100 g/L slurry concentration and shaking at 250 rpm. Slurry concentration had a strong effect on the extraction efficiency, similar to acid concentration. Here, decreasing the slurry concentration from 200 to 10 g/L resulted in an increase in the extraction efficiency of Ga from 3% (~3.7 mg/kg) to 47% (~53.9 mg/kg) under the following conditions: 1 M $H_2C_2O_4$, contact time 24 h, 60°C and shaking at 250 rpm.

Similar trends were identified for Al and Fe extraction (see Figure 3.3). Using 1 M $H_2C_2O_4$ resulted in extraction efficiencies of 57% (~52,316 mg/kg) for Al and 22% (~75,447 mg/kg) for Fe under the following conditions: 24 h contact time, 60°C, 100 g/L slurry concentration and shaking at 250 rpm. Increasing the temperature increased the extraction efficiency for Al to 63% (~58,102 mg/kg), with the extraction efficiency for Fe remaining at 21% (~74,345 mg/kg), under conditions of 1 M $H_2C_2O_4$, 24 h contact time, 100 g/L slurry concentration and shaking at 250 rpm. The optimum Al and Fe extraction efficiencies were achieved by decreasing the slurry concentration to 10 g/L, resulting in extraction efficiencies of 62% (~54,775 mg/kg) for Al and 62% (~216,378 mg/kg) for Fe using 1 M $H_2C_2O_4$, 24 h contact time, 60°C and shaking at 250 rpm.

Table 3.3. Extraction efficiencies for leaching bauxite residue with HCl, H_2SO_4, HNO_3 and $H_2C_2O_4$[a]

Acid	pH	Extraction efficiency (%)[b]		
		Ga	Al	Fe
HCl	0.1	32.5 ± 2.5 (37.2 ± 2.7 mg/kg)	55.4 ± 1.3 (51,056 ± 1265 mg/kg)	16.5 ± 1.5 (57,455 ± 3680 mg/kg)
HNO_3	0.2	26.0 ± 2.0 (29.8 ± 2.2 mg/kg)	54.5 ± 2.6 (50,293 ± 2613 mg/kg)	1.5 ± 0.1 (5299 ± 295 mg/kg)
H_2SO_4	0.8	26.7 ± 1.0 (30.6 ± 1.1 mg/kg)	57.9 ± 1.0 (53,382 ± 971 mg/kg)	1.7 ± 0.1 (5790 ± 84 mg/kg)
$H_2C_2O_4$	1.1	39.2 ± 2.1 (44.8 ± 2.4 mg/kg)	54.0 ± 0.4 (49,802 ± 415 mg/kg)	23.4 ± 1.1 (81,563 ± 2781 mg/kg)

[a]Under the following conditions: normality = 2 N, 24 h contact time, 60°C, 100 g/L slurry concentration and shaking at 250 rpm.

[b]Based on aqua regia-accessible content.

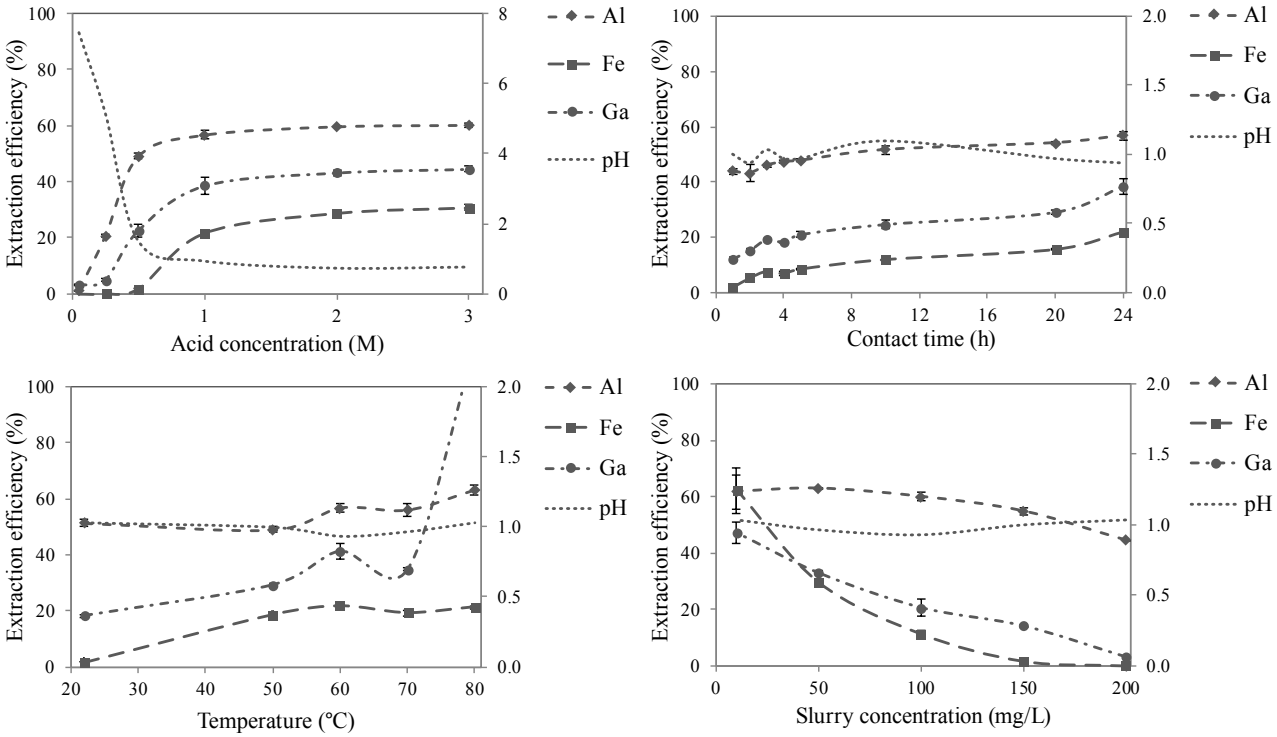

Figure 3.3. Effect of leaching parameters ($H_2C_2O_4$ concentration, contact time, temperature, slurry concentration) on extraction efficiency (primary *y*-axis) and pH (secondary *y*-axis) of Al, Fe and Ga. Single parameters were varied with all other parameters kept constant (1 M $H_2C_2O_4$, 24 h contact time, 60°C, 100 g/L slurry concentration).

3.2.5 Design of experiment approach to predict the optimal parameters for leaching experiments

To determine the optimal extraction conditions to extract the maximal amount of Ga from bauxite residue a DOE approach was used to account for interaction effects between acid concentration (0.05–3 M $H_2C_2O_4$), contact time (1–24 h), temperature (50–80°C) and slurry concentration (10–200 g/L). The response surface reduced linear model considered linear effects between the investigated parameters (equation 3.1) when all linear effects of the four tested factors had a significant ($p \leq 0.05$) effect on the amount of extracted Ga.

Equation 3.1 shows the final equation of the response surface model in terms of actual factors for leaching experiments:

$$\text{Ga conc. (mg/kg)} = 4.71 + 16.56 \times \text{acid conc. (M)} + 0.575 \times \text{contact time (h)} + 0.395 \times \text{temperature (°C)} - 0.2662 \times \text{slurry conc. (g/L)} \quad (3.1)$$

Figure 3.4 shows the two-factor interaction effects between contact time and $H_2C_2O_4$ concentration (Figure 3.4a), temperature and $H_2C_2O_4$ concentration (Figure 3.4b) and slurry concentration and $H_2C_2O_4$ concentration (Figure 3.4c).

The $H_2C_2O_4$ concentration and slurry concentration had the most pronounced effects on the extracted Ga (ranging from 3.0 to 63.1 mg/kg, with the other factors held constant at the optimal values) and are therefore the most important factors to optimise. Contact time and temperature had considerably lower impacts.

The optimal conditions predicted by the model regarding maximal extraction of Ga from bauxite residue were $H_2C_2O_4$ concentration of 2.5 M, contact time of 21.7 h, temperature of 80.0°C and slurry concentration of 10 g/L. The model predicted a maximal extracted concentration of Ga of 85.8 mg/kg. The corresponding leaching experiment at these conditions was conducted and yielded a maximal extracted Ga concentration of 81.1 mg/kg. As the experimentally determined and predicted maximal extractable Ga concentration did not differ significantly (the value obtained was 93% of that predicted), the model was considered to be accurate. Using these optimal conditions, 71% of the aqua regia-accessible Ga content was extracted from the bauxite residue.

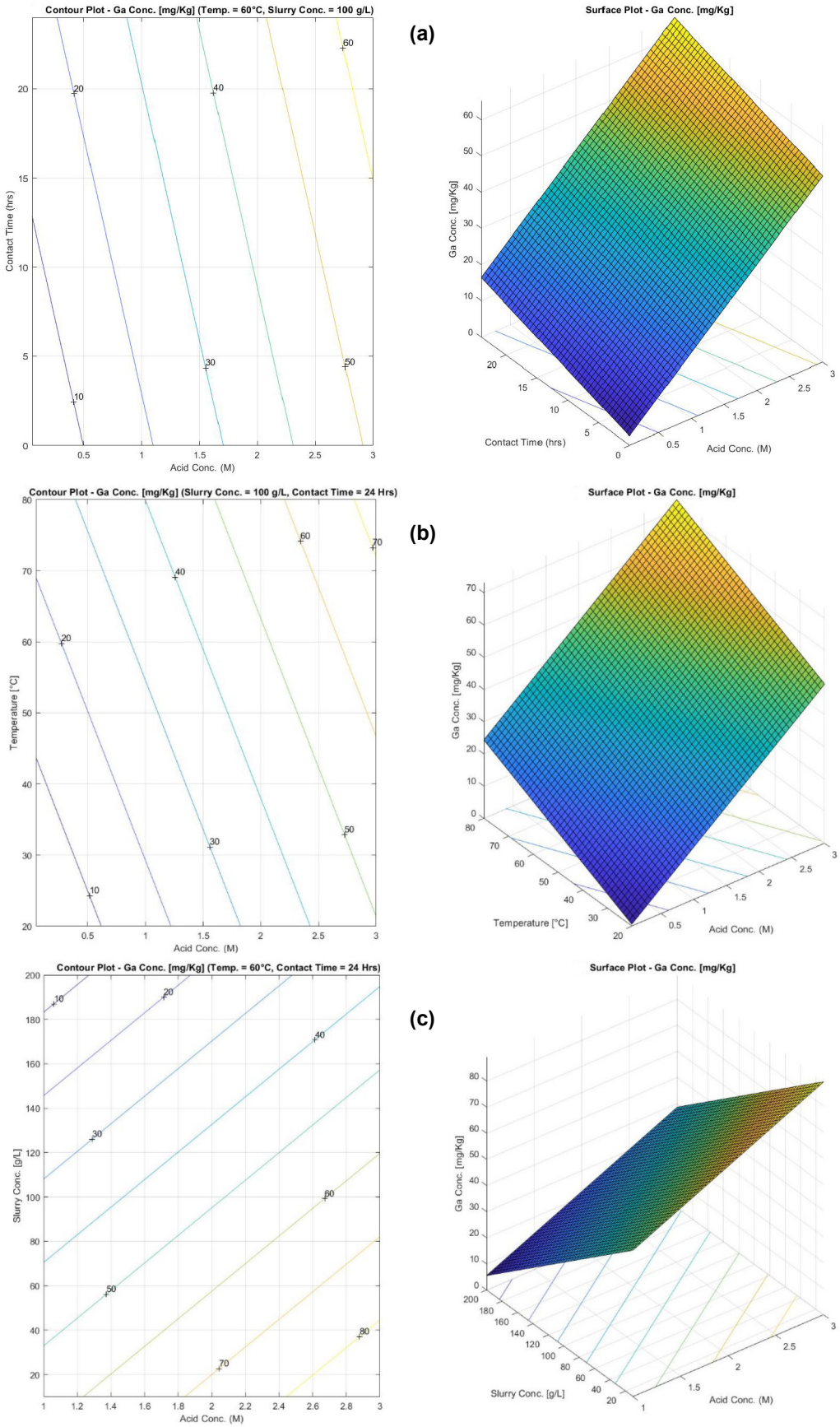

Figure 3.4. Two-factor interaction effects (left, contour plot; right, surface plot) on the extracted Ga. (a) Contact time and $H_2C_2O_4$ concentration; (b) temperature and $H_2C_2O_4$ concentration; (c) slurry concentration and $H_2C_2O_4$ concentration. Factors that are not shown in the graphs were held constant at the predicted optimal values.

3.2.6 Adsorption study

For the first time this study showed a process combination of acid leaching and adsorption on zeolites for the recovery of Ga from bauxite residue; therefore, process parameters were developed for the study in batch experiments.

In the batch study, the removal of Ga from Ga solution (50 mg/L) by three types of zeolites (CBV 500, CP 811E-75 and CBV 2314) were compared (see Table 3.1). Among the investigated zeolite products, the zeolite CBV 500 showed the highest Ga adsorption capacity from the Ga solution, with 99% (~49.6 mg/L) Ga removal efficiency under the following conditions: 10 mg/mL of adsorbent, 24 h contact time and temperature of 20°C (Table 3.4).

Further, the effects of adsorbent dosage, temperature and contact time on the removal of Ga from Ga solution by the zeolite CBV 500 were studied (Figure 3.5).

Increasing the adsorbent dosage from 0 to 25 mg/mL increased the removal efficiency for Ga from 0% (~0.1 mg/L) to 100% (~49.9 mg/L), with a contact time of 24 h and temperature of 20°C. The Ga removal efficiency was already 90% at an absorbent dosage of 5 mg/mL; therefore, this absorbent dosage was used to investigate the effect of temperature and contact time. Temperature in the range of 20–80°C had no particular effect on the removal of Ga. Increasing the contact time from 0 to 24 h increased the extraction efficiency of Ga from 5% (~2.6 mg/L) to 90% (~44.8 g/L) using 5 g/mL of adsorbent at 20°C. Ga adsorption on the zeolite CBV 500 showed rapid kinetics as 82% (~40.0 g/L) of the Ga was adsorbed from the solution after 10 min.

Similar to the extraction study, to determine the optimal conditions for the removal of maximal Ga from the solution a DOE approach was used to account for interaction effects between adsorbent dosage (0.4–25 mg/mL), contact time (0–24 h) and temperature (20–80°C). The response surface reduced linear model considered linear effects between adsorbent dosage and contact time (equation 3.2) as they had a significant ($p \leq 0.05$) effect on the Ga removal efficiency.

Table 3.4. Removal efficiencies for adsorption of Ga with the zeolites CBV 500, CP 811E-75 and CBV 2314[a]

Adsorbent	Removal of Ga (%)
Zeolite CBV 500	99.1 ± 0.1
Zeolite CP 811E-75	16.8 ± 0.2
Zeolite CBV 2314	21.0 ± 3.2

[a]Under the following conditions: 10 mg/mL adsorbent, 24 h contact time and temperature of 20°C.

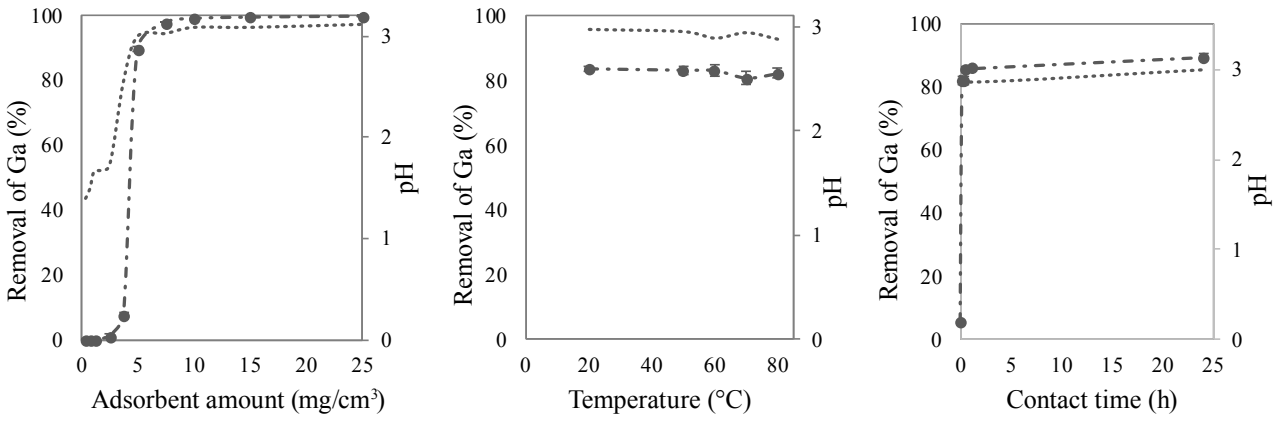

Figure 3.5. Effect of adsorption parameters (adsorbent dosage, temperature, contact time) on Ga removal efficiency (primary *y*-axis) and pH (secondary *y*-axis) from synthetic Ga solution (50 mg/L) by the zeolite CBV 500. Single parameters were varied whereas all other parameters were kept constant (5 mg/mL adsorbent, 24 h contact time and temperature of 20°C).

Equation 3.2 shows the final equation of the response surface model in terms of actual factors for adsorption experiments:

$$\text{Removal of Ga (\%)} = 52.24 + 4.636 \times \text{amount of adsorbent (mg/cm}^3\text{)} - 1.014 \times \text{contact time (h)} \quad (3.2)$$

The adsorbent dosage had the most pronounced effect on the Ga removal efficiency and is therefore the most important factor to optimise (Figure 3.6).

The optimal conditions predicted by the model for the maximal removal of Ga from solution were 5 mg/mL adsorbent dosage and 1 h contact time at 20°C. The model predicted a maximal Ga removal efficiency of 99.8%. The corresponding adsorption experiment at these conditions was conducted and yielded a maximal Ga removal efficiency of 99.4%. As the experimentally determined and predicted maximal Ga removal efficiency did not differ significantly (the value obtained was 99.6% of that predicted), the model was considered to be accurate.

The optimal adsorption parameters (5 mg/mL adsorbent dosage, 1 h contact time and temperature of 20°C) were applied to the bauxite residue leachate to separate Ga from the leachate. In contrast to the batch study, 16.1% (~17.8 mg/kg) of Ga was adsorbed, with the presence of major elements in the bauxite residue (Al: 9.8%, ~13,419 mg/kg; Ca: 14.0%, ~2739 mg/kg; Fe: 11.7%, ~39,018 mg/kg; Na: 7.2%, ~5708 mg/kg; Ti: 17.7%, ~7045 mg/kg) (Figure 3.7 and Table 3.5). The most efficient adsorption was achieved for Si, with a removal efficiency of 98% (~33,934 mg/kg). Another economically interesting element in bauxite residue, V, was adsorbed from the leachate with a removal efficiency of 14.2% (~210 mg/kg).

3.2.7 Liquid–liquid extraction study

Following acidic extraction, Ga was also purified by LLE using D2EHPA. With the organic system consisting of 1 M D2EHPA in kerosene at an O/A (organic to acidic) ratio of 3 at room temperature (Ujaczki *et al*., 2017b), over 72.9% of the Ga (~57.6 mg/kg) was extracted (Figure 3.8 and Table 3.5). In addition, 73.5% of Al (~60,577 mg/kg), 75.8% of Ca (~10,567 mg/kg), 74.4% of Fe (~172,994 mg/kg), 73.8% of Na (~30,922 mg/kg), 75.7% of Si (~25,807 mg/kg), 73.1% of Ti (~24,040 mg/kg) and 73.8% of V (~772 mg/kg) were co-extracted.

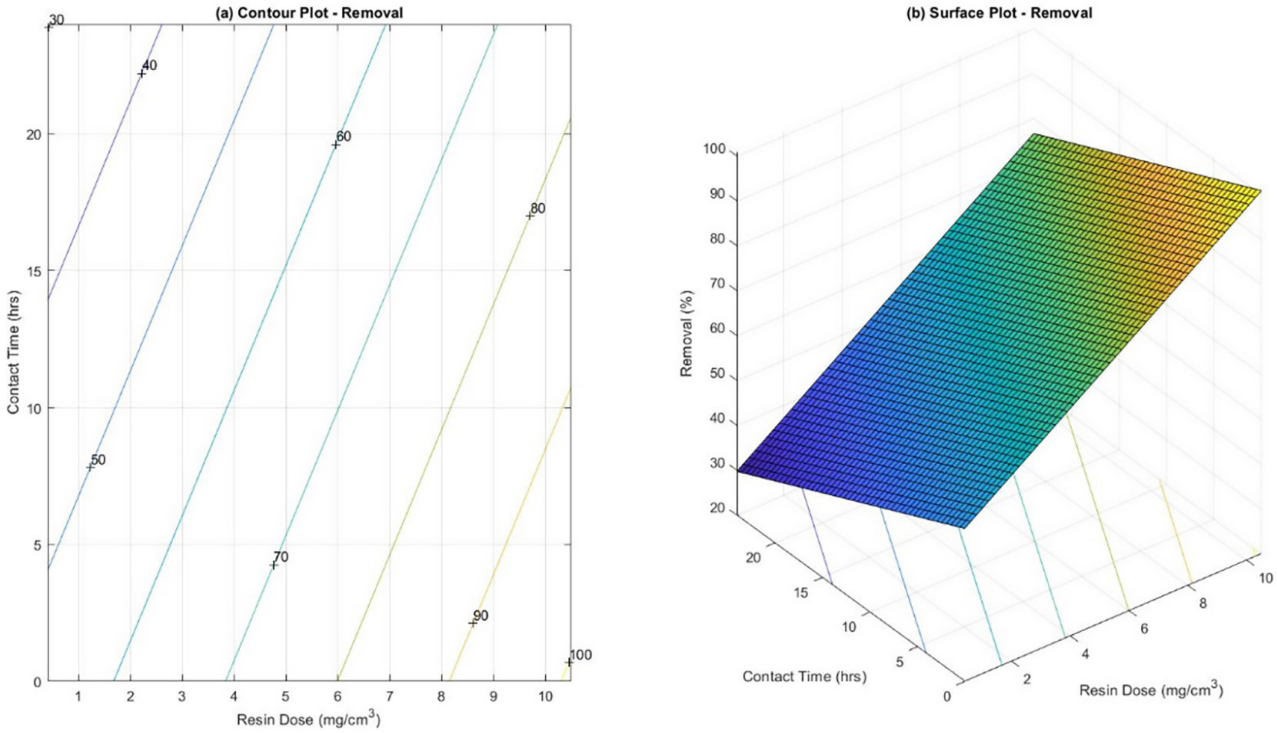

Figure 3.6. Two-factor interactions effects (left, contour plot; right, surface plot) on the extracted Ga: adsorbent dosage and contact time. Factors that are not shown in the graphs were held constant at the predicted optimal values.

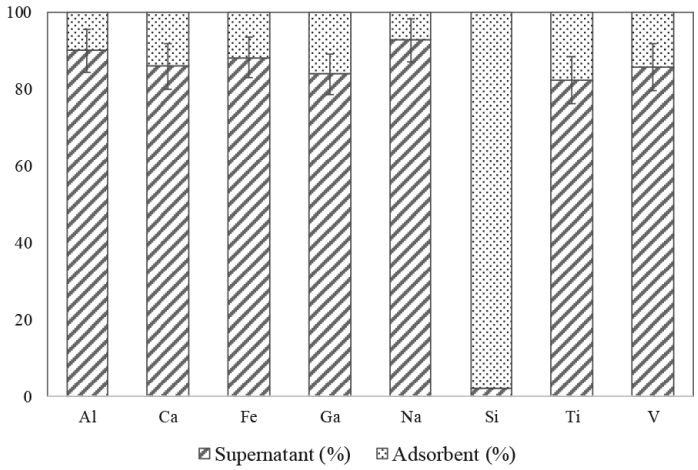

Figure 3.7. Bauxite residue leachate compounds partitioning into supernatant and adsorbent during adsorption on the zeolite CBV 500 under the following conditions: 5 mg/mL absorbent dosage, 1 h contact time and temperature of 20°C (pH 0.5).

Table 3.5. Aqua regia-accessible composition of bauxite residue and partitioning of metal(loid)s during leaching, LLE and adsorption

Elements	Aqua regia-accessible (mg/kg)	Oxalic acid leachate (mg/kg)[a]	LLE organic solvent phase (mg/kg)[b]	Adsorbent (mg/kg)[c]
Al	90,782 ± 1726	84,717 ± 7901	60,577 ± 7839	13,419 ± 4751
Ca	39,827 ± 805	14,192 ± 1739	10,567 ± 1036	2739 ± 846
Fe	347,952 ± 25,269	238,084 ± 8838	172,994 ± 19073	39,018 ± 12493
Ga	114 ± 5.2	81.1 ± 6.9	57.6 ± 7.3	17.8 ± 4.3
Na	44,372 ± 8794	42,573 ± 2021	30,922 ± 2775	5708 ± 2394
Si	43,808 ± 5711	34,558 ± 3256	25,807 ± 2506	33,934 ± 9
Ti	33,784 ± 967	30,828 ± 3003	24,040 ± 2773	7045 ± 1915
V	1226 ± 203	1072 ± 38	772 ± 89	210 ± 65

[a]Leaching parameters: 2.5 M $H_2C_2O_4$, 21.7 h contact time, 80°C, 10 g/L slurry concentration.
[b]LLE parameters: 1 M D2EHPA in kerosene, 1 h contact time, 20°C, O/A ratio 3:1.
[c]Adsorption parameters: 5 mg/mL adsorbent dosage, 1 h contact time, 20°C (pH 0.5).

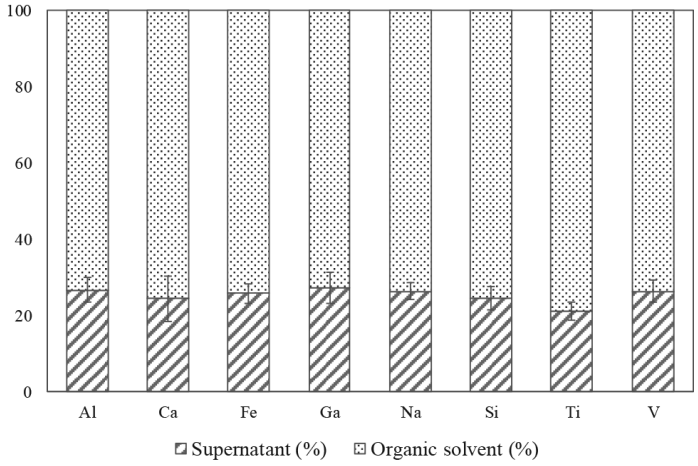

Figure 3.8. Bauxite residue leachate compounds partitioning into organic solvent and leachate during LLE under the following conditions: 1 M D2EHPA in kerosene, 1 h contact time, temperature of 20°C and O/A ratio of 3:1.

3.2.8 Study on the by-product of leaching

The pH of the acidic solid residue was 0.3 and the EC was 39.1 mS. The EDS mapping of the bauxite residue after the extraction process, discussed above, displays the presence of Fe, Al, Si, Ti, Ca and Na oxides (Figure 3.9).

The SEM analysis showed that residue formed large aggregates containing oxalic acid crystals (see Figure 3.9). EDS mapping showed that elements remaining in the acidic solid residue accumulated on the surface of the large aggregates.

Major minerals present in the bauxite residue were not identifiable by XRD analysis so only Fe- and Si-containing peaks were found (Figure 3.10).

3.3 Discussion

The typical order of elemental abundance in bauxite residue is Fe > Si ~ Ti > Al > Ca > Na (Gräfe *et al.*, 2011). In this study, the elemental composition of the bauxite residue was dominated by Fe (~43.3%), Al (~16.5%), Si (~9.4%), Ti (~8.9%), Ca (~6.2%) and Na (~6.0%) oxides (see Table 3.2) and the aqua regia-accessible Ga concentration was 114.5 ± 5.2 mg/kg (see Table 3.5). Similar Ga contents have been described, for instance 89 mg/kg in Australian bauxite residue (Wang *et al.*, 2013) and 91 mg/kg in Indian bauxite residue (Mohapatra *et al.*, 2012).

Similarly to Ujaczki *et al.* (2017a), in this study the extraction efficiency of Ga was higher using

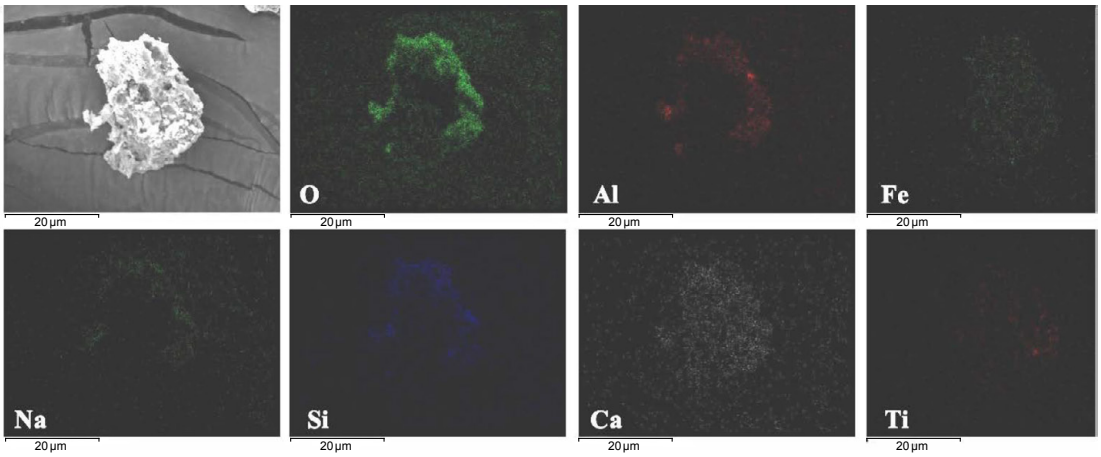

Figure 3.9. Morphology and chemical composition of the by-product of leaching detected by SEM-EDS (10.0 kV, 17.5 mm, ×3.00k).

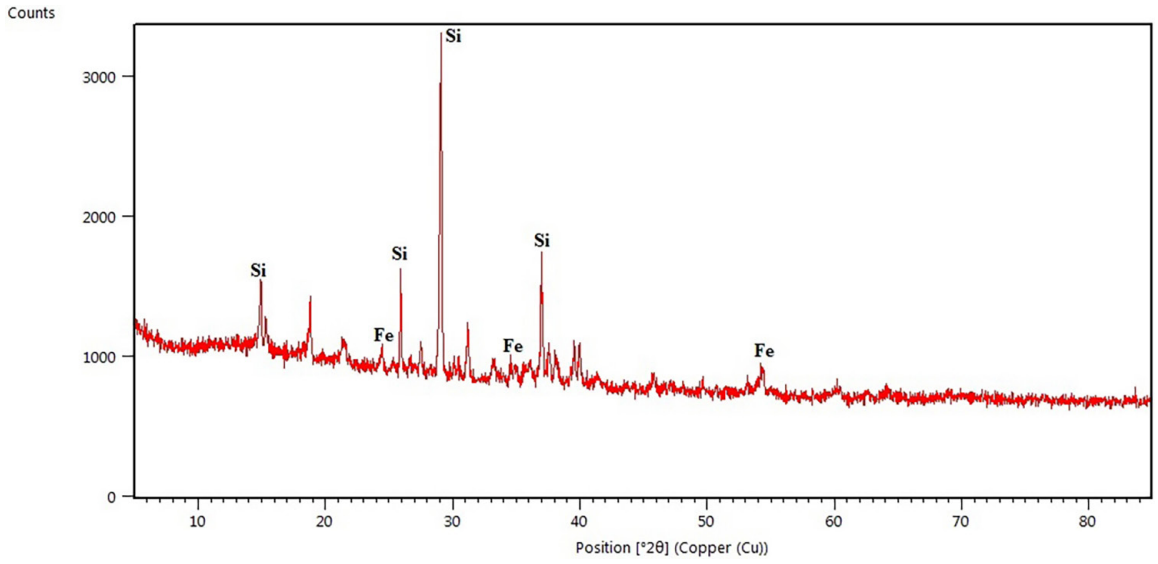

Figure 3.10. The XRD pattern obtained from the dried and sieved by-product of the leaching sample annotated with the major phase peaks detected.

$H_2C_2O_4$ than using HCl, HNO_3 and H_2SO_4 under normality = 2 N, a contact time of 24 h, a temperature of 60°C and a slurry concentration of 100 g/L (see Table 3.3). Lu *et al*. (2018) also evaluated the effects of different mineral acids (4.4 M HCl, 2.2 M H_2SO_4, 4.1 M HNO_3) on Ga extraction from bauxite residue under the following conditions: 4 h contact time, 60°C and 125 g/L slurry concentration. In their study, leaching with HCl resulted in a greater efficiency than leaching with H_2SO_4 or HNO_3, in accordance with the current study and that of Ujaczki *et al*. (2017a).

Considering leaching parameters such as acid concentration, contact time, temperature and slurry concentration, general trends were observed. The extraction efficiencies depended largely on the acid concentration, with higher efficiencies achieved at higher acid concentrations (Lu *et al*., 2018; Ujaczki *et al*., 2017a). For instance, Lu *et al*. (2018) reported a significant increase in Al and Ga extraction efficiency, from 81% to 95%, when the HCl concentration increased from 4.4 M to 6.5 M using a contact time of 4 h, temperature of 100°C and slurry concentration of 125 g/L. They found a slight improvement in Al and Ga extraction efficiency from 4.4 M to 5.8 M HCl, and a large increase in extraction efficiency from 5.8 M to 6.5 M HCl. They attributed this to the initial extraction of only the most easily digested Al (Ga) phases in the bauxite residue, e.g. kaolinite, at lower acid concentrations. Here, increasing the $H_2C_2O_4$ concentration from 0.05 M to 3 M increased the extraction efficiencies of Al and Ga from 3% and 1% to 44% and 60%, respectively, using a contact time of 24 h, temperature of 60°C and slurry concentration of 100 g/L (see Figure 3.3).

Other studies showed similar effects of contact time on the extraction of Ga from bauxite residue. For example, Lu *et al*. (2018) reported that increasing the contact time from 1 to 5 h led to an increased extraction efficiency, from 82% to 95%, under the following conditions: 4.4 M HCl, 55°C and 125 g/L slurry concentration. They found an increase in Ga extraction efficiency from 94% to 95% from 4 to 5 h contact time; therefore, 4 h was chosen as the optimal contact time in their study. In the study by Ujaczki *et al*. (2017a), the best results were achieved using a contact time of 3 h, with a Ga extraction efficiency of 63% under the following conditions: 4 M HCl, 60°C and 100 g/L slurry concentration. Ujaczki *et al*. (2017a) found a relatively low Fe extraction efficiency (21%) at 3 h but the Al extraction efficiency was already high after the first hour (72%). In this study, increasing the contact time from 1 to 24 h increased the extraction efficiency of Ga from 12% to 38% using 1 M $H_2C_2O_4$, a temperature of 60°C and a 100 g/L slurry concentration. A slight increase in extraction efficiency of Al was detectable on increasing the contact time from 1 to 24 h (from 44% to 57%) (see Figure 3.3).

According to Davris *et al*. (2016) and Pepper *et al*. (2016), temperature plays a crucial role in bauxite residue dissolution. The extraction of aluminosilicate (Ga) phases in bauxite residue has been shown to increase with rising reaction temperatures. In the study by Lu *et al*. (2018), the extraction efficiency of Ga increased rapidly from 89% to 94% when the temperature increased from 40°C to 55°C, with a slight increase in extraction efficiency seen when the temperature increased from 55°C to 100°C. In the present study, increasing the temperature from 22°C to 80°C resulted in a considerably increased extraction efficiency of Ga, from 18% to 40%, under the following conditions: 1 M $H_2C_2O_4$, 24 h contact time and 100 g/L slurry concentration (see Figure 3.3). Increasing the temperature increased the Al extraction efficiency to 63% whereas the extraction efficiency for Fe remained at 21%.

Slurry concentration had a strong effect on extraction efficiencies, similar to acid concentration. Decreasing the slurry concentration from 200 g/L to 10 g/L resulted in an increase in the extraction efficiency of Ga from 3% to 47% under the following conditions: 1 M $H_2C_2O_4$, 24 h contact time and temperature of 60°C (see Figure 3.3). The maximal Al (62%) and Fe (62%) extraction efficiencies were also achieved by decreasing the slurry concentration to 10 g/L. This is in accordance with the findings of Ujaczki *et al*. (2017a). However, Lu *et al*. (2018) did not find a significant improvement in the Ga and Al extraction efficiency on reducing the slurry concentration. They found that the slurry (bauxite residue and HCl acid solution) filtration was quite difficult when the slurry concentration was < 125 g/L, which could be attributed to a high concentration of formed silica gels in the slurry (Liu *et al*., 2016; Zheng and Gesser, 1996). Kinetic studies performed by Rivera *et al*. (2018) with HCl and H_2SO_4 demonstrated that, at ambient temperatures, silica dissolution increases with increasing acid concentration, which leads to the formation of silica gel.

Based on the experiments conducted, Lu *et al*. (2018) determined optimum leaching conditions for Ga extraction from bauxite residue to be as follows: 4.4 M HCl concentration, 4 h contact time, temperature of 55°C and 125 g/L slurry concentration. Under these optimal conditions, an average Ga extraction efficiency of 95% was reached. Here, an experimental design approach was used to determine the optimal conditions for Ga extraction using $H_2C_2O_4$. Extraction of maximal Ga from bauxite residue was chosen as the application-relevant response viable. Optimal conditions for the extraction of maximal Ga from bauxite residue were predicted as an $H_2C_2O_4$ concentration of 2.5 M, contact time of 21.7 h, temperature of 80.0°C and slurry concentration of 10 g/L. Indeed, the experimentally determined economic potential corresponded well with the predictions (93% of predicted), allowing a maximum extracted amount of Ga of 85.8 mg/kg. Using these optimal conditions, 71% of the aqua regia-accessible Ga content was extracted from the bauxite residue.

After extraction, dissolved Ga is mostly separated using solvent extraction (Chen *et al*., 2014; Lee *et al*., 2002; Mihaylov and Distin, 1993; Nishihama *et al*., 1999). Solvent extraction (LLE) is based on the partitioning of the dissolved metal into a non-miscible organic phase (extract), followed by recovery (stripping) of metal from the solvent phase (Free, 2013). Nishihama *et al*. (1998) investigated the feasibility of using several organophosphorus compounds for the extraction of Ga and In from chloride solution. Three organophosphorus compounds diluted in kerosene were studied: D2EHPA, 2-ethylhexyl phosphonic acid mono-2-ethylhexyl ester (EHPNA) and bis(2-ethylhexyl) phosphinic acid (PIA-226). The authors found that D2EHPA was the most suitable for separation of Ga and In with high purity (99.8% Ga and 97.4% In). Here, Ga was also purified by extraction using D2EHPA dissolved in kerosene at an O/A ratio of 3 at room temperature (Ujaczki *et al*., 2017b) and over 72.9% of the Ga was extracted (see Figure 3.6 and Table 3.5).

The adsorption technique is also available as another possibility because of its claimed lower environmental impact, high efficiency, easy operation and low price compared with conventionally used solvents (Zhao *et al*., 2015). In recent years, zeolites have been investigated with regard to the adsorption of metals owing to their net negative charge in the polymeric network and the fact that zeolite exchangeable ions are relatively innocuous (Bao *et al*., 2013; Chao and Chen, 2012; Erdem *et al*., 2004). Zeolites consist of a three-dimensional framework of SiO_4 and AlO_4 tetrahedra in which the Al ion is small enough to occupy the position in the centre of the tetrahedron of four oxygen atoms and the isomorphous replacement of Si^{4+} by Al^{3+} produces a negative charge in the lattice (Erdem *et al*., 2004). The net negative charge is balanced by the exchangeable cation (Na^+, K^+, NH^{4+} or Ca^{2+}) and these cations are exchangeable with certain cations such as lead, cadmium, zinc, and manganese (Erdem *et al*., 2004). In the study by Zhao *et al*. (2015), magnetic cobalt ferrite ($CoFe_2O_4$)-coated zeolite was prepared with a hydrothermal method and was used for the adsorption of Ga and In. The authors investigated the effects of pH and adsorption time as the adsorption capacity was influenced by these parameters. In their experiments, the adsorption equilibrium of Ga and In on the $CoFe_2O_4$-coated zeolite could be achieved very quickly. The optimum pH was chosen as 5.0 because at a lower pH more hydrogen ions exist, which can compete more effectively with Ga and In for active bonding sites, leading to a lower adsorption capacity (Zhao *et al*., 2015). However, a high pH also leads to a lower adsorption capacity, which is attributed to the formation of $Ga(OH)_3$ and $In(OH)_3$ (Zhao *et al*., 2015). According to Zhao *et al*. (2015), the rapidly achieved high adsorption efficiency was attributed to the active sites on the adsorbent's surface on a large scale. In the present study, Ga adsorption on the zeolite CBV 500 also showed rapid kinetics, as 82% of the Ga was adsorbed from the solution after 10 min (see Figure 3.4). The pH was kept low because the parameters developed in the batch experiments related to adsorbing Ga from an acidic (pH 0.5) leachate.

4 Phosphorus Recovery from Wastewater Using Bauxite Residue

4.1 Enhancement of Bauxite Residue As a Low-cost Adsorbent for Phosphorus in Aqueous Solution, Using Seawater and Gypsum Treatments

The objectives of this study were to (1) characterise bauxite residue from two different sources, before and after treatment with seawater and gypsum, and investigate their potential to release trace elements, (2) investigate the effect of the treated bauxite residue on P adsorption and (3) assess the impact of particle size and mineral and elemental (particularly Ca and Mg) composition of the bauxite residue on the adsorption of P.

4.1.1 Materials and methods

Sample preparation

A total of 1 kg of mud-farmed bauxite residue samples (treated by atmospheric carbonation and therefore non-hazardous) was obtained from a European refinery, which separates the fine (particle sizes of < 100 µm) and coarse (particle sizes of > 150 µm) fractions of bauxite residue before disposal (IAI, 2015) in a ratio of 9:1 (fine:coarse). The fine and coarse fractions will be referred to hereafter as UF (untreated fine) and UC (untreated coarse). A second bauxite residue sample was sourced from another European alumina refinery (untreated co-disposed or UFR).

Prior to analysis or experiments, all bauxite residue samples were dried at 105°C for 24 h. Dried samples were pulverised using a mortar and pestle and sieved to a particle size of < 2 mm. In total, 0.3 kg of each sample was then treated with either seawater or laboratory-grade gypsum (Lennox Ireland); therefore, two treatments were applied to each source of bauxite residue, with S (seawater) or G (gypsum) placed after the above abbreviations indicating the treatment applied. Gypsum was applied to the 0.3 kg bauxite residue samples at a ratio of 8% (w/w) (Lopez *et al*., 1998) and leached for 72 h in accordance with standard methods (BSI, 2002). Seawater amendment involved mixing with 0.3 kg of bauxite at a ratio of 5:1 (v/w) (after Johnston *et al*., 2010) for 1 h, followed by a 12 h settlement period overnight. The bauxite residue and seawater mixture was then filtered through a 0.45 µm membrane using a vacuum pump. The treated bauxite residue samples were then oven dried for 24 h, pulverised with a mortar and pestle and sieved to < 2 mm in size.

Characterisation study

Untreated and treated bauxite samples ($n = 3$) were characterised for their physical, chemical, elemental and mineralogical properties. Soil pH and EC were determined as described in section 3.1.1. The bulk density (ρ_b) was determined after Blake (1965) and the particle density (ρ_p) after Blake and Hartge (1986). Total pore space (S_t) was calculated using the values obtained for the bulk and particle densities (Danielson and Sutherland, 1986). The effective particle size analysis was determined on particle sizes of < 53 µm using optical laser diffraction on the Malvern Zetasizer 3000HS® with an online autotitrator and a Horiba LA-920, and reported at specific cumulative percentages (10%, 50% and 90%). Surface morphology and elemental detection were carried out using SEM and EDS on a Hitachi SU-70 (Berkshire, UK). Quantification of the elemental content was determined following acid digestion using inductively coupled plasma atomic emission spectroscopy (ICP-AES) (Brookside Laboratories, OH, USA) and elemental composition was quantified using XRF. Measurement of the point of zero charge (PZCpH) was after Vakros *et al*. (2002) and cation exchange capacity (CEC) was determined using the K saturation technique (Thomas, 1982). Brunauer–Emmett–Teller specific surface area (SSA) and pore volume analysis were conducted on samples, which were degassed at 120°C for 3 h prior to analysis, which was carried out by Glantreo Laboratories (Cork, Ireland).

Phosphorus adsorption batch study

The P adsorption capacity of nine bauxite samples (untreated and gypsum/seawater treated samples) was examined in a bench-scale experiment. To

conduct a P adsorption isotherm test, orthophosphorus (PO_4^{3-}-P) solutions were made up to known concentrations using potassium dihydrogen phosphate (K_2HPO_4) in distilled water. In total, 1 g of each of the sieved media was placed into a series of 50-ml-capacity containers and was overlain with 25 ml of the solutions. Each sample was then shaken in a reciprocal shaker at 250 rpm for 24 h. At $t = 24$ h, the supernatant water from each sample container was filtered using a 0.45 µm filter and analysed immediately using a nutrient analyser (Konelab 20, Thermo Clinical Labsystems, Finland). The data obtained from the P adsorption batch studies were modelled using the Langmuir adsorption isotherm (McBride, 2000), which assumes monolayer adsorption on adsorption sites and allows for the estimation of the maximum P adsorption capacity (q_{max}) of the media:

$$q_i = q_{max}\left(\frac{k_a C_e}{1+k_a C_e}\right) \quad (4.1)$$

where q_i is the quantity of the contaminant adsorbed per gram of media (g/g), C_e is the equilibrium contaminant concentration in the water (g/m³), k_a is a measure of the affinity of the contaminant for the media (m³/g) and q_{max} is the maximum amount of the contaminant that can be adsorbed onto the media (g/g).

Statistical analysis

Linear regression analysis was utilised to examine the extent of correlation between the individual characteristic parameters of the bauxite residue samples and bauxite adsorption, using Minitab. A Pearson correlation coefficient and a correlation *p*-value were determined to quantify the correlation. The *p*-value represents the probability that the correlation between the bauxite residue characteristic in question and the response variable (adsorption) is zero, i.e. the probability that there is no relationship between the two.

4.1.2 Results and discussion

Effect of treatments on elemental and mineralogical composition

The mineral and total elemental composition of the three untreated bauxite residues (UF, UC and UFR) are shown in Tables 4.1 and 4.2. Bauxite residues are typically high in Fe and Al oxides (Liu *et al*., 2007a), which was found to be the case in this study. The mineralogical composition of all untreated samples was dominated by Fe_2O_3, Al_2O_3, SiO_2 and CaO. A decrease in Al_2O_3 was noted following treatment with gypsum and seawater in all samples, with an increase in CaO content noted in samples treated with gypsum.

Effect of treatments on physicochemical properties

The untreated bauxite residues had a high pH (10.8–11.9) and EC (704–1184 µS/cm) (Table 4.3). Following treatment with gypsum and seawater, the pH decreased and EC increased. Changes in pH after treatment with either seawater or gypsum are due to precipitation of calcium carbonates such as calcite, brucite and aragonite, which behave as buffers and maintain a reduced pH (Menzies *et al*., 2004), whereas the increase in EC is attributed to the introduction of excess Na^+ and Ca^{2+} (Gräfe *et al*., 2009). The pH of bauxite residue is normally within

Table 4.1. Mineralogical composition of the bauxite residues (untreated and treated)

Oxides	UF (%)	UFG (%)	UFS (%)	UC (%)	UCG (%)	UCS (%)	UFR (%)	UFRG (%)	UFRS (%)
Fe_2O_3	43.9±1.1	40.6±0.6	41.8±1.2	64.0±5.1	61.4±3.0	69.9±3.8	43.9±0.6	47.9±0.5	53.3±5.8
Al_2O_3	12.7±0.6	11.3±1.0	11.1±2.5	19.4±1.8	11.1±0.6	7.4±0.7	14.0±1.0	11.2±0.3	11.4±2.2
CaO	5.9±0.2	8.2±0.5	4.4±0.3	1.1±0.2	7.6±0.4	1.2±0.1	5.6±0.1	7.7±0.3	3.2±0.5
MgO	3.6±1.3	3.5±0.8	3.1±1.0	4.7±1.8	3.6±0.8	2.6±0.6	4.1±0.6	3.8±0.9	3.2±1.6
SiO_2	8.6±0.7	8.5±0.9	8.6±1.7	2.6±0.3	1.3±0.2	1.4±0.2	9.4±0.5	5.1±0.4	4.3±0.3
TiO_2	2.4±0.3	2.1±0.6	2.7±0.1	0.9±0.1	1.0±0.1	2.1±0.6	2.5±0.02	2.3±0.1	2.3±0.5
P_2O_5	0.6±0.04	0.4±0.02	0.4±0.1	0.3±0.02	0.2±0.02	0.2±0.06	0.5±0.01	0.5±0.02	0.5±0.01

Table 4.2. Elemental composition of the bauxite residues (untreated and treated) (mg/kg)

Elements	UF	UFG	UFS	UC	UCG	UCS	UFR	UFRG	UFRS
B	470±8.8	425±29	448±13	615±13.3	622±29	722±32.1	566±18.9	539±25	483.8±31
Al	72,538±1390	81,095±1219	80,608±3090	45,854±2769	48,851±2336	45,917±2080	67,295±3343	65,389±1326	64,189±595
As	21.9±1.7	9.70±0.4	<LOD	<LOD	<LOD	<LOD	8.1±0.2	9.75±0.6	6.51±0.4
Ba	43.8±1.2	29.4±5	33.3±0.7	13.9±1.0	18.3±3.4	12.7±2.8	45.7±1.5	41.4±1.4	49.4±3.8
Cd	8.03±0.2	7.02±0.3	7.33±0.2	10.7±0.2	10.8±0.5	11.8±0.59	9.31±0.2	8.87±0.3	8.21±0.3
Cr	1698±37.2	933±44	1170±12.9	880±4	817±13	803±21.3	1184±15.9	1090±9	1159±31.2
Fe	33,8571±3057	289,459±1859	298,282±4937	434,739±9980	460,078±23,043	471,204±25,753	353,392±10,003	328,114±4498	33,2251±3435
Pb	34.9±0.5	27.8±2.8	36.9±0.8	29.6±3.0	24.6±3.0	22.1±2.5	34.5±0.9	32.3±0.8	37.4±2.1
Mg	122±5.0	163±37	1047±26	18.3±4.8	8.5±2.2	512±25	109±3.9	150±9	2203.8±134
Mn	163±2.6	140±6	167±7	187±16	223±99	185±31	134±0.9	139±1.9	142.9±4.2
Ni	18.6±0.9	<LOD[1]	2.25±0.2	3.54±0.3	3.15±0.5	4.18±0.2	1.1±0.1	1.24±0.2	1.23±0.3
K	391±13.7	454±29	1108±41	255±38	195±23	557±67	399±13	359±11	1048±63.2
Si	224±46.1	256±92	246±35	213±7	234±34	194±11	276±20	285±34	258.5±11.7
Na	28,347±553	38,180±352	41,864±2012	8804±666	5935±114	11,102±1122	25,514±317	23,703±499	31,974±1087
Ti	1395±196	1309±100	1265±22	<LOD	<LOD	<LOD	1382±38	1288±120	1233±46
V	1050±22	781±29	777±8	786±23.6	731±20	731±23	1036±12	920±7	983±21
Zn	50.7±0.7	40.6±1.2	42.6±1.3	86.7±1.7	82±5	84.7±4.2	55.8±0.5	55.6±1.2	57.3±0.9
Ga	78.9±2.0	81.2±0.5	73.9±0.6	71.8±1.0	69.3±2.3	73.5±1.6	86.8±1.3	78.6±2.0	78.8±0.9
Ca	46,657±832	51,641±485	17,159±413	4152±490	12,771±823	4089±588	15,084±358	42,703±2383	14,820±926
P	955±1	962±99	1018±15	1040±23	1011±59	1040±23	1298±26	1220±10	1320±54
Be	<LOD	<LOD	<LOD	<LOD	<LOD	<LOD	<LOD	<LOD	<LOD
Cu	<LOD	<LOD	<LOD	<LOD	<LOD	<LOD	<LOD	<LOD	<LOD
Hg	<LOD	<LOD	<LOD	<LOD	<LOD	<LOD	<LOD	<LOD	<LOD
Mo	<LOD	<LOD	<LOD	<LOD	<LOD	<LOD	<LOD	<LOD	<LOD
Se	<LOD	<LOD	<LOD	<LOD	<LOD	<LOD	<LOD	<LOD	<LOD

<LOD, below the limits of detection.

Table 4.3. Physical and chemical characterisation of the bauxite residues (untreated and treated)

Parameter	UF	UFG	UFS	UC	UCG	UCS	UFR	UFRG	UFRS
pH	10.8±0.1	8.70±0.04	9.02±0.1	11.4±0.3	6.79±0.1	7.95±0.2	11.9±0.1	9.17±0.02	9.49±0.01
EC (µS/cm)	704±90.8	1338±4	3080±17	856±1	909±2	916±2	1184±49	1219±7	5323±172
% water	23.5±0.7	28.9±0.6	32.1±1.7	0.39±0.2	0.82±0.2	3.13±0.7	28±0.5	35.3±1.3	36.5±0.2
d_{10} (µm)[a]	0.60±0.1	1.37±0.2	1.26±0.1	1.27±0.5	1.11±0.2	1.66±0.8	1.30±0.04	1.49±0.1	1.08±0.7
d_{50} (µm)[b]	2.43±0.3	3.56±0.6	3.52±0.1	5.13±0.6	3.69±0.5	3.68±0.4	3.70±0.1	4.11±0.4	3.47±1.0
d_{90} (µm)[c]	6.02±0.9	7.12±2.0	7.69±2.0	12.0±1.3	9.51±0.3	7.00±0.1	10.1±2.4	9.81±2.7	7.17±3.2
Total pore space (%)[d]	50.0±2.3	50.7±9.0	50.0±1.8	9.63±6.5	10.82±1.1	7.65±5.3	61.8±1.2	53.6±2.0	53.9±0.8
Bulk density (g/cm^3)[e]	1.50±0.02	1.5±0.01	1.49±0.01	2.53±0.01	2.48±0.03	2.55±0.01	1.31±0.03	1.32±0.03	1.31±0.02
Particle size density (g/cm^3)[f]	2.99±0.1	3.11±0.5	2.94±0.1	2.81±0.2	2.65±0.4	2.7±0.1	3.41±0.1	2.85±0.1	2.85±0.1
PZCpH[g]	6.96±1.2	3.43±0.7	6.28±1.0	6.89±0.1	3.11±0.1	6.39±0.5	6.16±0.2	6.32±0.5	4.43±0.1
CEC (K) (cmol/kg)	63.3±2.6	64.1±3.4	60.1±3.0	NA	NA	NA	57.5±2.1	56.4±3.5	48.9±13.7
Total pore volume (cm^3/g)	0.03	0.03	0.03	0.02	0.02	0.03	0.03	0.04	0.03
BET SSA (m^2/g)[h]	11.7	12.8	13.8	12.6	13.2	15.4	15.2	17.6	17.6

[a] d_{10} = the size of particles at 10% of the total particle distribution, expressed in µm.

[b] d_{50} = the median; the size of particles at 50% of the total particle distribution, expressed in µm.

[c] d_{90} = the size of particles at 90% of the total particle distribution, expressed in µm.

[d] Total pore space, calculated from particle density and bulk density.

[e] Bulk density = the mass of soil per unit volume, expressed as g/cm^3.

[f] Particle size density = the density of the solid particles, excluding pore spaces between them, expressed as g/cm^3.

[g] PZCpH = the pH at which the point of zero charge is occurring.

[h] BET SSA = the specific surface area analysed using the Brunauer–Emmett–Teller isotherm and expressed as m^2/g.

NA, not available.

the range of 11–13 (Newson *et al*., 2006), but varies according to the type of bauxite ore, Bayer process and neutralisation techniques used in the refinery. Both seawater (Johnston *et al*., 2010; Menzies *et al*., 2004) and gypsum (Courtney and Kirwan, 2012; Jones and Haynes, 2011; Lehoux *et al*., 2013) applications are recognised methods of reducing the alkalinity of bauxite residues.

No change was observed in the particle size or particle size density following the addition of the gypsum and seawater treatments to the various bauxite residue samples (see Table 4.3). Similarly, the addition of gypsum or seawater did not have any impact on bulk density.

Phosphorus adsorption study

All nine bauxite residue samples in this study were successful at removing P from aqueous solution (Table 4.4). Bauxite residue has been shown in numerous P adsorption studies to have a high P retention capacity, particularly following treatment or modification (Grace *et al*., 2015; Ye *et al*., 2014). In this study, gypsum or seawater treatment had a positive impact on P removal, with the gypsum-treated bauxite residue performing best (see Table 4.4).

Following seawater treatment, the P adsorption capacity of the bauxite residues increased to *q*max values of 0.48, 0.66 and 1.92 mg P/g media for UFS, UCS and UFRS, respectively. In previous studies, following treatment with seawater, bauxite residue had a higher adsorption capacity for P. Akhurst *et al.* (2006) reported a maximum adsorption of 6.5 mg/g when using a bauxite residue treated with brine (Bauxsol™). This relatively high adsorption may be attributed to the higher concentrations of Ca^{2+} and Mg^{2+} in the brines (or products such as Bauxsol™, developed by Basecon™) compared with the raw seawater (0.41, 1.29 and 10.77 g/kg of Ca^{2+}, Na and Mg^{2+}, respectively) used in this study (Gräfe *et al*., 2009). The gypsum-treated bauxite residues had the highest *q*max values: 2.46, 1.39 and 2.73 mg P/g media for UFG, UCG and UFRG, respectively. However, these values were lower than those in a P adsorption study carried out by Lopez *et al*. (1998), who used the same application rate of gypsum to the bauxite residue samples and reported a *q*max of 7.03 mg P/g. The lower rate observed in the current study may be attributed to the 72 h leaching process that the gypsum-treated bauxite residue underwent before use in the adsorption study, which may have allowed for further exchange and removal of Ca^{2+} following the leaching process.

Overall, the bauxite residue in the current study had a higher P adsorbency than that in other studies of zeolite (0.01 mg P/g, Grace *et al*., 2015) and granular ceramics (0.9 mg P/g; Chen *et al*., 2012), but lower than those of fly ash, granular blast furnace slag and pyritic fill (6.48, 3.61 and 0.88 mg/g, respectively; Grace *et al*., 2015), crushed concrete (19.6 mg P/g; Egemose *et al*., 2012), untreated biochar (32 mg P/g; Wang *et al*., 2015) and NaOH-modified coconut shell powder (200 mg P/g; de Lima *et al*., 2012).

Factors affecting phosphorus adsorption

The adsorption of P onto media is influenced by many factors, including particle size, pH, component and surface characteristics (Wang Z. *et al*., 2016). Numerous studies have investigated the effect of parameters such as the kinetics of P adsorption (Akhurst *et al*., 2006; Grace *et al*., 2015; Liu *et al*., 2007b; Ye *et al*., 2014), ionic solution (Akhurst *et al*.,

Table 4.4. Maximum adsorbency (mg P/g media) of P using each of the bauxite residue samples (untreated and treated)[a]

Media	Treatment method employed (mg/g media)		
	Untreated	Gypsum	Seawater
UFR	1 (0.99)	2.73 (0.99)	1.92 (0.99)
UF	0.38 (0.99)	2.46 (0.97)	0.48 (0.99)
UC	0.35(0.98)	1.39 (0.99)	0.66 (0.99)

[a]**Level of fit of the data, R^2, to the Langmuir isotherm is included in parentheses.**

2006) and pH (Grace *et al*., 2015; Huang *et al*., 2008; Liu *et al*., 2007b) on the adsorption of P from aqueous solution. Although all bauxite residue samples in this study did remove P from aqueous solution, it is clear that the application of treatments such as gypsum or seawater has an effect on the adsorption capability, and that the rate of adsorption will vary as a result of the source of bauxite residue and treatments used (Wang *et al*., 2008).

The parameters that showed a statistically significant positive correlation of medium strength with P adsorption in this study were Ca concentration [correlation coefficient = 0.47, $p = 0.01$, degrees of freedom (df) = 25] and CaO concentration (correlation coefficient = 0.39, $p = 0.04$, df = 25). The influence of Ca on P adsorption can be due to the high level of Ca^{2+} and Mg^{2+} present in the bauxite residue, particularly after seawater and gypsum treatments, when the majority of PO_4^{3-} is removed from solution as a result of the formation of magnesium phosphate [$Mg_3(PO_4)_2$] and calcium phosphate [$Ca_3(PO_4)_2$] (Akhurst *et al*., 2006). A statistically significant negative correlation of medium strength was also detected between pH and P adsorption (correlation coefficient = –0.38, $p = 0.05$, df = 25). pH was a contributing factor in the adsorption process, with the amount of phosphate adsorbed increasing with a decrease in pH in the media following treatments as follows: UFRG > UFRS > UFR, UFG > UFS > UF and UCG > UCS > UC. This was a similar finding to that in several studies carried out by Li *et al*. (2006), Liu *et al*. (2007b), Huang *et al*. (2008) and Grace *et al*. (2015).

The pH at which net charges are neutral on the surface of the adsorbent – the PZCpH – influences the rate of adsorption of P (Jacukowicz-Sobala *et al*., 2015). When the pH is higher than the PZCpH, the surface of the adsorbent media becomes more negative (attracting more cations) as a result of the adsorption of OH^- from the surrounding solution (Prajapati *et al*., 2016). The PZCpH ranged from 6.16 to 6.96 in the three untreated samples (see Table 4.3). Following treatment with gypsum and seawater, there were notable changes, but no statistical relevance was detected for the interaction between the PZCpH and P adsorption in this study. However, as bauxite residue is composed of numerous minerals, each with its own individual PZCpH (which, as noted in the literature, can range between pH 2 and pH 9.8; Gräfe *et al*., 2009), this results in the bauxite residue being able to cater for a wide range of pH (Gräfe *et al*., 2009) and also having the capability of removing both cations and anions from solution.

The SSA analysis carried out on the bauxite residues shows an increase in SSA in all samples following treatment with gypsum or seawater (see Table 4.3). There was also an increase in pore volume following the addition of either gypsum or seawater. This is attributed to the formation of precipitates in the neutralisation process for both gypsum and seawater and the effect of Ca acting as a flocculant to the finer particles present. This increase in surface area also contributes to the increase in P adsorption following treatments. Although particle size affects adsorption onto media, because of the availability of sites for P uptake, no significant correlation was observed in the current study.

4.1.3 Implications of the findings of the phosphorus adsorption study

The use of gypsum and seawater treatments of bauxite residue improved the overall P adsorption capacity of the bauxite residue samples, but mixing the bauxite residue and treatments with actual wastewater will be necessary to fully understand the total adsorption behaviour of the bauxite residue. In addition to improving the P adsorption, alkalinity was significantly reduced following both treatments. However, the EC was increased, which may limit the growth of plants on the gypsum- or seawater-treated bauxite residues. One solution may be to increase the rinsing period of the bauxite residue following treatment to remove the excess Ca^{2+} and Na^+ ions in solution. Lowering the alkalinity, increasing the P, Ca^{2+} and Mg^{2+} content and improving the physical structure may enable the treated bauxite residue to be reused as a growth medium.

For a refinery, the cost of neutralisation techniques is an obvious consideration when deciding which technique(s) to use. The use of seawater as a neutralisation technique would be a cheap and feasible option for a refinery that is located close to the sea. The establishment of a pipeline (if not already in place) would be the dominant capital cost. The use of a nanofiltration system to concentrate the Ca^{2+}, Mg^{2+} and Na^+ ions in the seawater (Couperthwaite *et al*., 2014) could allow for a reduction in the volume of seawater needed for the neutralisation process,

but may add to the cost. Gypsum, however, may be a more expensive option, requiring machinery such as amphirolls for the mixing and spreading of the gypsum. However, depending on the location of a refinery, waste gypsum from construction sites or fossil fuel-powered power stations may be used (Jones and Haynes, 2011).

4.2 Efficiency of Bauxite Residue As a Low-cost Adsorbent in the Removal of Dissolved Reactive Phosphorus from Agricultural Wastewaters

The objectives of this study were to (1) investigate the removal rate and retention capacity of bauxite residue for dissolved reactive P removal from dairy soiled water and forest run-off, (2) identify any potential trace metal mobilisation from the bauxite residue media during the loading period of the columns when treating the wastewater and (3) investigate the mechanism and speciation of P adsorption onto the bauxite residue media.

4.2.1 Materials and methods

Sample collection

Bauxite residue was obtained from a European refinery. Residue was sampled to a depth of 30 cm and the bulk samples were stored in 1 L containers, returned to the laboratory and dried at 105°C for 24 h. Once dry, the samples were pulverised using a mortar and pestle and sieved to a particle size of < 0.5 mm. The pH and EC were determined as described in section 3.1.1. Dairy soiled water was collected from Teagasc Agricultural Research Centre, Moorepark, County Cork, Ireland (52° 9′ 48.114″ N, 8° 15′ 34.6464″ W) and forest run-off was collected from Kilmoon, County Clare, Ireland (53° 2′ 48.0372″ N, 9° 16′ 21.1368″ W).

The dairy soiled water and forest run-off were transferred directly to a temperature-controlled room (11°C). The dissolved reactive P was measured using filtered (0.45 µm) subsamples using a nutrient analyser (Konelab20, Thermo Clinical Lab systems, Espoo, Finland) and the pH was measured using a Eutech Instruments pH 700 meter (Thermo Scientific, USA).

Media characterisation

The bauxite residue media was characterised before and after use in the columns. Mineralogical detection was conducted using XRD on a Philips X'Pert PRO MPD® (California, USA) at 40 kV, 40 mA, 25°C by Cu X-ray tube (Kα-radiation). The patterns were collected in the angular range from 5° to 80° (2ɵ) with a step size of 0.008° (2ɵ) (Castaldi *et al*., 2011), whereas surface morphology and elemental detection were carried out using SEM and EDS on a Hitachi SU-70 system (Berkshire, UK). XRF analysis was carried out onsite at the refinery using a Panalytical Axios XRF system. Fourier transform infrared (FT-IR) analysis was carried out using a PerkinElmer Spectrum 100 (PerkinElmer, USA). The FT-IR spectra were recorded in the 4000–650/cm range and were collected after 256 scans at 4 cm resolution (Castaldi *et al*., 2010).

Rapid small-scale column study

Small-bore adsorption columns were prepared after Callery *et al*. (2016) using polycarbonate tubes with an internal diameter of 0.94 cm and lengths of 20, 30 and 40 cm. The tubes were packed with a mixture of bauxite residue. The bauxite residue media was held in place within the column by friction fit using plastic syringes with an internal diameter equal to the outside diameter of the polycarbonate tubes. Acid-washed glass wool was placed at the top and bottom of each of the polycarbonate tube columns to retain the bauxite residue media. To each polycarbonate tube column, flexible silicone tubing was attached to the syringe ends to provide lines for the influent and effluent. The columns were secured on a metal frame, allowing a stable vertical orientation to be maintained. A Masterflex® L/S Variable-Speed Drive peristaltic pump (Gelsenkirchen, Germany) with a variable speed motor was used to pump the influent, dairy soiled water and forest run-off into the base of each column at an estimated flow rate of 30.49 ± 0.85 mL/h, preventing the occurrence of channelling. The pump was operated in 12 h on/off cycles to achieve loading periods of 24–36 h. Every 2 h, aliquots were collected and the volume and pH were measured, the instantaneous PO_4-P was analysed using a nutrient analyser (Konelab20) and the cumulative mass of P adsorbed by the filter media was calculated using the following equation:

$$q_e = \sum_{i=1}^{n} \frac{\left(c_O - c_{e_i}\right) v_i}{m} \quad (4.2)$$

where q_e is the cumulative mass of contaminant adsorbed per gram of filter media, n is the number of containers in which the total volume of effluent ($\sum V_i$) is collected, C_o is the influent contaminant concentration, C_{e_i} is the effluent contaminant concentration in the ith container, V_i is the volume of effluent contained in the ith container and m is the mass of filter media contained in the filter column.

The performance of the adsorption column media was predicted using a model described by Callery and Healy (2017) using the following equation:

$$C_e = C_o - \frac{q_e M}{V_B} \quad (4.3)$$

where C_e is the filter effluent contaminant concentration and C_o is the influent contaminant concentration, M is the mass of the filter media, V is the volume of the influent loaded onto the filter, B is a model constant and q_e is the mass of adsorbate adsorbed per unit mass of filter media, as modelled by the following equation:

$$q_e = A V_B^{\left(\frac{1}{B}\right)} \quad (4.4)$$

where A is a model constant and V_B is the number of bed columns of influent filtered.

The solution adsorbate concentration at any given filter depth, C_t, can be found using the following equation:

$$C_t = C_o - \frac{q_t M}{V_B} \quad (4.5)$$

A description of the relationship between bed depth and volume of solution treated to any breakthrough concentration, C_t, can be found using the following arrangement of the equation:

$$V = \frac{q_t M}{B\left(C_o - C_t\right)} \quad (4.6)$$

The filter service time can then be found from equation 4.6 by dividing the volume treated, V (in L), by the loading rate (L/s).

Trace metal analysis

Every 2 h, 10 mL of the aliquot collected from the columns was preserved in HNO_3 to a pH of < 2 and refrigerated before the elemental analysis was carried out using ICP-OES. The calibration curve was constructed by fitting through the origin using standard solutions of 100, 50, 10, 5 and 1 g/L of a multi-element standard (Inorganic Ventures, Ireland). A 1 M HNO_3 solution was used for the dilutions of the standard solutions and as a calibration blank. The following analytical lines (in nm) were used for the calculations: Al 237.312, 396.152; Ca 396.847, 422.673; Cd 214.439, 226.502, 228.802; Cr 205.560, 267.716, 357.868; Cu 213.598, 324.754, 327.395; Fe 234.350, 238.204, 259.940; Ga 287.423, 294.363, 417.204; Hg 184.887, 194.164; Mg 279.553, 280.270, 285.213; Mn 257.610, 259.372, 260.568; Mo 202.032, 203.846, 204.598; Na 589.592; Ni 216.555, 221.648, 231.604; Pb 220.353, 283.305; Se 196.026, 203.985; Si 250.690, 251.611, 288.158; V 268.796, 292.401, 309.310; Zn 202.548, 206.200, 213.857 (Bridger and Knowles, 2000). XRF analysis was carried out onsite at the refinery using a Panalytical Axios XRF (Malvern Panalytical Ltd, UK).

RHIZOtest

The effect of using P-saturated media on soil properties and plant growth was assessed following completion of the rapid small-scale column study. The plant growth trial was set up after ISO 16198 (Bravin *et al*., 2010), using *Lolium perenne*. Briefly, seeds were germinated and, once germinated, were exposed to a pre-culture period in a hydrophonic solution; the seeds and seedlings were allowed to develop a dense and planar mat of roots. Once established, the seedlings were transferred to individual plant pots containing a P-deficient solution for the 2-week test culture period. Gypsum amended bauxite residue (GR) and Callery mix (PR) were saturated fully with dairy soiled water. The P-saturated spend media from the columns was then applied at a rate of 30 kg/ha. A superphosphate fertiliser was used as a third treatment and a control was also included in the plant trial, which included the soil being used on an “as is” basis (nothing added). Dry weight measurements of the root and shoot biomass were determined at harvest. Plant material was placed in an oven at 60°C for 72 h. Once a steady dry mass was achieved, the roots and shoots were ground and sieved to a size of < 2 mm.

Soil phosphorus extractions

Soil P extractions were performed on the dried and sieved (< 2 mm) soil samples. Water-soluble P was measured using 1 g of soil in 20 mL of deionised water, after shaking for 1 h (Tessier *et al*., 1979). Soil P was examined by Morgan P analysis using 0.54 M CH_3COOH and 0.7 M $NaCH_3COO$ at pH 4.8 in a ratio of 6 mL:30 mL. The soil and Morgan solution was then placed on a reciprocating shaker for 30 min at 180 rpm (Peech and English, 1944). Olsen P analysis was carried out using 0.5 M $NaHCO_3$ at pH 8.5 in a ratio of 1 g:20 ml, followed by shaking on a reciprocating shaker for 30 min at 180 rpm (Olsen *et al*., 1954).

4.2.2 Results

Media characterisation

The main mineralogical composition of the bauxite residue used (Table 4.5) consisted of Fe_2O (47.5%) and Al_2O_3 (14.8%). The remaining composition consisted of TiO_2, SiO_2 and CaO.

The XRD (Figure 4.1) revealed the dominance of Fe oxides, present as haematite (Fe_2O_3). Spent media from both the dairy soiled water and forest run-off columns showed new peaks in the XRD patterns, demonstrating the presence of calcium hydrogen phosphate (III) hydrate (CaH_3PO_4), tetracalcium diphosphide oxide (Ca_4P_2O) and hydroxylapatite

Table 4.5. Main mineralogical composition (%) of the bauxite residue used, as determined by XRF analysis

Mineral oxide	%
Al_2O_3	14.8 ± 1.5
Fe_2O	47.5 ± 2.0
SiO_2	7.20 ± 1.0
TiO_2	10.3 ± 0.9
CaO	6.1 ± 1.0

Reprinted from *Journal of Environmental Management*, Vol. 241, Cusack, P.B., *et al*., The use of rapid, small-scale column tests to determine the efficiency of bauxite residue as a low-cost adsorbent in the removal of dissolved reactive phosphorus from agricultural waters, pp. 273–283, Copyright 2019, with permission from Elsevier.

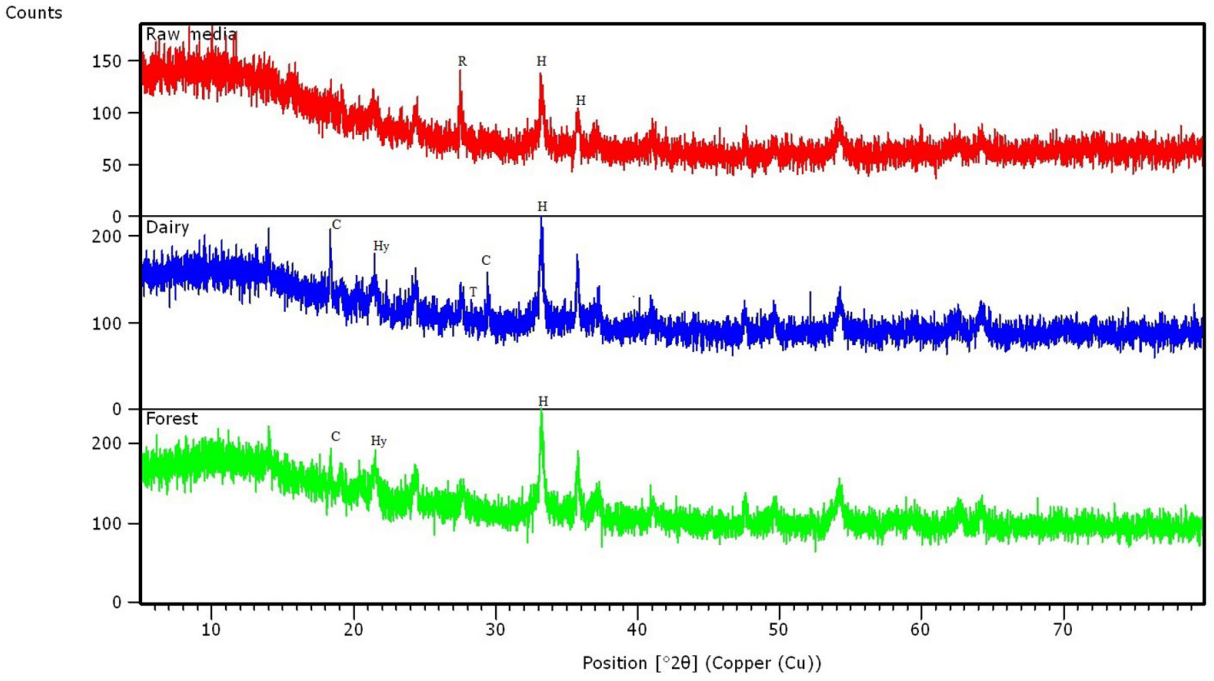

Figure 4.1. The XRD pattern as determined for the column media before and after the loading period with dairy soiled water or forest run-off. H, haematite (Fe_2O_3); R, rutile (TiO_2); C, calcium hydrogen phosphate (III) hydrate (CaH_3PO_4); T, tetracalcium diphosphide oxide (Ca_4P_2O); Hy, hydroxylapatite [$Ca_5(PO_4)_3(OH)$]. Reprinted from *Journal of Environmental Management*, Vol. 241, Cusack, P.B., *et al*., The use of rapid, small-scale column tests to determine the efficiency of bauxite residue as a low-cost adsorbent in the removal of dissolved reactive phosphorus from agricultural waters, pp. 273–283, Copyright 2019, with permission from Elsevier.

[$Ca_5(PO_4)_3(OH)$]. This highlights the P retention capacity of the bauxite residue media.

Rapid small-scale column study

The breakthrough curves of the adsorption columns for the three different lengths for dairy soiled water can be seen in Figure 4.2a. As would be expected, the 20 cm column (the shortest column) approached the saturation point before the 30 and 40 cm columns. A total of 0.275 mg P/g bauxite residue media was retained following the treatment of the dairy soiled water over a 36 h loading period (Figure 4.2b).

The breakthrough curves for the columns treating the forest run-off show that the shortest columns (the 20 cm column) was approaching the media saturation point before the longer columns, as would be expected because of the difference in the media volume (Figure 4.3a). Modelling the data showed that the amount of P retained following treatment of the forest run-off over the 36 h loading period was 0.0366 mg P/g bauxite residue media (Figure 4.3b).

Increases in the pH values of the effluent for both the forest run-off and the dairy soiled water were evident with the running of the columns (Figure 4.4). The initial pH of the dairy soiled water influent was 7.79; this increased to 8.86 ± 0.06. The pH of the forest run-off influent was 7.57; this increased to 8.51 ± 0.07.

The FT-IR analysis of the bauxite residue media before and after treatment of the dairy soiled water showed little difference (Figure 4.5). Intensive IR absorption bands are typically in the range of 560–600/cm and 1000–1100/cm for PO_4^{3-} (Berzina-Cimdina and Borodajenko, 2012).

Similar to the FT-IR analysis of the bauxite residue media before and after treatment with the dairy soiled water, the forest run-off analysis showed little difference before and after treatment (Figure 4.6).

Trace metal analysis

The Al and Fe content showed an increase in the dairy soiled water effluent compared with the influent (increases of 0.095 mg/L and 0.052 mg/L, respectively)

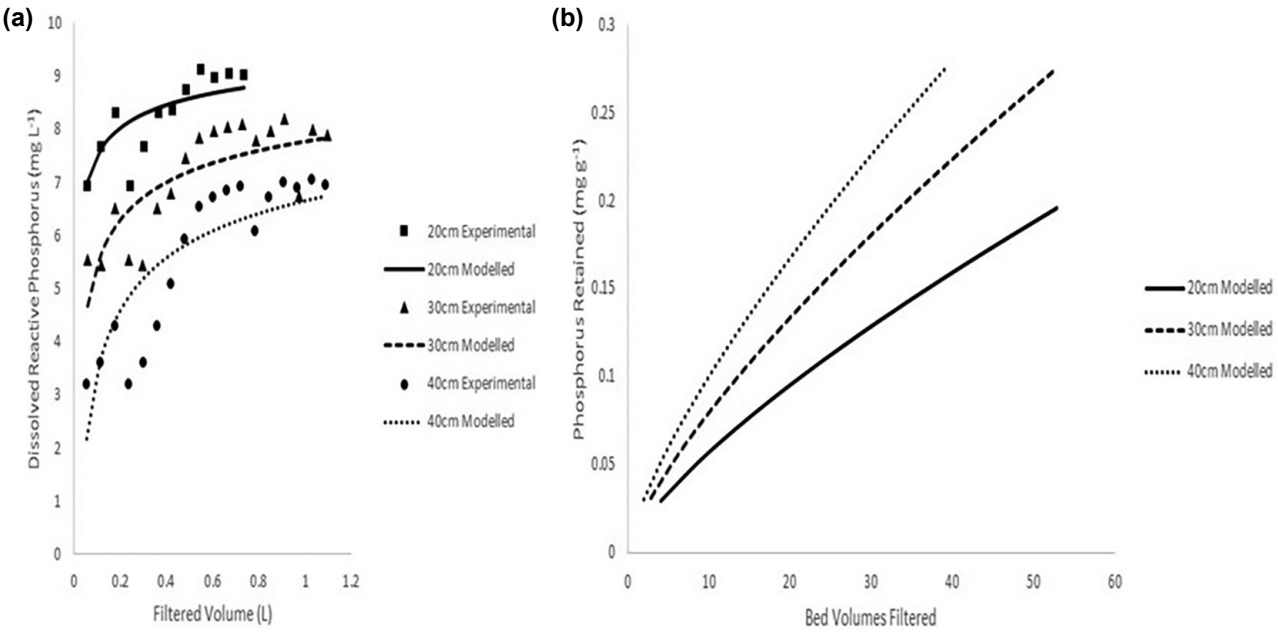

Figure 4.2. (a) The breakthrough curves showing the effluent dissolved reactive P content versus loading time for dairy soiled water using experimental and modelled data and (b) the predicted modelled retention behaviour of P for the bauxite residue media. Reprinted from *Journal of Environmental Management*, Vol. 241, Cusack, P.B., *et al*., The use of rapid, small-scale column tests to determine the efficiency of bauxite residue as a low-cost adsorbent in the removal of dissolved reactive phosphorus from agricultural waters, pp. 273–283, Copyright 2019, with permission from Elsevier.

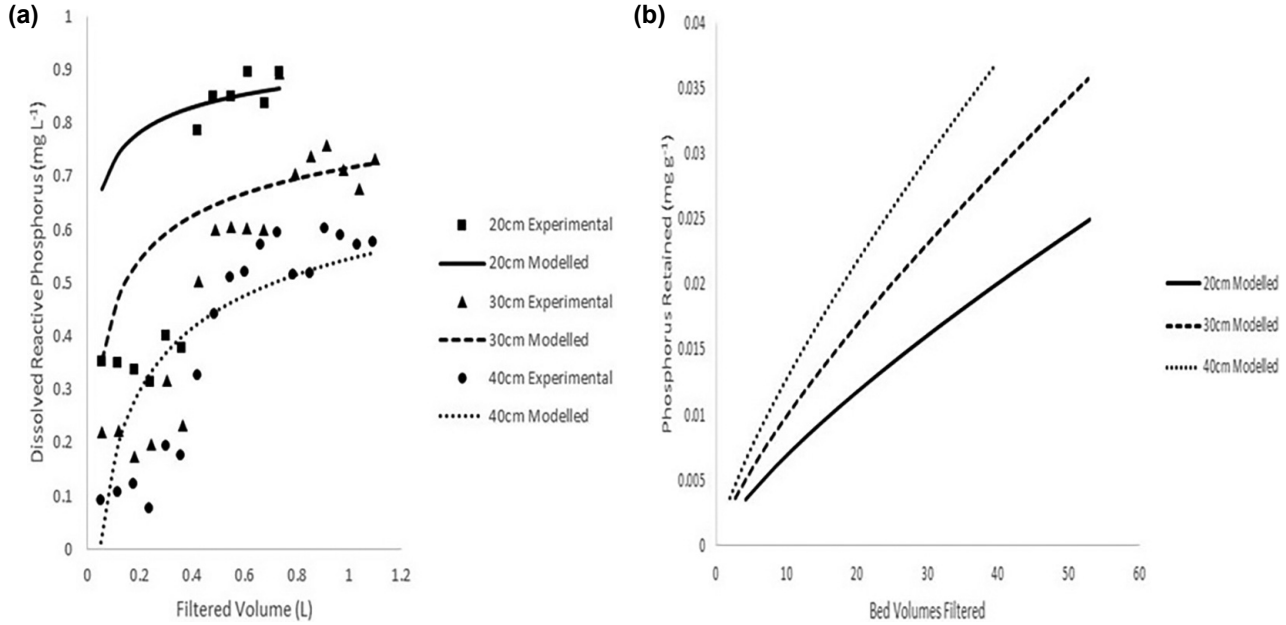

Figure 4.3. (a) The breakthrough curves showing the effluent dissolved reactive P content versus loading time for forest run-off using experimental and modelled data and (b) the modelled predicted P retention of the bauxite residue media. Reprinted from *Journal of Environmental Management*, Vol. 241, Cusack, P.B., *et al*., The use of rapid, small-scale column tests to determine the efficiency of bauxite residue as a low-cost adsorbent in the removal of dissolved reactive phosphorus from agricultural waters, pp. 273–283, Copyright 2019, with permission from Elsevier.

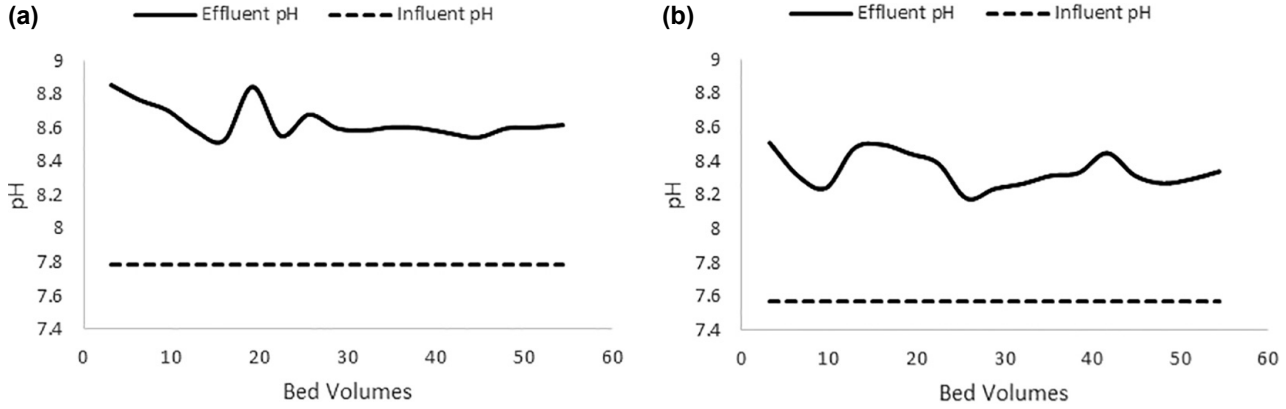

Figure 4.4. The mean pH values of (a) the dairy soiled water and (b) the forest run-off effluent from the columns over the 24–36 h loading period. Reprinted from *Journal of Environmental Management*, Vol. 241, Cusack, P.B., *et al*., The use of rapid, small-scale column tests to determine the efficiency of bauxite residue as a low-cost adsorbent in the removal of dissolved reactive phosphorus from agricultural waters, pp. 273–283, Copyright 2019, with permission from Elsevier.

(Figure 4.7). Copper also showed an increase, from 0.91 mg/L in the influent to 2.02 mg/L in the effluent; however, it did decrease and show retention with loading time. The Mn content in the dairy soiled water effluent was lower than that in the influent (decrease of 0.18 mg/L), showing a retention capacity of the bauxite residue media for this element.

Similar to the dairy soiled water, the columns treating the forest run-off showed increases in the Al and Fe content of the effluent compared with the influent values (Figure 4.8). Cu was also elevated in the effluent compared with the influent, and Mn, similar to the dairy soiled water-treated columns, showed a retention capacity of the media.

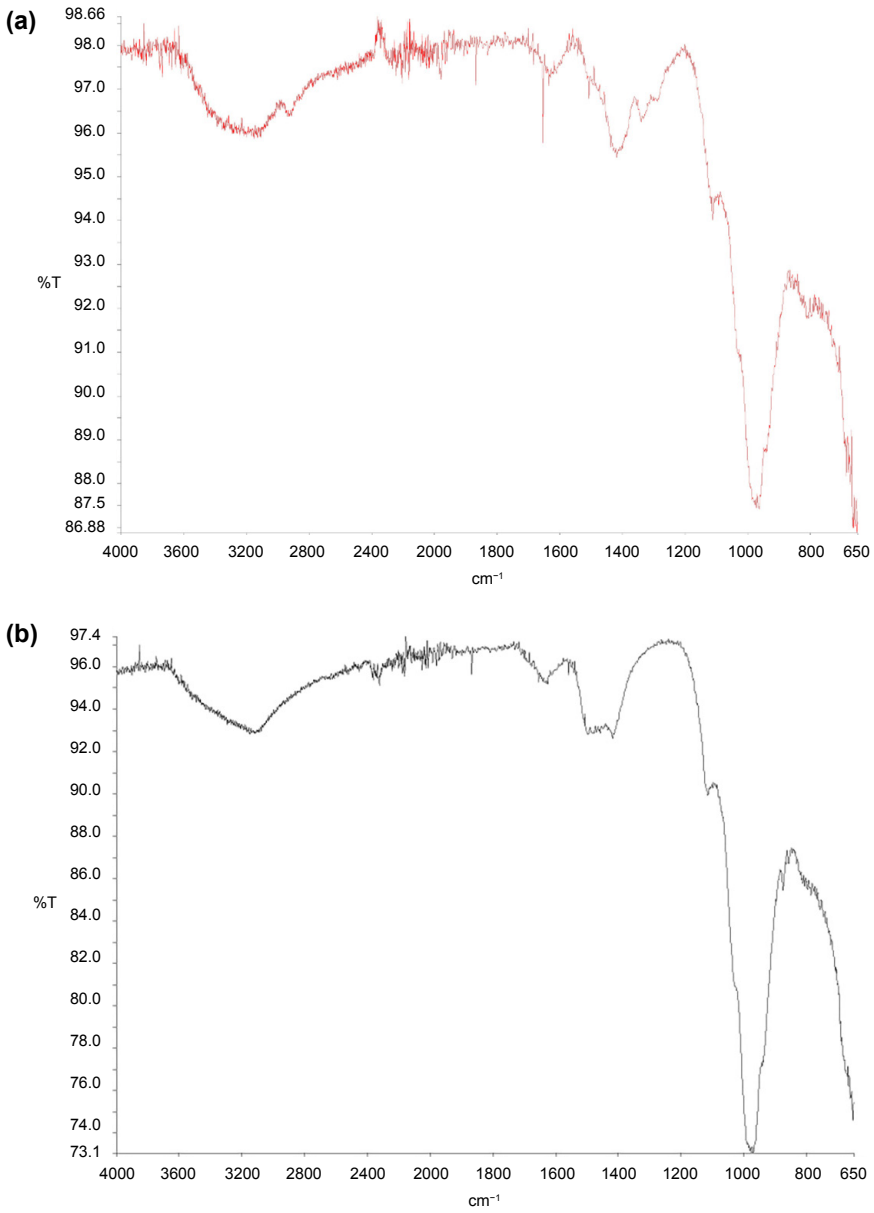

Figure 4.5. FT-IR analysis of the bauxite residue media (a) before and (b) after use in the column treating dairy soiled water. Reprinted from *Journal of Environmental Management*, Vol. 241, Cusack, P.B., *et al.*, The use of rapid, small-scale column tests to determine the efficiency of bauxite residue as a low-cost adsorbent in the removal of dissolved reactive phosphorus from agricultural waters, pp. 273–283, Copyright 2019, with permission from Elsevier.

RHIZOtest and soil phosphorus analysis

The results of the growth trial using the RHIZOtest (Table 4.6) show that the greatest biomass (dry weight) accumulated for the growth period was observed for the superphosphate (SR) sample, followed by the GR and then the PR samples, with the least amount observed for the control (CR) plants. Morgan's extractable soil P analysis shows that the highest value was found again for the SR sample, followed by the GR and then the PR samples, with the lowest value found for the control sample, where no P source had been applied to the soil.

4.2.3 Discussion

Media characterisation

Bauxite residue typically has a high composition of Fe, Al, Ti, Si, Na and Ca, mainly in the form of oxides (Gräfe *et al.*, 2009). Because of the high level of

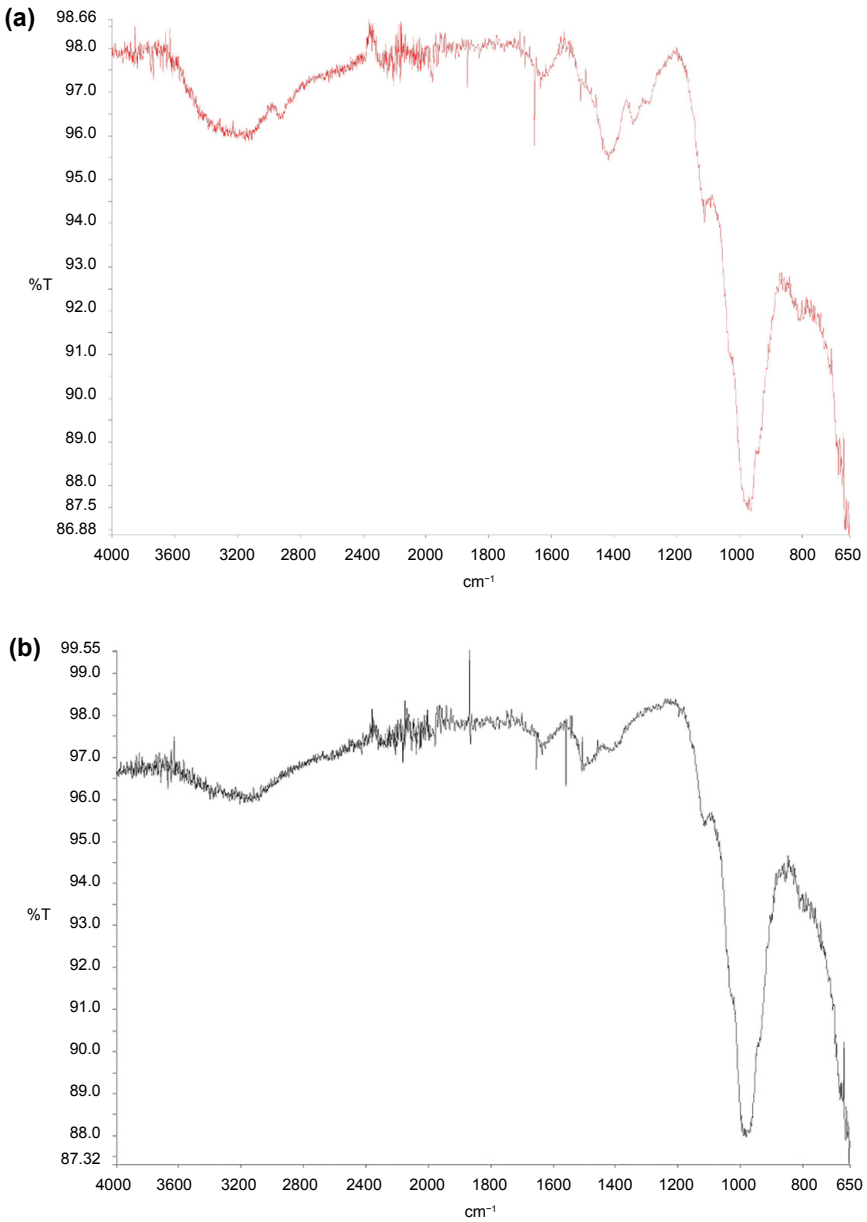

Figure 4.6. FT-IR analysis of the bauxite residue media before (a) and after (b) use in the column treating forest run-off. Reprinted from *Journal of Environmental Management*, Vol. 241, Cusack, P.B., *et al*., The use of rapid, small-scale column tests to determine the efficiency of bauxite residue as a low-cost adsorbent in the removal of dissolved reactive phosphorus from agricultural waters, pp. 273–283, Copyright 2019, with permission from Elsevier.

Fe and Al oxides, which can range from 5% to 60% and from 5% to 30%, respectively (Evans, 2016), bauxite residue has previously been identified as a potential adsorbent for both cations and anions from aqueous solutions (Arco-Lázaro *et al*., 2018; Atasoy and Bilgic 2018; Bhatnagar *et al*., 2011; Caporale *et al*., 2013; Castaldi *et al*., 2011; Cusack *et al*., 2018; Grace *et al*., 2015, 2016; Ha *et al*., 2017; Kocabas and Yürüm, 2011; Sahu *et al*., 2010, 2011; Zhou and Haynes, 2012).

Rapid small-scale column study

Previous studies that have highlighted the high retention capacity of bauxite residue, in particular for P, have found adsorption rates between 0.2 and 202.9 mg P/g of bauxite residue. In this study, the higher retention rate for phosphate observed in the column media treating the forest run-off may be attributed to the composition of the wastewater being treated. The dairy soiled water is typically

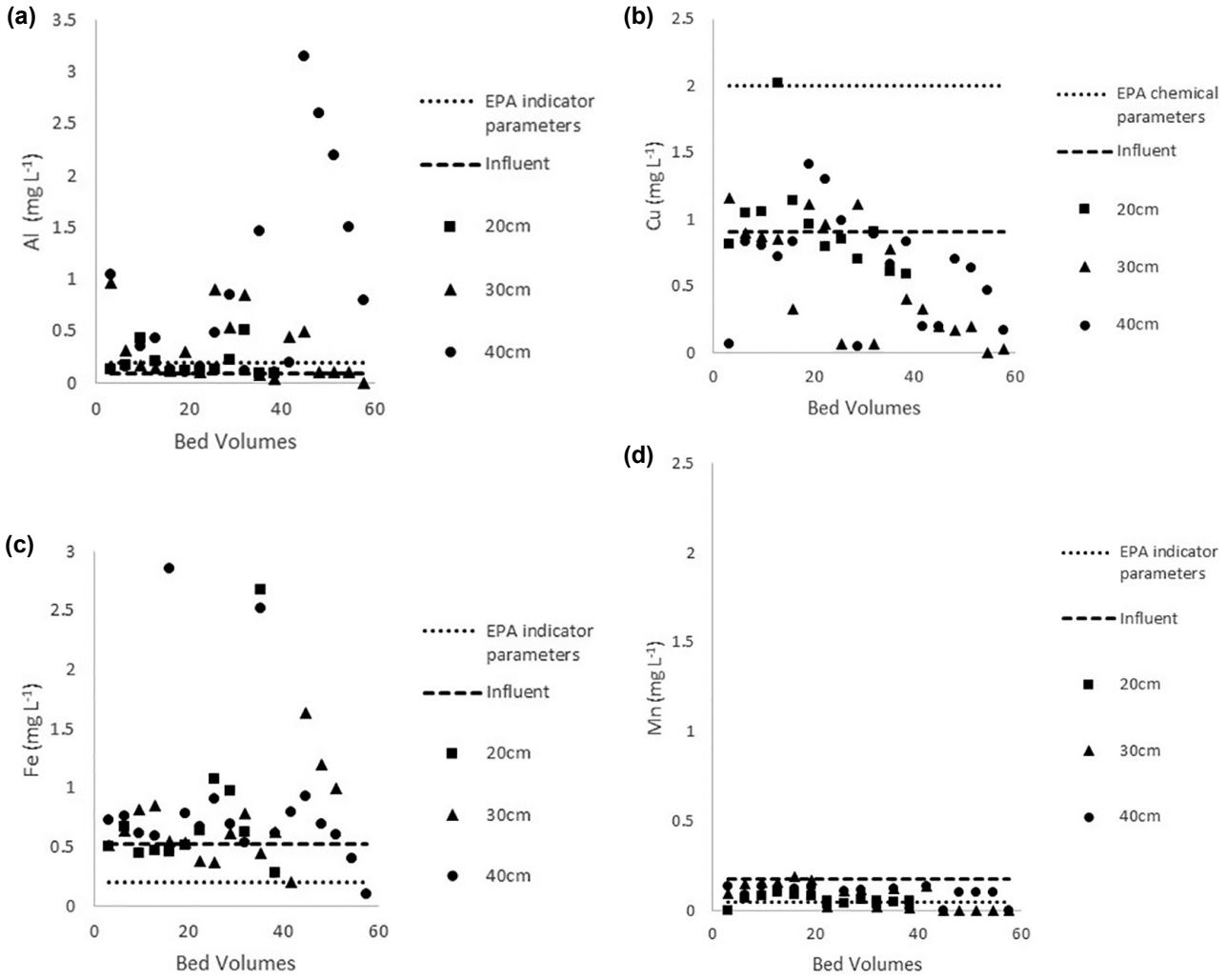

Figure 4.7. Comparison of the composition of (a) Al, (b) Cu, (c) Fe and (d) Mn in influent and effluent in the columns treating dairy soiled water over the 24–36 h loading period. The indicator parameters or chemical parameters defined by the Environmental Protection Agency (EPA) are included for each element. Reprinted from *Journal of Environmental Management*, Vol. 241, Cusack, P.B., *et al.*, The use of rapid, small-scale column tests to determine the efficiency of bauxite residue as a low-cost adsorbent in the removal of dissolved reactive phosphorus from agricultural waters, pp. 273–283, Copyright 2019, with permission from Elsevier.

composed of a total P concentration of 20–100 mg/L and a total N concentration of 70–500 mg/L (Minogue *et al*., 2015), as well as being composed of milk parlour and holding area washings (Murnane *et al*., 2016). Forest run-off mainly includes a low level of phosphate (approximately 1 mg/L; Finnegan *et al*., 2012). Naturally, there are far more anions present in the dairy soiled water and therefore there is greater competitiveness for available adsorption sites and interferences between the adsorbent surface and the ions present in the aqueous solution. As a result, a lower retention rate was observed for the bauxite residue when treating the dairy soiled water in this study.

The bauxite residue used in this study demonstrated a lower level of P adsorption than that found by Despland *et al*. (2011), who used Bauxsol™ (neutralised bauxite residue produced using the Basecon™ procedure) to treat secondary treated effluent and found a P removal capacity of 2.85–8.74 mg/g. Herron *et al*. (2016) found a maximum retention capacity of 25 mg/g for the bauxite residue used in their study; however, this was used on synthetic water and this may be a reason for the higher

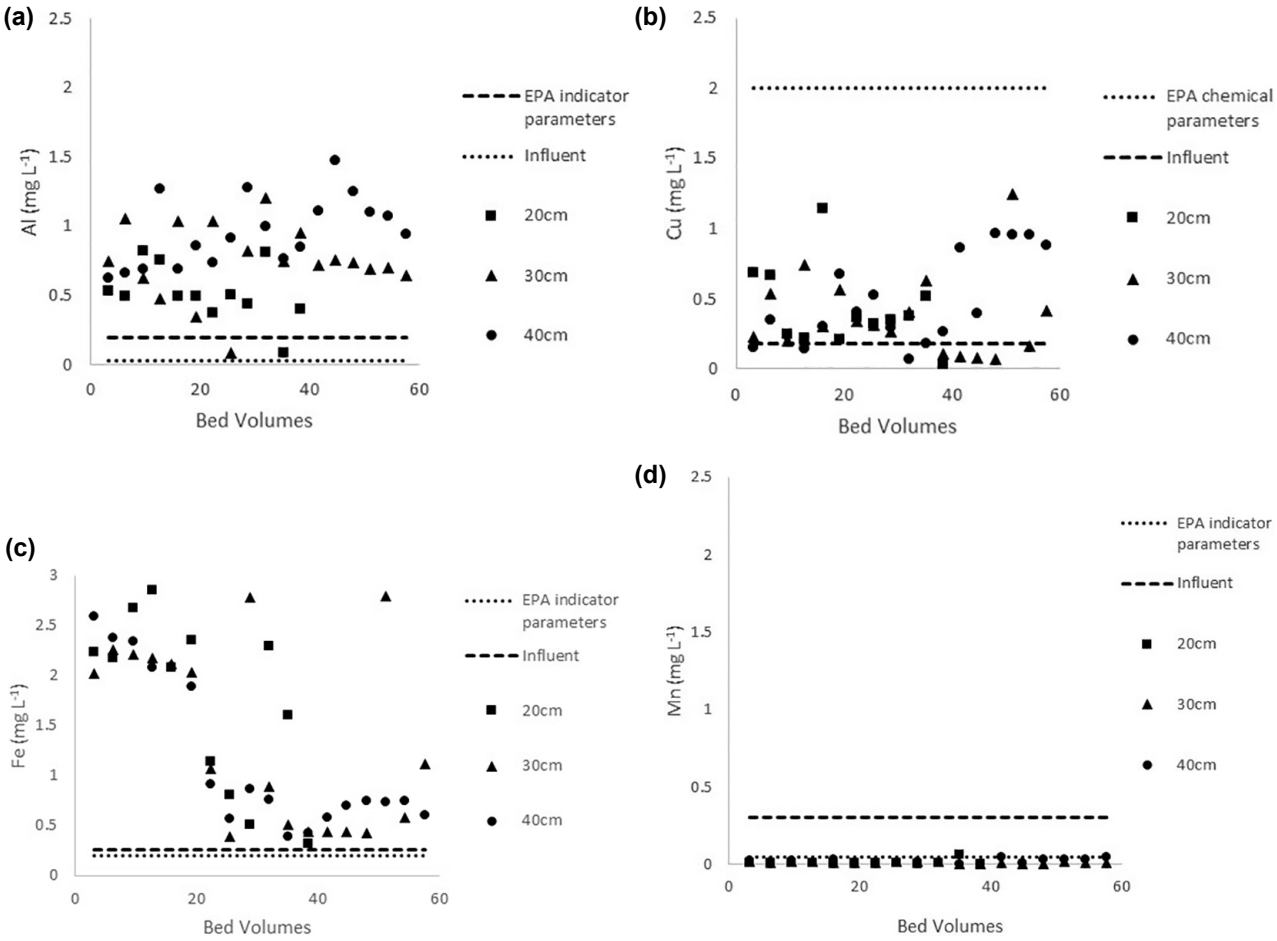

Figure 4.8. Comparison of the composition of (a) Al, (b) Cu, (c) Fe and (d) Mn in influent and effluent in the columns treating forest run-off over the 24–36 h loading period. The EPA indicator parameters or EPA chemical parameters are included for each element. Reprinted from *Journal of Environmental Management*, Vol. 241, Cusack, P.B., *et al*., The use of rapid, small-scale column tests to determine the efficiency of bauxite residue as a low-cost adsorbent in the removal of dissolved reactive phosphorus from agricultural waters, pp. 273–283, Copyright 2019, with permission from Elsevier.

Table 4.6. Soil and plant analysis following the RHIZOtest

Analysis	CR	GR	PR	SR
Plant data (*n* = 20)				
Plant biomass (g dry weight)	1.25 ± 0.4	1.61 ± 0.2	1.49 ± 0.4	1.65 ± 0.3
Soil data (*n* = 20)				
P – Morgan analysis (mg/L)	0.13 ± 0.02	0.43 ± 0.1	0.25 ± 0.04	0.30 ± 0.1
P – Olsen analysis (mg/L)	< LOD	< LOD	< LOD	< LOD
P – water soluble (mg/L)	0.07 ± 0.003	0.077 ± 0.01	0.06 ± 0.01	0.10 ± 0.01
pH	6.45 ± 0.1	6.6 ± 0.2	6.62 ± 0.1	6.58 ± 0.2
EC (mS/cm)	162 ± 24	235 ± 24	147 ± 20	192 ± 35

< LOD, below the limits of detection.

retention rate observed. The P retention capacity of the bauxite residue used in this study may also be compared with that of a conventional sand filter, which has a P retention capacity of approximately 1.9 g/kg (Vohla *et al*., 2007).

The main mechanism of phosphate adsorption (and other anions and cations) onto the surface of Fe and Al oxides may be separated into two processes: specific and non-specific adsorption (Cornell and Schwertmann, 2003; Stumm, 1992). Specific adsorption takes place through the process of ligand exchange (Jacukowicz-Sobala *et al*., 2015). A phosphate ion exchanges with one or more hydroxyl groups, with the release of OH_2 and/or OH^- back into the surrounding solution, contributing to the alkalisation of the surrounding environment (Cornell and Schwertmann, 2003), as shown in the following equations:

$$FeOH + An^- \leftrightarrow \equiv FeAn + OH^- \quad (4.7)$$

$$Fe(OH)_2 + An^- \leftrightarrow \equiv Fe_2 + An^+ + 2OH^- \quad (4.8)$$

Non-specific adsorption is inclusive of electrostatic interactions between the surface of the adsorbent and the phosphate ion (Jacukowicz-Sobala *et al*., 2015). The results of this study show that there was an increase in the pH of the effluent for both the dairy soiled water and the forest run-off treated wastewater. No clear indication of what species was adsorbed was provided by the FT-IR analysis. However, it is well documented that, depending on the pH of the solution, the species of P found in aqueous solution are H_3PO_4, $H_2PO_4^-$, HPO_4^{2-} and PO_4^{3-} (Despland *et al*., 2011; Karageorgiou *et al*., 2007).

Trace metal analysis

Because of the complex nature of bauxite residue and its composition, there is the potential for trace metal leaching (Evans, 2016). The effluent analysis shows that Al and Fe are the dominant metals released or mobilised in the solution. Adsorption and retention were also noted for Cu, Zn, Mg and Mn, with Na and Fe adsorbed and retained to an extent. This was shown in both of the wastewaters treated, with the exception of Fe, which was adsorbed to only a small extent in the dairy soiled water columns. Previous work by Lopez *et al*. (1998) highlighted the ability of bauxite residue to remove and retain Ni, Cu and Zn. Despland *et al*. (2014) showed that Bauxsol™ had the ability to remove trace amounts of As, Pb, Cd, Cr, Cu, Ni, Se, Zn, Mn and Al. This again highlights the potential of bauxite residue to remove both cations and anions from aqueous solution.

RHIZOtest and soil phosphorus analysis

Bauxite residue is normally deficient and limited in P content (Barrow, 1982). The results of the growth trial were as expected, with the plants supplied with a conventional superphosphate (SR sample) achieving the highest biomass yield, and the control (CR sample), which had no P supply, having the lowest biomass. This is a similar trend to that seen in the Morgan's P soil extraction tests. Of the two spent column media trials, the GR (gypsum) sample had a higher biomass yield than the PR (Callery mix) sample. The overall Morgan's results indicate that the soil is in the very low P index for grassland, with an overall P index of 1 (Coulter *et al*., 2008).

5 Further Development of Results

5.1 Evaluation of Techniques for Gallium Recovery from Bauxite Residue

There are only a few publications on the extraction of Ga from bauxite residue. These papers discuss leaching of Ga by mineral acids (Lu *et al*., 2018; Ujaczki *et al*., 2017a) and by alkaline solution, called the hydrogarnet process (Abdulvaliyev *et al*., 2015). In the latter, the extraction of Ga from bauxite residue was carried out in high modulus alkaline solution (240 g/L Na_2O; $\alpha\kappa = 30$) at high temperature (240–260°C) in the presence of lime, followed by treatment of the leached solution by CO_2-enriched air (Abdulvaliyev *et al*., 2015).

Lu *et al*. (2018) presented a method called the acidic leaching ion exchange process (ALIEP) to extract Ga from bauxite residue. The ALIEP method consisted of three main steps: extraction of Ga from bauxite residue by mineral acid (HCl), removal of Fe^{3+} from the leaching solution by chlorinated polystyrene macroporus (LSD-369) resin, and recovery of Ga from the leaching solution using LSC-500S resin. LSC-500S resin contained the reactive groups [-NH-CH_2-P(O)$(OH)_2$] and was able to form stable complexes through reactive groups binding with metal ions.

Ujaczki *et al*. (2017a,b) explored the extraction of Ga and REEs from bauxite residue by selective acid leaching. Both conventional extracting agents (mineral acids) and small-molecular-weight complexing agents (organic acids) were evaluated for their ability to extract CRMs such as Ga from bauxite residue. After acidic extraction, REEs were purified by LLE using D2EHPA dissolved in kerosene.

In the research undertaken within this project, the feasibility of acidic leaching of Ga from bauxite residue combined with adsorption on zeolite was investigated. First, the extraction of Ga from bauxite residue by a number of mineral acids (HCl, HNO_3, H_2SO_4) and a low-molecular-weight organic acid ($H_2C_2O_4$) was explored. Then, the most efficient acid was selected to investigate the process parameters of acid concentration, contact time, temperature and slurry concentration. Consequently, an experimental design approach was used to determine the optimal conditions for Ga extraction. Adsorption on zeolite was used for the separation of Ga from the acidic solution. Here, three zeolite products were compared for Ga adsorption from solution. Then, the most efficient zeolite was applied to investigate the process parameters of adsorbent dosage, contact time and temperature. The most efficient parameters were applied to the bauxite residue acidic leachates. Comparison with another technique, the most commonly used LLE complexing agent (D2EHPA:kerosene) for selective recovery, was also carried out.

Figure 5.1 shows the mass balance calculation for the optimised conditions found in this study for the LLE process. The maximum economic potential was derived as total Ga extracted × economic value of Ga from the US Geological Survey (USGS) website (USGS, 2017), which represents the highest value of Ga that could potentially be extracted. Costs for the chemicals were taken from the Sigma-Aldrich Ireland website (https://www.sigmaaldrich.com/ireland.html). The maximum economic value should not be seen as a value that can actually be recovered (as it is based on pure, refined metal). In addition, costing of the chemicals was calculated using the higher grade options and thus represents the maximum costs. In this experiment, 1 kg of bauxite residue contained 0.114 kg of Ga, with an overall maximum value of €43.30 (see Figure 5.1). By optimising acidic extraction (2.5 M $H_2C_2O_4$, 21.7 h contact time, 80°C, 10 g/L slurry concentration), 0.081 kg of Ga could be extracted, with an overall maximum cost of €30.80. After extraction from bauxite residue, purification of Ga was achieved using LLE with D2EHPA dissolved in kerosene under the following conditions: 1 h contact time, 20°C, O/A ratio 3:1. Here, 0.058 kg of Ga was extracted from the leachate in the organic solvent phase, with an overall maximum value of €21.90. The costs for the process are high in this stage as 90 L of oxalic acid (at a cost of €2755) is required to achieve the maximal extractable level of Ga from the bauxite reside. In the LLE step, the total organic solvent cost is €6296; however, the organic solvent from the process could be recycled.

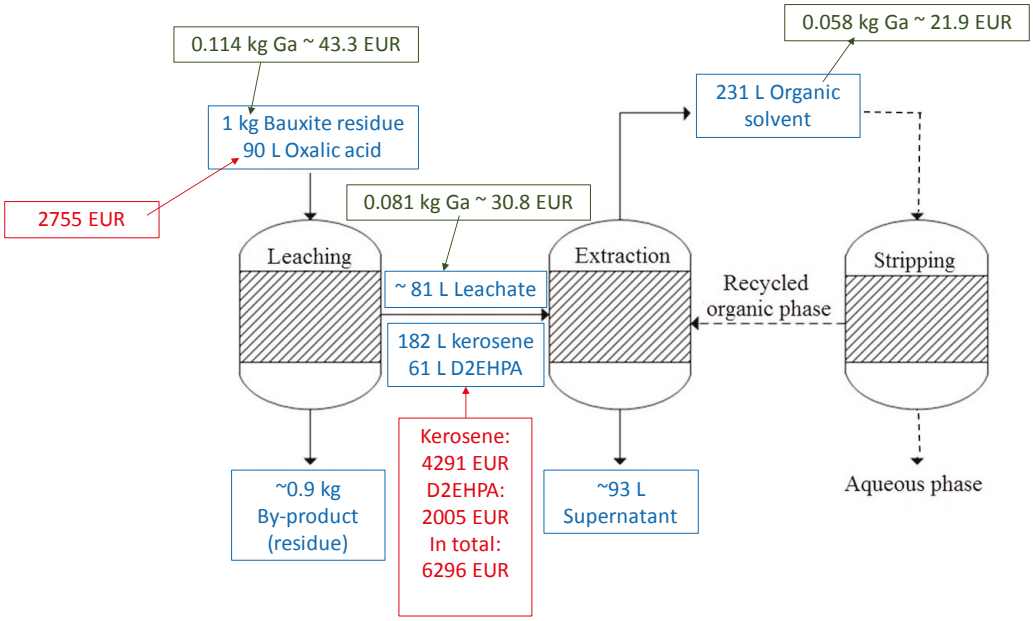

Figure 5.1. Mass balance calculation for the LLE process. Values and costs are also indicated. Leaching parameters: 2.5 M $H_2C_2O_4$, 21.7 h contact time, 80°C 10 g/L slurry concentration. LLE parameters: 1 M D2EHPA in kerosene, 1 h contact time, 20°C, O/A ratio 3:1. Prices: USGS (2017) and Sigma-Aldrich Ireland website (https://www.sigmaaldrich.com/ireland.html).

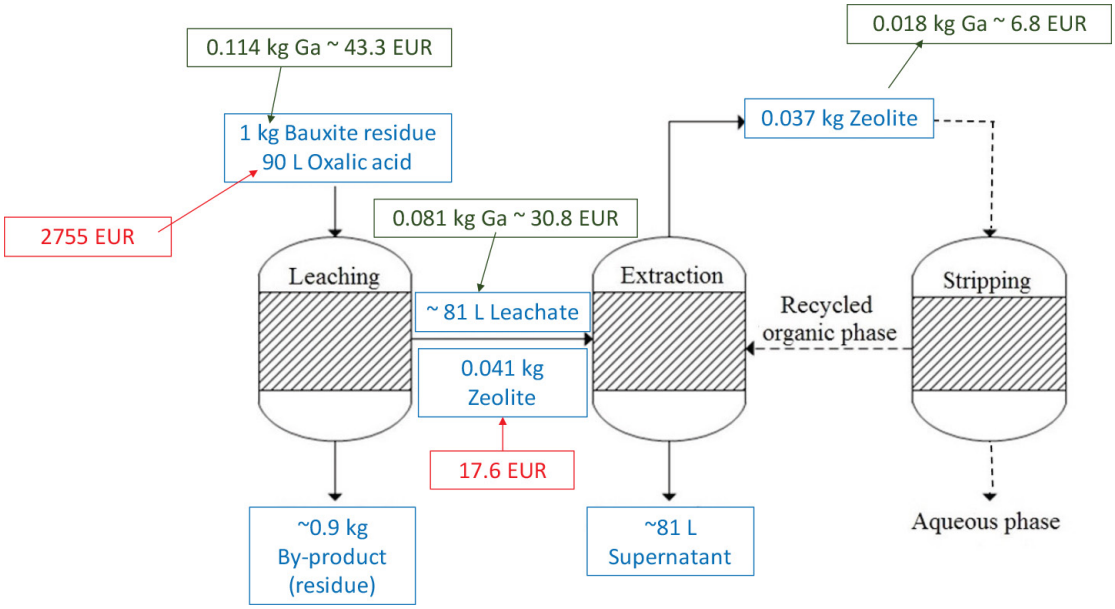

Figure 5.2. Mass balance calculation for the adsorption process. Values and benefits are also indicated. Leaching parameters: 2.5 M $H_2C_2O_4$, 21.7 h contact time, 80°C, 10 g/L slurry concentration. Adsorption parameters: 5 g/cm³, 1 h contact time, 20°C (pH 0.5). Prices: USGS (2017) and Sigma-Aldrich Ireland website (https://www.sigmaaldrich.com/ireland.html).

In the second purification study carried out in this project, 16.1% (~17.8 mg/kg) of the Ga was adsorbed onto the zeolite CBV 500.

Figure 5.2 shows the mass balance calculation for the adsorption process applied in this study. In this experiment, purification of Ga was achieved by an adsorption technique using the zeolite CBV-500 under the following conditions: 5 g/cm³ packing density, 1 h contact time and 20°C (pH 0.5). Here, 0.018 kg of Ga was extracted from the leachate in the adsorbent, with an overall maximum value of €6.80.

The future challenges relating to the investigated adsorption techniques are (1) the concentration of Ga in the adsorbent from the leachate, (2) decreasing the volume of acid used, (3) improvement of the selectivity of Ga against major components (e.g. Al and Fe), (4) development of a recovery step from the adsorbent or finding a market where Ga bound to a zeolite network can be utilised, (5) regeneration of the adsorbent and (6) development of a technique for the utilisation of the acidic by-product generated during the extraction. Similarly, the LLE technique will also involve challenges in the future: (1) find a Ga selectivity solvent, (2) develop a recovery step from the organic (solvent) phase and (3) recovery of the solvent. In addition, it may be that, although the solvents used during LLE perform well technologically, certain processing steps will have a higher environmental impact (Vahidi and Zhao, 2017).

Moreover, there is a challenge related to the reprocessed residue produced during Ga extraction from bauxite residue. Because of the application of oxalic acid for the extraction of Ga, the bauxite residue was transformed from an alkaline (pH 10.9) to an acidic (pH 0.3) material, which may have an impact on reuse options and warrants further investigation.

It should be noted that many strategies for the recovery of valuable elements from bauxite residue require large amounts of energy and chemicals (Abhilash *et al*., 2014; Borra *et al*., 2015a,b, 2016a; Davris *et al*., 2016; Hatzilyberis *et al*., 2018; Lu *et al*., 2018; Ochsenkühn-Petropoulou *et al*., 1996; Paramguru *et al*., 2006; Ujaczki *et al*., 2017a). Private operators and investors often take into account only immediate financial costs and benefits in their decisions. However, the extraction of strategically important elements from bauxite residue is not only attractive financially in terms of the recovered elements alone; it is also motivated by a number of other factors such as social, environmental and technological benefits (Ujaczki *et al*., 2018).

Following on from this research there are two ongoing projects being carried out at the University of Limerick. BIOMIMIC focuses on developing innovative biotechnological methods for energy-efficient metal recovery from acid mine drainage, bauxite residue and incineration waste in the form of ashes. The RemovAL project will deliver and validate a complete feasibility study of technologies to extract Fe, Si, alumina, soda and rutile, as well as REE and Ga raw materials, from bauxite residue.

5.2 Evaluation of the Technique for Phosphorus Recovery from Wastewater Using Bauxite Residue

Gypsum was applied to the bauxite residue at a rate of 8% (w/w). The gypsum application had a direct effect on pH, reducing it from 10.8 to 8.7. The P adsorption capacity of the bauxite residue was also increased, from 0.38 to 2.46 g P/kg bauxite residue media.

Figure 5.3 shows the mass balance calculation for P recovery from wastewater using gypsum-neutralised bauxite residue. In this experiment, 1 kg of bauxite residue was neutralised with 0.092 kg of gypsum, which cost €3.40. The maximum total adsorbed P from the wastewater was 2.46 g/kg of the gypsum-neutralised bauxite residue, as determined using

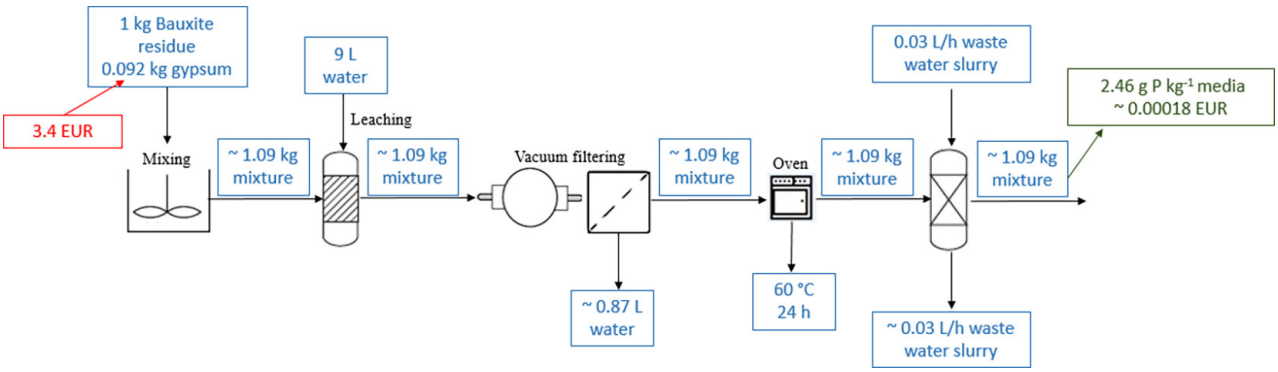

Figure 5.3. Mass balance calculation for P recovery from wastewater using gypsum-neutralised bauxite residue. This is based on the use of a synthetic P water using batch studies. The corresponding P value is based on the current price of phosphate rock from USGS (2017) and the price of gypsum as supplied by Lennox Ireland (http://lennox.ie).

P synthetic water and batch studies. The estimated value of the recovered P is €0.00018 based on the current phosphate rock price, available from USGS (2017).

In relation to this process the by-products and the volume generated are listed in Table 5.1.

Another technique developed by Oisín Callery (under patent process) was also applied to the bauxite residue, transforming it into a stable media. This technique also had a direct effect on the pH of the bauxite residue, reducing it to 8.13 from the original pH of 10.6. The columns were successfully run without clogging using both the forest run-off and the dairy soiled water.

Figure 5.4 shows the mass balance calculation for P recovery from wastewater using the Callery mix and bauxite residue. In this experiment, 1 kg of bauxite residue was neutralised with 0.03 kg of Callery mix (cost unavailable as it is under a patent process). The amount of P adsorbed after the 36 h loading period was 0.27 g/kg. It is important to note that this is the amount of P adsorbed from dairy soiled water after a 36 h loading period and is not based on the saturation of the bauxite residue media. The estimated value of the recovered P is €0.00002 based on the current phosphate rock price, available from USGS (2017).

In relation to this process the by-products and the volume generated are listed in Table 5.2.

Bauxite residue has potential as an adsorbent; however, the recovery efficiency is minimal with low economic value. Future challenges include (1) permeability issues around the bauxite residue, (2) stabilising trace element mobilisation from the column media when treating the influent, (3) finding a suitable reuse for the spent column media and (4) improving overall P recovery efficiencies.

Table 5.1. The list of by-products formed per 1 kg of bauxite residue column media used

By-product produced	Volume	Reuse/disposal of by-product
Water from the leaching step	~0.87 L	Disposal required as Ca and potential metals from bauxite residue present
Column effluent	~0.03 L/h	Potential for reuse for land application, pending the presence of any metals leaching from the bauxite residue column media

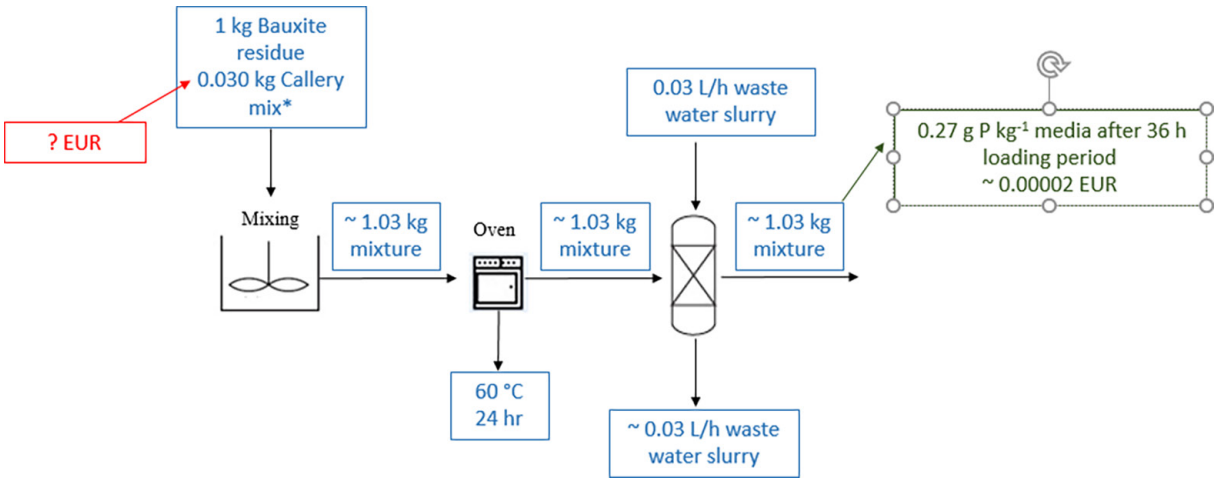

Figure 5.4. Mass balance calculation for P recovery from wastewater using the Callery mix and bauxite residue. This is based on the use of columns treating forest run-off and dairy soiled water. The corresponding P value is based on the current price of phosphate rock from USGS (2017).

Table 5.2. The list of by-products formed per 1 kg of bauxite residue column media used

By-product produced	Volume	Reuse/disposal of by-product
Column effluent	~0.03 L/h	Potential for reuse for land application, pending the presence of any metals leaching from the bauxite residue column media

6 Conclusions

This project investigated the potential for recovery or reuse of CRMs from bauxite residue. Following assessment of the CRM content in bauxite residue, Ga was selected as the specific CRM for optimum extraction and recovery determination.

Bauxite residue was also used as a medium for P removal from synthetic and agri-effluents to determine the adsorption mechanisms and removal rates. Following saturation of the bauxite residue media with P, the media were then assessed as a potential source of nutrients in plant growth trials.

6.1 Gallium Recovery

- In a comparison of the acids H_2SO_4, HCl, HNO_3 and $H_2C_2O_4$, $H_2C_2O_4$ yielded the highest Ga recovery rate.
- The optimal extraction parameters for Ga were 2.5 M $H_2C_2O_4$, 21.7 h contact time, 80.0°C and 10 g/L slurry concentration.
- Under optimal conditions, extraction of 71% (81.1 mg/kg) of the aqua regia-accessible Ga content from bauxite residue was achieved.
- Adsorption by zeolite may be applicable for selective element recovery (e.g. Ga) from bauxite residue leachate.
- There are future challenges related to the adsorption technique: (1) the concentration of Ga in the adsorbent from the leachate, (2) improvement of the selectivity of Ga against major components (e.g. Al and Fe), (3) development of a recovery step from the adsorbent or finding a market where Ga bound to a zeolite network can be utilised and (4) regeneration of the adsorbent.
- There is also a challenge related to the utilisation of the reprocessed residue produced during Ga extraction from bauxite residue.

6.2 Phosphorus Recovery

6.2.1 Synthetic phosphorus solutions

- The mineralogical composition of untreated bauxite residues was dominated by Fe_2O_3, Al_2O_3, SiO_2 and CaO.
- Following treatment with gypsum and seawater, the pH decreased and EC increased, but no change was observed in particle size or density. The SSA and pore volume of the bauxite increased following both treatments, which contributed to the increase in P adsorbency.
- Although the P adsorbency measured in this study was not as high as that measured in other studies using different media, it still indicates that reuse in water or wastewater treatment facilities may be an appropriate option for bauxite residue.

6.2.2 Phosphorus recovery from agri-effluents and reuse

- Bauxite residue media have a high potential for the treatment of both low- and high-P-concentrated agricultural wastewaters, dairy soiled water and forest run-off.
- There was evidence of mobilisation of some metal(loid)s while treating the wastewater, but this may be overcome by including a rinse/wash period prior to packing the columns.
- Bauxite residue media have a retention capacity for Cu and Zn ions. This highlights the potential of the bauxite residue in treating wastewaters containing other contaminants.
- The results of the growth trial indicate that the spent column media show a P supply to the soil compared with a conventional superphosphate fertiliser.

References

Abdulvaliyev, R.A., Akcil, A., Gladyshev, S.V., Tastanov, E.A., Beisembekova, K.O., Akhmadiyeva, N.K. and Deveci, H., 2015. Gallium and vanadium extraction from red mud of Turkish alumina refinery plant: hydrogarnet process. *Hydrometallurgy* 157: 72–77.

Abhilash, Sinha, S., Sinha, M.K. and Pandey, B.D., 2014. Extraction of lanthanum and cerium from Indian red mud. *International Journal of Mineral Processing* 127: 70–73.

Acelas, N.Y., Martin, B.D., López, D. and Jefferson, B., 2015. Selective removal of phosphate from wastewater using hydrated metal oxides dispersed within anionic exchange media. *Chemosphere* 119: 1353–1360.

Agatzini-Leonardou, S., Oustadakis, P., Tsakiridis, P.E. and Markopoulos, C., 2008. Titanium leaching from red mud by diluted sulfuric acid at atmospheric pressure. *Journal of Hazardous Materials* 157: 579–586.

Akhurst, D.J., Jones, G.B., Clark, M. and McConchie, D., 2006. Phosphate removal from aqueous solutions using neutralised bauxite refinery residues (Bauxsol™). *Environmental Chemistry* 3: 65–74.

Alexandratos, S.D., 2009. Ion-exchange resins: a retrospective from industrial and engineering chemistry research. *Industrial and Engineering Chemistry Research* 48: 388–398.

Arco-Lázaro, E., Pardo, T., Clemente, R. and Bernal, M.P., 2018. Arsenic adsorption and plant availability in an agricultural soil irrigated with As-rich water: effects of Fe-rich amendments and organic and inorganic fertilisers. *Journal of Environmental Management* 209: 262–272.

Atasoy, A.D. and Bilgic, B., 2018. Adsorption of copper and zinc ions from aqueous solutions using montmorillonite and bauxite as low-cost adsorbents. *Mine Water and the Environment* 37: 205–210.

Balram, V., Manikyamba, C., Ramesh, S.L. and Saxena, V.K., 1990. Determination of rare earth elements in Japanese rock standards by inductively coupled plasma mass spectrometry. *Atomic Spectroscopy* 11: 19–23.

Bánvölgyi, G.Y. and Huan, T.M., 2010. De-watering, disposal and utilization of red mud: state of the art and emerging technologies. *Travaux* 35: 431–443.

Bao, W.W., Zou, H.F., Gan, S.C., Xu, X.C., Ji, G.J. and Zheng, K.Y., 2013. Adsorption of heavy metal ions from aqueous solutions by zeolite based on oil shale ash: kinetic and equilibrium studies. *Chemical Research in Chinese Universities* 29: 126−131.

Barca, C., Gérente, C., Meyer, D., Chazarenc, F. and Andrès, Y., 2012. Phosphate removal from synthetic and real wastewater using steel slags produced in Europe. *Water Research* 46: 2376–2384.

Bárdossy, G., 1982. Karst bauxites, bauxite deposits on carbonate rocks. In Laznicka P. (ed.), *Developments in Economic Geology*. Elsevier, Amsterdam.

Bárdossy, G. and Aleva, G.J.J., 1990. *Lateritic Bauxites*. Elsevier, Amsterdam.

Barrow, N.J., 1982. Possibility of using caustic residue from bauxite for improving the chemical and physical properties of sandy soils. *Australian Journal of Agricultural Research* 33: 275–285.

Berzina-Cimdina, L. and Borodajenko, N., 2012. Research of calcium phosphates using Fourier transform infrared spectroscopy. *Infrared Spectroscopy – Materials Science, Engineering and Technology* 12: 251–263.

Bhatnagar, A. and Sillanpää, M., 2010. Utilization of agro-industrial and municipal waste materials as potential adsorbents for water treatment – a review. *Chemical Engineering Journal* 157: 277–296.

Bhatnagar, A., Vilar, V.J., Botelho, C.M. and Boaventura, R.A., 2011. A review of the use of red mud as adsorbent for the removal of toxic pollutants from water and wastewater. *Environmental Technology* 32: 231–249.

Binnemans, K., Jones, PT., Blanpain, B., Van Gerven, T. and Pontikes, Y., 2015. Towards zero-waste valorisation of rare-earth-containing industrial process residues: a critical review. *Journal of Cleaner Production* 99: 17–38.

Blake, G.R., 1965. Bulk density. In Black, C.A. (ed.), *Methods of Soil Analysis. Part 1. Physical and Mineralogical Properties, Including Statistics of Measurement and Sampling*. American Society of Agronomy, Inc., Madison, WI, pp. 374–390.

Blake, G.R. and Hartge, K.H., 1986. Particle density. In Klute, A. (ed.), *Methods of Soil Analysis: Part 1. Physical and Mineralogical Methods*. American Society of Agronomy, Inc., Madison, WI, pp. 377–382.

Bolster, C.H., Forsberg, A., Mittelstet, A., Radcliffe, D.E., Storm, D., Ramirez-Avila, J., Sharpley, A.N. and Osmond, D., 2017. Comparing an annual and a daily time-step model for predicting field-scale phosphorus loss. *Journal of Environmental Quality* 46: 1314–1322.

Borra, C.R., Pontikes, Y., Binnemans, K. and Van Gerven, T., 2015a. Leaching of rare earths from bauxite residue (red mud). *Minerals Engineering* 76: 20–27.

Borra, C.R., Blanpain, B., Pontikes, Y., Binnemans, K. and Van Gerven, T., 2015b. Smelting of bauxite residue (red mud) in view of iron and selective rare earths recovery. *Journal of Sustainable Metallurgy* 2: 28–37.

Borra, C.R., Mermans, J., Blanpain, B., Pontikes, Y., Binnemans, K. and Van Gerven, T., 2016a. Selective recovery of rare earths from bauxite residue by combination of sulfation, roasting and leaching. *Minerals Engineering* 92: 151–159.

Borra, C.R., Blanpain, B., Pontikes, Y., Binnemans, K. and Van Gerven, T., 2016b. Recovery of rare earths and other valuable metals from bauxite residue (red mud): a review. *Journal of Sustainable Metallurgy* 2: 365–386.

Bravin, M.N., Michaud, A.M., Larabi, B. and Hinsinger, P., 2010. RHIZOtest: a plant-based biotest to account for rhizosphere processes when assessing copper bioavailability. *Environmental Pollution* 158: 3330–3337.

Bray, A.W., Stewart, D.I., Courtney, R., Rout, S.P., Humphreys, P.N., Mayes, W.M. and Burke, I.T., 2018. Sustained bauxite residue rehabilitation with gypsum and organic matter 16 years after initial treatment. *Environmental Science and Technology* 52: 152−161.

Bridger, S. and Knowles, M., 2000. A complete method for environmental samples by simultaneous axially viewed ICP-AES following US EPA guidelines. Available online: https://www.agilent.com/cs/library/applications/ICPES-29.pdf (accessed 24 May 2018).

BSI (British Standard Institution), 2002. *BS EN 12457-2:2002 Characterisation of Waste – Leaching – Compliance Test for Leaching of Granular Waste Materials and Sludges. One Stage Batch Test at a Liquid to Solid Ratio of 10 l/kg for Materials with Particle Size Below 4 mm (without or with Size Reduction*). Available online: https://www.thenbs.com/PublicationIndex/documents/details?Pub=BSI&DocID=262433 (accessed 4 October 2019).

Cablik, V., 2007. Characterization and applications of red mud from bauxite processing. *Gospodarka surowcami mineralnymi* 23: 27–38.

Callery, O. and, Healy, M.G., 2017. Predicting the propagation of concentration and saturation fronts in fixed-bed filters. *Water Research* 123: 556–568.

Callery, O., Healy, M.G., Rognard, F., Barthelemy, L. and Brennan, R.B., 2016. Evaluating the long-term performance of low-cost adsorbents using small-scale adsorption column experiments. *Water Research* 101: 429–440.

Caporale, A.G., Punamiya, P., Pigna, M., Violante, A. and Sarkar, D., 2013. Effect of particle size of drinking-water treatment residuals on the sorption of arsenic in the presence of competing ions. *Journal of Hazardous Materials* 260: 644–651.

Castaldi, P., Silvetti, M., Enzo, S. and Melis, P., 2010. Study of sorption processes and FT-IR analysis of arsenate sorbed onto red muds (a bauxite ore processing waste). *Journal of Hazardous Materials* 175: 172–178.

Castaldi, P., Silvetti, M., Enzo, S. and Deiana, S., 2011. X-ray diffraction and thermal analysis of bauxite ore-processing waste (red mud) exchanged with arsenate and phosphate. *Clays and Clay Minerals* 59: 189–199.

Çengeloglu, Y., Kir, E. and Ersöz, M., 2001. Recovery and concentration of Al(III), Fe(III), Ti(IV), Ti(IV), and Na(I) from red mud. *Journal of Colloid and Interface Science* 244: 342–346.

Chao, H.P. and Chen, S.H., 2012. Adsorption characteristics of both cationic and oxyanionic metal ions on hexadecyltrimethylammonium bromide-modified NaY zeolite. *Chemical Engineering Journal* 193−194: 283–289.

Chen, N., Feng, C., Zhang, Z., Liu, R., Gao, Y., Li, M. and Sugiura, N., 2012. Preparation and characterization of lanthanum (III) loaded granular ceramic for phosphorus adsorption from aqueous solution. *Journal of the Taiwan Institute of Chemical Engineers* 43: 783–789.

Chen, W.-S., Huang, S.-L., Chang, F.-C., Chang, J.-E. and Wang, Y.-N., 2014. Separation of gallium and copper from hydrochloric acid by D2EHPA. *Desalination and Water Treatment* 54: 1–5.

Claveau-Mallet, D., Wallace, S. and Comeau, Y., 2013. Removal of phosphorus, fluoride and metals from a gypsum mining leachate using steel slag filters. *Water Research* 47: 1512–1520.

Cordell, D. and White, S., 2011. Peak phosphorus: clarifying the key issues of a vigorous debate about long-term phosphorus security. *Sustainability* 3: 2027–2049.

Cornell, R.M. and Schwertmann, U., 2003. *The Iron Oxides: Structure, Properties, Reactions, Occurrences and Uses*. John Wiley, Weinheim, Germany.

Coulter, S., Lalor, S., Alex, C.S., Black, A., Bol, A., Burke, J., Carton, O.T., Coulter, B.S., Culleton, N., Dillon, P. and Humphreys, J., 2008. *Major and Micro Nutrient Advice for Productive Agricultural Crops*. Teagasc, Johnstown Castle, Ireland.

Couperthwaite, S.J., Johnstone, D.W., Mullett, M.E., Taylor, K.J. and Millar, G.J., 2014. Minimization of bauxite residue neutralization products using nanofiltered seawater. *Industrial and Engineering Chemistry Research* 53: 3787–3794.

Courtney, R. and Harrington, T., 2010. Assessment of plant-available phosphorus in a fine textured sodic substrate. *Ecological Engineering* 36: 542–547.

Courtney, R. and Kirwan, L., 2012. Gypsum amendment of alkaline bauxite residue – plant available aluminium and implications for grassland restoration. *Ecological Engineering* 42: 279–282.

Courtney, R.G., Jordan, S.N. and Harrington, T., 2009. Physico-chemical changes in bauxite residue following application of spent mushroom compost and gypsum. *Land Degradation and Development* 20: 572–581.

Cusack, P.B., Healy, M.G., Ryan, P.C., Burke, I.T., O'Donoghue, L.M., Ujaczki, É. and Courtney, R., 2018. Enhancement of bauxite residue as a low-cost adsorbent for phosphorus in aqueous solution, using seawater and gypsum treatments. *Journal of Cleaner Production* 179: 217–224.

Cusack, P.B., Callery, O., Courtney, R., Ujaczki, É., O'Donoghue, L.M.T. and Healy, M.G., 2019. The use of rapid, small-scale column tests to determine the efficiency of bauxite residue as a low-cost adsorbent in the removal of dissolved reactive phosphorus from agricultural waters. *Journal of Environmental Management* 241: 273–283.

Danielson, R.E. and Sutherland, P.L., 1986. Porosity. In Klute, A. (ed.), *Methods of Soil Analysis: Part 1. Physical and Mineralogical Methods*. American Society of Agronomy, Inc., Madison, WI, pp. 443–461.

Davris, P., Balomenos, E., Panias, D. and Paspaliaris, I., 2016. Selective leaching of rare earth elements from bauxite residue (red mud), using a functionalized hydrophobic ionic liquid. *Hydrometallurgy* 164: 125–165.

Deady, É., Mouchos, E., Goodenough, K., Williamson, B. and Wall, F., 2014. Rare earth elements in karst-bauxites: a novel untapped European resource. Proceedings of the ERES2014: 1st European Rare Earth Resources Conference, 4–7 September, Milos, Greece.

Deep, A., Malik, P. and Gupta, B., 2001. Extraction and separation of Ti(IV) using thiophosphinic acids and its recovery from ilmenite and red mud. *Separation Science and Technology* 36: 671–685.

de Lima, A.C.A., Nascimento, R.F., de Sousa, F.F., Josue Filho, M. and Oliveira, A.C., 2012. Modified coconut shell fibers: a green and economical sorbent for the removal of anions from aqueous solutions. *Journal of Chemical Engineering* 185: 274–284.

Desmidt, E., Ghyselbrecht, K., Zhang, Y., Pinoy, L., Van der Bruggen, B., Verstraete, W., Rabaey, K. and Meesschaert B., 2015. Global phosphorus scarcity and full-scale P-recovery techniques: a review. *Critical Reviews in Environmental Science and Technology* 45: 336–384.

Despland, L.M., Clark, M.W., Vancov, T., Erler, D. and Aragno, M., 2011. Nutrient and trace-metal removal by Bauxsol pellets in wastewater treatment. *Environmental Science & Technology* 45: 5746–5753.

Despland, L.M., Clark, M.W., Vancov, T. and Aragno, M., 2014. Nutrient removal and microbial communities' development in a young unplanted constructed wetland using Bauxsol™ pellets to treat wastewater. *Science of the Total Environment* 484: 167–175.

Dodoo-Arhin, D., Konadu, D.S., Annan, E., Buabeng, F.P., Yaya, A. and Agyei-Tuffour, B., 2013. Fabrication and characterisation of Ghanaian bauxite red mud-clay composite bricks for construction applications. *American Journal of Materials Science* 3: 110–119.

Dursun, S., Guclu, D., Berktay, A. and Guner, T., 2008. Removal of chromate from aqueous system by activated red-mud. *Asian Journal of Chemistry* 20: 6473–6478.

EC (European Commission), 2014a. *Annexes to the Report on Critical Raw Materials for the EU. Report of the Ad Hoc Working Group on Defining Critical Raw Materials*. Available online: https://ec.europa.eu/growth/sectors/raw-materials/specific-interest/critical_en (accessed 13 August 2019).

EC (European Commission), 2014b. *On the Review of the List of Critical Raw Materials for the EU and the Implementation of the Raw Materials Initiative*. Available online: http://ec.europa.eu/enterprise/policies/raw-materials/files/docs/crmcommunication_en.pdf (accessed 25 January 2016).

EC (European Commission), 2017. Communication from the Commission to the European Parliament, the Council, the European Economic and Social Committee and the Committee of the Regions. COM(2017) 490 final, 13.9.2017. Brussels. Available online: http://eur-lex.europa.eu/legal-content/EN/ALL/?uri=COM:2017:0490:FIN (accessed 31 October 2017).

Egemose, S., Sønderup, M.J., Beinthin, M.V., Reitzel, K., Hoffmann, C.C. and Flindt, M.R., 2012. Crushed concrete as a phosphate binding material: a potential new management tool. *Journal of Environmental Quality* 41: 647–653.

Erçağ, E. and Apak, R., 1997. Furnace smelting and extractive metallurgy of red mud: recovery of TiO_2, Al_2O_3 and pig iron. *Journal of Chemical Technology and Biotechnology* 70: 241–246.

Erdem, E., Karapinar, N. and Donat, R., 2004. The removal of heavy metal cations by natural zeolites. *Journal of Colloid Interface Science* 280: 309−314.

Evans, K., 2015. Successes and challenges in the management and use of bauxite residue. *Proceedings of Bauxite Residue Valorisation and Best Practices*, Leuven, Belgium, pp. 113–128.

Evans, K., 2016. The history, challenges, and new developments in the management and use of bauxite residue. *Journal of Sustainable Metallurgy* 2: 316–331.

Fergusson, L., 2009. *Commercialisation of Environmental Technologies Derived from Alumina Refinery Residues: A Ten-year Case History of Virotec*. Available online: http://citeseerx.ist.psu.edu/viewdoc/download?doi=10.1.1.458.2073&rep=rep1&type=pdf (accessed 8 December 2017).

Finnegan, J., Regan, J.T., De Eyto, E., Ryder, E., Tiernan, D. and Healy, M.G., 2012. Nutrient dynamics in a peatland forest riparian buffer zone and implications for the establishment of planted saplings. *Ecological Engineering* 47: 155–164.

Free, M.L., 2013. *Hydrometallurgy: Fundamentals and applications*. John Wiley, Hoboken, NJ.

Ge, H., Batstone, D.J. and Keller, J., 2015. Biological phosphorus removal from abattoir wastewater at very short sludge ages mediated by novel PAO clade *Comamonadaceae*. *Water Research* 69: 173–182.

Ghorbani, A. and Fakhariyan, A., 2013. Recovery of Al_2O_3, Fe_2O_3 and TiO_2 from bauxite processing waste (red mud) by using combination of different acids. *Journal of Basic and Applied Scientific Research* 3: 187–191.

Gomes, H.I., Jones, A., Rogerson, M., Burke, I.T. and Mayes, W.M., 2016. Vanadium removal and recovery from bauxite residue leachates by ion exchange. *Environmental Science and Pollution Research* 23: 23034–23042.

Grace, M.A., Healy, M.G. and Clifford, E., 2015. Use of industrial by-products and natural media to adsorb nutrients, metals and organic carbon from drinking water. *Science of the Total Environment* 518: 491–497.

Grace, M.A., Clifford, E. and Healy, M.G., 2016. The potential for the use of waste products from a variety of sectors in water treatment processes. *Journal of Cleaner Production* 137: 788–802.

Gräfe, M., Power, G. and Klauber, C., 2009. Review of bauxite residue alkalinity and associated chemistry. CSIRO, Karawara, WA, Australia. Available online: http://enfo.agt.bme.hu/drupal/sites/default/files/vörösiszpa%20kémia%20és%20lúgosság.pdf (accessed 12 December 2017).

Gräfe, M., Power, G. and Klauber, C., 2011. Bauxite residue issues: III. Alkalinity and associated chemistry. *Hydrometallurgy* 108: 60–79.

Guo, Y.H., Gao, J.J., Xu, H.J., Zhao, K. and Shi, X.F., 2013. Nuggets production by direct reduction of high iron red mud. *Journal of Iron and Steel Research, International* 20: 24–27.

Gupta, C.K., 2017. Chapter 3: Metal recovery processes. In Gupta, C.K. and Mukherjee, T.K. (eds), *Hydrometallurgy in Extraction Processes, Volume II*. CRC Press, Boca Raton, FL.

Ha, X.L., Hoang, N.H., Nguyen, T.T.N., Nguyen, T.T., Nguyen, T.H., Dang, V.T. and Nguyen, N.H., 2017. Removal of Cd (II) from aqueous solutions using red mud/graphene composite. In Tran-Nguyen, H.H., Wong, H., Ragueneau, F. and Ha-Minh, C. (eds), *Proceedings of the 4th Congrès International de Géotechnique – Ouvrages – Structures*. Lecture Notes in Civil Engineering, Vol. 8. Springer, Singapore, pp. 1044–1052.

Hammond, K., Apelian, B.M.D. and Blanpain, B., 2013. CR3 communication: red mud – a resource or a waste? *Journal of the Minerals, Metals & Materials Society* 65: 340–341.

Hanahan, C., McConchie, D., Pohl, H., Creelman, R., Clark, M. and Stocksiek, C., 2004. Chemistry of seawater neutralization of bauxite refinery residues (red mud). *Environmental Engineering Science* 21: 125–138.

Hannachi, Y., Shapovalov, N.A. and Hannachi, A., 2010. Adsorption of nickel from aqueous solution by the use of low-cost adsorbents. *Korean Journal of Chemical Engineering* 27: 152–158.

Hatzilyberis, K., Lymperopoulou, T., Tsakanika, L.-A., Ochsenkühn, K.-M., Georgiou, P., Defteraios, N., Tsopelas, F. and Ochsenkühn-Petropoulou, M., 2018. Process design aspects for scandium – selective leaching of bauxite residue with sulfuric acid. *Minerals* 8: 79.

Hauduc, H., Takács, I., Smith, S., Szabo, A., Murthy, S., Daigger, G.T. and Spérandio, M., 2015. A dynamic physicochemical model for chemical phosphorus removal. *Water Research* 73: 157–170.

Hennebel, T., Boon, N., Maes, S., Lenz, M., 2015. Biotechnologies for critical raw materials recovery from primary and secondary sources: R&D priorities and future perspectives. *New Biotechnol*ogy 32: 121–127.

Herron, S.L., Sharpley, A.N., Brye, K.R. and Miller, D.M., 2016. Optimizing hydraulic and chemical properties of iron and aluminum byproducts for use in on-farm containment structures for phosphorus removal. *Journal of Environmental Protection* 7: 1835.

Hertel, T., Blanpain, B. and Pontikes, Y., 2016. A proposal for a 100% use of bauxite residue towards inorganic polymer mortar. *Journal of Sustainable Metallurgy* 2: 394–404.

Higgins, D., Curtin, T., Pawlett, M. and Courtney, R., 2016. The potential for constructed wetlands to treat alkaline bauxite-residue leachate: *Phragmites australis* growth. *Environmental Science & Pollution Research* 23: 24305–24315.

Hoogerstraete, T.V., Onghena, B. and Binnemans, K., 2013. Homogenous liquid–liquid extraction of metal ions with a functionalized ionic liquid. *Journal of Physical Chemistry Letters* 4: 1659–1663.

Huang, W., Wang, S., Zhu, Z., Li, L., Yao, X., Rudolph, V. and Haghseresht, F., 2008. Phosphate removal from wastewater using red mud. *Journal of Hazardous Materials* 158: 35–42.

IAI (International Aluminium Institute), 2012. *Refining Process*. Available online: http://bauxite.world-aluminium.org/refining/process.html (accessed 11 February 2016).

IAI (International Aluminium Institute), 2015. *Bauxite Residue Management: Best Practice*. Available online: http://www.world-aluminium.org/media/filer_public/2015/10/15/bauxite_residue_management_-_best_practice_english_oct15edit.pdf (accessed 14 October 2017).

Jacukowicz-Sobala, I., Ociński, D. and Kociołek-Balawejder, E., 2015. Iron and aluminium oxides containing industrial wastes as adsorbents of heavy metals: application possibilities and limitations. *Waste Management & Research* 33: 612–629.

Jamieson, E., Jones, A., Cooling, D. and Stockton, N., 2006. Magnetic separation of red sand to produce value. *Minerals Engineering* 19: 1603–1605.

Jayasankar, K., Ray, P.K., Chaubey, A.K., Padhi, A., Satapathy, B.K. and Mukherjee, P.S., 2012. Production of pig iron from red mud waste fines using thermal plasma technology. *International Journal of Minerals, Metallurgy and Materials* 19: 679–684.

Johnston, M., Clark, M.W., McMahon, P. and Ward, N., 2010. Alkalinity conversion of bauxite refinery residues by neutralization. *Journal of Hazardous Materials* 182: 710–715.

Jones, B.E.H. and Haynes, R.J., 2011. Bauxite processing residue: a critical review of its formation, properties, storage and revegetation. *Critical Reviews in Environmental Science and Technology* 41: 271–315.

Karageorgiou, K., Paschalis, M. and Anastassakis, G.N., 2007. Removal of phosphate species from solution by adsorption onto calcite used as natural adsorbent. *Journal of Hazardous Materials* 139: 447–452.

Kasliwal, P. and Sai, P.S.T., 1999. Enrichment of titanium dioxide in red mud: a kinetic study. *Hydrometallurgy* 53: 73–87.

Kawamoto, H., 2008. Japan's policies to be adopted on rare metal resources. *Quarterly Review* 27: 57–76.

Klauber, C., Gräfe, M. and Power, G., 2011. Bauxite residue issues: II. options for residue utilization. *Hydrometallurgy* 108: 11–32.

Kocabaş, Z.Ö. and Yürüm, Y., 2011. Kinetic modeling of arsenic removal from water by ferric ion loaded red mud. *Separation Science and Technology* 46: 2380–2390.

Ku, A.Y. and Hung, S., 2014. *Manage Raw Material Supply Risks*. Available online: http://www.aiche.org/sites/default/files/cep/20140928.pdf (accessed 30 January 2017).

Kumar, R.A.S., Srivastava, J.P and Premchand, 1998. Utilization of iron values of red mud for metallurgical applications. In Bandopadhyay, A., Goswami, N.G. and Rao, P.R. (eds), *Environmental and Waste Management*. National Metallurgical Laboratory, Jamshedpur, India, pp. 108–119.

Kumar, S., Kumar, R. and Bandopadhyay, A., 2006. Innovative methodologies for the utilisation of wastes from metallurgical and allied industries. *Resources, Conservation & Recycling* 48: 301–314.

Laskou, M. and Economou-Eliopoulos, M., 2013. Bio-mineralization and potential biogeochemical processes in bauxite deposits: genetic and ore quality significance. *Mineralogy and Petrology* 107: 471–486.

Lawson, D., Rijkeboer, A., Dajkovich, D., Jackson, M. and Lawrence, H., 2014. Approaches to the processing of Jamaican bauxite with high goethite content. In Grandfield, J. (ed.) *Light Metals 2014*. Springer, pp 11–18.

Lee, M.S., Ahn, J.G. and Lee, E.C., 2002. Solvent extraction separation of indium and gallium from sulphate solutions using D2EHPA. *Hydrometallurgy* 63: 269−276.

Lehoux, A.P., Lockwood, C.L., Mayes, W.M., Stewart, D.I., Mortimer, R.J., Gruiz, K. and Burke, I.T., 2013. Gypsum addition to soils contaminated by red mud: implications for aluminium, arsenic, molybdenum and vanadium solubility. *Environmental Geochemistry & Health* 35: 643–656.

Li, Y., Liu, C., Luan, Z., Peng, X., Zhu, C., Chen, Z., Zhang, Z., Fan, J. and Jia, Z., 2006. Phosphate removal from aqueous solutions using raw and activated red mud and fly ash. *Journal of Hazardous Materials* 137: 374–383.

Li, X.B., Xiao, W., Liu, W., Liu, G.H., Peng, Z.H., Zhou, Q.S. and Qi, T.G., 2009. Recovery of alumina and ferric oxide from Bayer red mud rich in iron by reduction sintering. *Transactions of Nonferrous Metals Society of China* 19: 1342–1347.

Li, Y., Wang, J., Wang, X., Wang, B. and Luan, Z., 2011. Feasibility study of iron mineral separation from red mud by high gradient superconducting magnetic separation. *Physica C: Superconductivity and its Applications* 471: 91–96.

Liu, Y. and Naidu, R., 2014. Hidden values in bauxite residue (red mud): recovery of metals. *Waste Management* 34: 2662–2673.

Liu, X. and Zhang, N., 2011. Utilization of red mud in cement production: a review. *Waste Management & Resources* 29: 1053–1063.

Liu, Y., Lin, C. and Wu, Y., 2007a. Characterization of red mud derived from a combined Bayer process and bauxite calcination method. *Journal of Hazardous Materials* 146: 255–261.

Liu, C.J., Li, Y.Z., Luan, Z.K., Chen, Z.Y., Zhang, Z.G. and Jia, Z.P., 2007b. Adsorption removal of phosphate from aqueous solution by active red mud. *Journal of Environmental Sciences* 19: 1166–1170.

Liu, W., Yang, J. and Xiao, B., 2009. Application of Bayer red mud for iron recovery and building material production from alumosilicate residues. *Journal of Hazardous Materials* 161: 474–478.

Liu, W., Sun, S., Zhang, L., Jahanshahi, S. and Yang, J., 2012. Experimental and simulative study on phase transformation in Bayer red mud soda-lime roasting system and recovery of Al, Na and Fe. *Minerals Engineering* 39: 213–218.

Liu, W., Chen, X., Li, W., Yu, Y. and Yan, K., 2014. Environmental assessment, management and utilization of red mud in China. *Journal of Cleaner Production* 84: 606–610.

Liu, F.P., Liu, Z.H., Li, Y.H., Liu, Z.Y., Li, Q.H. and Li, Z., 2016. Extraction of Ga and germanium from zinc refinery residues by pressure acid leaching. *Hydrometallurgy* 164: 313–332.

Logomerac, V.G., 1979. Complex utilisation of red mud by smelting and solvent extraction. *Travaux du Comité International pour l'Etude des Bauxites, de l'Alumine et de l'Aluminium* 15: 279–285.

Lopez, E., Soto, B., Arias, M., Nunez, A., Rubinos, D. and Barral, M.T., 1998. Adsorbent properties of red mud and its use for wastewater treatment. *Water Research* 32: 1314–1322.

Lu, F., Xiao, T., Lin, J., Li, A., Long, Q., Huang, F., Xiao, L., Li, X., Wang, J., Xiao, Q. and Chen, H., 2018. Recovery of gallium from Bayer red mud through acidic-leaching-ion-exchange process under normal atmospheric pressure. *Hydrometallurgy* 175: 124–132.

Lumley, R., 2010. *Fundamentals of Aluminium Metallurgy: Production, Processing, and Applications*. Woodhead Publishing, Cambridge.

McBride, M.B., 2000. Chemisorption and precipitation reactions. In Sumner, M.E. (ed.), *Handbook of Soil Science*. CRC Press, Boca Raton, FL, pp. B265–B302.

McConchie, D., Clark, M. and Davies-McConchie, F., 2001. *Processes and Compositions for Water Treatment*. Patent application filed by Nauveau Technology Investments.

Maksimović, Z., 1976. Genesis of some Mediterranean karstic bauxite deposits. *Travaux ICSOBA* 13: 1–14.

Maksimović, Z. and Roaldset, E., 1976. Lanthanide elements in some Mediterranean karstic bauxite deposits. *Travaux ICSOBA* 13: 199–220.

Mayes, W.M., Burke, I.T., Gomes, H.I., Anton, Á.D., Molnár, M., Feigl, V. and Ujaczki, É., 2016. Advances in understanding environmental risks of red mud after the Ajka spill, Hungary. *Journal of Sustainable Metallurgy* 2: 332–343.

Menzies, N.W., Fulton, I.M. and Morrell, W.J., 2004. Seawater neutralization of alkaline bauxite residue and implications for revegetation. *Journal of Environmental Quality* 33: 1877–1884.

Meyer, F.M., 2004. Availability of bauxite reserves. *Natural Resources Research* 13: 161–172.

Mihaylov, I. and Distin, P.A., 1993. Solvent extraction of gallium with D2EHPA from acidic sulphate solutions – equilibria and complexation. *Canadian Metallurgical Quarterly* 32: 21–30.

MineralsUK, 2017. Commodities & statistics. Critical raw materials. Available online: http://www.bgs.ac.uk/mineralsuk/statistics/criticalRawMaterials.html (accessed 9 February 2017).

Minogue, D., French, P., Bolger, T. and Murphy, P.N.C., 2015. Characterisation of dairy soiled water in a survey of 60 Irish dairy farms. *Irish Journal of Agricultural and Food Research* 54: 1–16.

Mohapatra, B.K., Mishra, B.K. and Mishra, C.R., 2012. Studies on metal flow from khondalite to bauxite to alumina and rejects from an alumina refinery, India. In Suarez, C.E. (ed.), *Proceedings of the Technical Sessions Presented by the TMS Aluminium Committee at the TMS 2012 Annual Meeting and Exhibition*, Springer, pp. 87–90.

Murnane, J.G., Brennan, R.B., Healy, M.G. and Fenton, O., 2016. Assessment of intermittently loaded woodchip and sand filters to treat dairy soiled water. *Water Research* 103: 408–415.

Murray, H.H., 1981. Alumina from non-bauxite sources. *Natural Resources* 5: 85–89.

Nadaroglu, H., Kalkan, E. and Demir, N., 2010. Removal of copper from aqueous solution using red mud. *Desalination* 251: 90–95.

Natural Resources Canada, 2017. *The Minerals and Metals Policy of the Government of Canada*. Available online: http://www.nrcan.gc.ca/mining-materials/policy/8690 (accessed 9 February 2017).

Newson, T., Dyer, T., Adam, C. and Sharp, S., 2006. Effect of structure on the geotechnical properties of bauxite residue. *Journal of Geotechnical & Geoenvironmental Engineering* 132: 143–151.

Nishihama, S., Hino, A., Hirai, T. and Komasawa, I., 1998. Extraction and separation of gallium and indium from aqueous chloride solution using several organophosphorus compounds as extractants. *Journal of Chemical Engineering Japan* 31: 818–827.

Nishihama, S., Hirai, T. and Komasawa, I., 1999. Separation and recovery of gallium and indium from simulated zinc refinery residue by liquid–liquid extraction. *Industrial & Engineering Chemistry Research* 38: 1032−1039.

Nowak, B., Aschenbrenner, P. and Winter, F., 2013. Heavy metal removal from sewage sludge ash and municipal solid waste fly ash – a comparison. *Fuel Processing Technology* 105: 195–201.

Nur, T., Johir, M.A.H., Loganathan, P., Nguyen, T., Vigneswaran, S. and Kandasamy, J., 2014. Phosphate removal from water using an iron oxide impregnated strong base anion exchange resin. *Journal of Industrial and Engineering Chemistry* 20: 1301–1307.

Ochsenkühn-Petropoulou, M., Lyberopulu, T., Ochsenkühn, K.M. and Parissakis, G., 1996. Recovery of lanthanides and yttrium from red mud by selective leaching. *Analytica Chimica Acta* 319: 249–254.

Olsen, S.R., 1954. *Estimation of Available Phosphorus in Soils by Extraction with Sodium Bicarbonate*. United States Department of Agriculture, Washington, DC.

Önal, M., Borra, C., Guo, M., Blanpain, B. and Van Gerven, T., 2015. Recycling of NdFeB magnets using sulfation, selective roasting, and water leaching. *Journal of Sustainable Metallurgy* 1: 199–215.

Palmer, S.J. and Frost, R.L., 2009. Characterisation of bauxite and seawater neutralised bauxite residue using XRD and vibrational spectroscopic techniques. *Journal of Material Sciences* 44: 55–63.

Paramguru, R.K., Rath, P.C. and Misra, V.N., 2006. Trends in red mud utilization – a review. *Mineral Processing and Extractive Metallurgy Review* 26: 1–29.

Patel, S. and Pal, B.K., 2015. Current status of an industrial waste: red mud an overview. *IJLTEMAS* 4: 1–16.

Peech, M. and English, L., 1944. Rapid microchemical soil tests. *Soil Science* 57: 167–196.

Penn, C., McGrath, J., Bowen, J. and Wilson, S., 2014. Phosphorus removal structures: a management option for legacy phosphorus. *Journal of Soil and Water Conservation* 69: 51A–56A.

Pepper, R.A., Couperthwaite, S.J. and Millar, G.J., 2016. Comprehensive examination of acid leaching behaviour of mineral phases from red mud: recovery of Fe, Al, Ti, and Si. *Minerals Engineering* 99: 8–18.

Petrakova, O.V., Panov, A.V., Gorbachev, S.N., Klimentenok, G.N., Perestoronin, A.V., Vishnyakov, S.E. and Anashkin, V.S., 2015. Improved efficiency of red mud processing through scandium oxide recovery. In Hyland, M. (ed.), *Light Metals 2015*. Springer, Cham, Switzerland, pp. 93–96.

Pontalier, P.Y., Ismail, A. and Ghoul, M., 1997. Mechanisms for the selective rejection of solutes in nanofiltration membranes. *Separation & Purification Technology* 12: 175−181.

Pontikes, Y. and Angelopoulos, G., 2013. Bauxite residue in cement and cementitious applications: current status and a possible way forward. *Resources, Conservation & Recycling* 73: 53–63.

Pontikes, Y., Rathossi, C., Nikolopoulos, P., Angelopoulos, G.N., Jayaseelan, D.D. and Lee, W.E., 2009. Effect of firing temperature and atmosphere on sintering of ceramics made from Bayer process bauxite residue. *Ceramics International* 35: 401–407.

Power, G., Grafe, M. and Klauber, C., 2011. Bauxite residue issues: I. Current management, disposal and storage practices. *Hydrometallurgy* 108: 33–45.

Pradhan, J., Das, S.N., Das, J., Rao, S.B. and Thakur, R.S., 1996. Characterization of Indian red muds and recovery of their metal values. In *Light Metals: Proceedings of Sessions, TMS Annual Meeting*. Springer, Warrendale, PA, pp. 87–92.

Prajapati, S.S., Najar, P.A. and Tangde, V.M., 2016. Removal of phosphate using red mud: an environmentally hazardous waste by-product of alumina industry. *Advances in Physical Chemistry* 2016: 9075206.

Qu, Y., Lian, B., Mo, B. and Liu, C., 2013. Bioleaching of heavy metals from red mud using *Aspergillus niger*. *Hydrometallurgy* 136: 71–77.

Qu, Y., Li, H., Tian, W., Wang, X., Wang, X., Jia, X., Shi, B., Song, G. and Tang, Y., 2015. Leaching of valuable metals from red mud via batch and continuous processes by using fungi. *Mineralogical Engineering* 81: 1–4.

Rivera, R.M., Ulenaers, B., Ounoughene, G., Binnemans, K. and Van Gerven, T., 2018. Extraction of rare earths from bauxite residue (red mud) by dry digestion followed by water leaching. *Minerals Engineering* 119: 82–92.

Roach, G.I.D., Jamieson, E., Pearson, N. and Yu, A.B., 2001. Effect of particle characteristics on the solids density of Bayer mud slurries. In Anjier, J. (ed.), *Light Metals: Proceedings of Sessions, TMS Annual Meeting*. Springer, Warrendale, PA, pp. 417–424.

Rollat, A., Guyonnet, G., Planchon, M. and Tuduri, J., 2016. Prospective analysis of the flows of certain rare earths in Europe at the 2020 horizon. *Waste Management* 49: 427–436.

Roosen, J., Van Roosendael, S., Borra, C.R., Van Gerven, T., Mullens, S. and Binnemans, K., 2016. Recovery of scandium from leachates of Greek bauxite residue by adsorption on functionalized chitosan–silica hybrid-materials. *Green Chemistry* 18: 2005–2013.

Sahu, R.C., Patel, R. and Ray, B.C., 2010. Utilization of activated CO_2-neutralized red mud for removal of arsenate from aqueous solutions. *Journal of Hazardous Materials* 179: 1007–1013.

Sahu, R.C., Patel, R. and Ray, B.C., 2011. Adsorption of Zn (II) on activated red mud: neutralized by CO_2. *Desalination* 266: 93–97.

Sargic, V. and Logomerac, V., 1974. Leaching and extraction in the complex processing of red mud. *Travaux du Comité International pur l'Etude des Bauxites, de l'Alumine et de l'Aluminium* 11: 71–78.

Schindler, D.W., Carpenter, S.R., Chapra, S.C., Hecky, R.E and Orihel, D.M., 2016. Reducing phosphorus to curb lake eutrophication is a success. Available online: https://pubs.acs.org/doi/abs/10.1021/acs.est.6b02204 (accessed 6 June 2018).

Senyuta, A., Panov, A., Suss, A. and Layner, Y., 2013. Innovative technology for alumina production from low-grade raw materials. In Sadler, B. (ed.), *Light Metals*. Springer, Cham, Switzerland, pp. 203–208.

Smiljanić, S., Smičiklas, I., Perić-Grujić, A., Lončar, B. and Mitrić, M., 2010. Rinsed and thermally treated red mud sorbents for aqueous Ni^{2+} ions. *Chemical Engineering Journal* 162: 75–83.

Smith, D.R., King, K.W. and Williams, M.R., 2015. What is causing the harmful algal blooms in Lake Erie? *Journal of Soil and Water Conservation* 70: 27A–29A.

Stumm, W., 1992. *Chemistry of the Solid–Water Interface: Processes at the Mineral–Water and Particle–Water Interface in Natural Systems*. John Wiley, New York.

Sukačová, K., Trtílek, M. and Rataj, T., 2015. Phosphorus removal using a microalgal biofilm in a new biofilm photobioreactor for tertiary wastewater treatment. *Water Research* 71: 55–63.

Taneez, M., Hurel, C., Marmier, N. and Lefèvre, G., 2017. Adsorption of inorganic pollutants on bauxite residues: an example of methodology to simulate adsorption in complex solids mixtures. *Applied Geochemistry* 78: 272–278.

Tessier, A., Campbell, P.G. and Bisson, M., 1979. Sequential extraction procedure for the speciation of particulate trace metals. *Analytical Chemistry* 51: 844–851.

Thomas, G.W., 1982. Exchangeable cations. In Page, A.L. (ed.), *Methods of Soil Analysis. Part 2. Chemical and Microbiological Properties*, 2nd edn. American Society of Agronomy, Soil Science Society of America, Madison, WI, pp. 159–165.

Tsai, H.-S. and Tsai, T.-H., 2013. Extraction equilibrium of gallium(III) from nitric acid solutions by di(2-ethylhexyl) phosphoric acid dissolved in kerosene. *Asian Journal of Chemistry* 25: 1429–1433.

Ujaczki, É., Klebercz, O., Feigl, V., Molnár, M., Magyar, Á., Uzinger, N. and Gruiz, K., 2015. Environmental toxicity assessment of the spilled Ajka red mud in soil microcosms for its potential utilisation as soil ameliorant. *Periodica Polytechnica: Chemical Engineering* 59: 253–261.

Ujaczki, É., Zimmermann, Y.S., Gasser, C.A., Molnár, M., Feigl, V. and Lenz, M., 2017a. Red mud as secondary source for critical raw materials – extraction study. *Journal of Chemical Technology and Biotechnology* 92: 2835–2844.

Ujaczki, É., Zimmermann, Y., Gasser, C., Molnár, M., Feigl, V. and Lenz, M., 2017b. Red mud as secondary source for critical raw materials – purification of rare earth elements by liquid/liquid extraction. *Journal of Chemical Technology and Biotechnology* 92: 2683–2690.

Ujaczki, É., Feigl, V., Molnár, M., Cusack, P., Curtin, T., Courtney, R., O'Donoghue, L., Davris, P., Hugi, C., Evangelou, M.W.H., Balomenos, E. and Lenz, M., 2018. Re-using bauxite residues: benefits beyond (critical raw) material recovery. *Journal of Chemical Technology and Biotechnology* 93: 2498–2510.

Urík, M., Bujdoš, M., Milová-Žiaková, B., Mikušová, P., Slovák, M. and Matúš, P., 2015. Aluminium leaching from red mud by filamentous fungi. *Journal of Inorganic Biochemistry* 152: 54–159.

US EPA (Environmental Protection Agency), 1996. *EPA Method 3050B: Acid Digestion of Sediments, Sludges, and Soils*. Available online: www.epa.gov/sites/production/files/2015-06/documents/epa-3050b.pdf (accessed 30 October 2017).

USGS (United States Geological Survey), 2016. Commodity statistics and information. Available online: http://minerals.usgs.gov/minerals/pubs/commodity/ (accessed 30 January 2018).

USGS (United States Geological Survey), 2017. Bauxite and alumina statistics and information. Available online: https://minerals.usgs.gov/minerals/pubs/commodity/bauxite/mcs-2017-bauxi.pdf (accessed 30 January 2018).

US National Research Council, 2008. *Minerals, Critical Minerals, and the U.S. Economy*. National Academies Press, Washington, DC.

Uzun, D. and Gulfen, M., 2007. Dissolution kinetics of iron and aluminium from red mud in sulphuric acid solution. *Indian Journal of Chemical Technology* 14: 263–268.

Vachon, P., Tyagi, R.D., Auclair, J.C. and Wilkinson, K.J., 1994. Chemical and biological leaching of aluminum from red mud. *Environmental Science & Technology* 28: 26–30.

Vahidi, E. and Zhao, F., 2017. Environmental life cycle assessment on the separation of rare earth oxides through solvent extraction. *Journal of Environmental Management* 1: 255–263.

Vakros, J., Kordulis, C. and Lycourghiotis, A., 2002. Potentiometric mass titrations: a quick scan for determining the point of zero charge. *Chemical Communications* 17: 1980–1981.

Vassiliadou, V., 2014. Bauxite–alumina–aluminium. Raw Materials University Day, 19 June 2014, Athens, Greece. Available online: https://ec.europa.eu/growth/tools-databases/eip-raw-materials/sites/rawmaterials/files/Bauxite%20-alumina%20-aluminium%20Presentation%20.pdf (accessed 10 February 2016).

Vind, J., Malfliet, A., Blanpain, B., Tsakiridis, P.E., Tkaczyk, A.H., Vassiliadou, V. and Panias, D., 2018. Rare earth element phases in bauxite residue. *Minerals* 8: 77.

Vohla, C., Alas, R., Nurk, K., Baatz, S. and Mander, Ü., 2007. Dynamics of phosphorus, nitrogen and carbon removal in a horizontal subsurface flow constructed wetland. *Science of the Total Environment* 380: 66–74.

Vohla, C., Kõiv, M., Bavor, H.J., Chazarenc, F. and Mander, Ü., 2011. Filter materials for phosphorus removal from wastewater in treatment wetlands – a review. *Ecological Engineering* 37: 70–89.

Wall, F., 2014. Rare earth elements. In Gunn, G. (ed.), *Critical Metals Handbook*. Wiley, New York, pp. 312–339.

Wang, S., Ang, H.M. and Tadé, M.O., 2008. Novel applications of red mud as coagulant, adsorbent and catalyst for environmentally benign processes. *Chemosphere* 72: 1621–1635.

Wang, W., Pranolo, Y. and Cheng, C.Y., 2013. Recovery of scandium from synthetic red mud leach solutions by solvent extraction with D2EHPA. *Separation and Purification Technology* 108: 96–102.

Wang, B., Lehmann, J., Hanley, K., Hestrin, R. and Enders, A., 2015. Adsorption and desorption of ammonium by maple wood biochar as a function of oxidation and pH. *Chemosphere* 138: 120–126.

Wang, X.X., Wu, Y.H., Zhang, T.Y., Xu, X.Q., Dao, G.H. and Hu, H.Y., 2016. Simultaneous nitrogen, phosphorous, and hardness removal from reverse osmosis concentrate by microalgae cultivation. *Water Research* 94: 215–224.

Wang, Z., Shen, D., Shen, F. and Li, T., 2016. Phosphate adsorption on lanthanum loaded biochar. *Chemosphere* 150: 1–7.

Xiang, Q., Liang, X., Schlesinger, M.E. and Watson, J.L., 2001. Low-temperature reduction of ferric iron in red mud. In Anjier, J. (ed.), *Light Metals: Proceedings of Sessions, TMS Annual Meeting*. Springer, Warrendale, PA, pp. 157–162.

Xie, F., Zhang, T.A., Dreisinger, D. and Doyle, F., 2014. A critical review on solvent extraction of rare earths from aqueous solutions. *Minerals Engineering* 56: 10–28.

Xue, S., Zhu, F., Kong, X., Wu, C., Huang, L., Huang, N. and Hartley, W., 2016. A review of the characterization and revegetation of bauxite residues (red mud). *Environmental Science and Pollution Research* 23: 120–1132.

Yang, Y., Wang, X., Wang, M., Wang, H. and Xian, P., 2015. Recovery of iron from red mud by selective leach with oxalic acid. *Hydrometallurgy* 157: 239–245.

Yaroshchuk, A., Martínez-Lladó, X., Llenas, L., Rovira, M., De Pablo, J., Flores, J. and Rubio, P., 2009. Mechanisms of transfer of ionic solutes through composite polymer nano-filtration membranes in view of their high sulfate/chloride selectivities. *Desalination and Water Treatment* 6: 48−53.

Ye, J., Zhang, P., Hoffmann, E., Zeng, G., Tang, Y., Dresely, J. and Liu, Y., 2014. Comparison of response surface methodology and artificial neural network in optimization and prediction of acid activation of Bauxsol for phosphorus adsorption. *Water, Air & Soil Pollution* 225: 2225.

Yue, Q., Zhao, Y., Li, Q., Li, W., Gao, B., Han, S., Qi, Y. and Yu, H., 2010. Research on the characteristics of red mud granular adsorbents (RMGA) for phosphate removal. *Journal of Hazardous Materials* 176: 741–748.

Zhang, R., Zheng, S., Ma, S. and Zhang, Y., 2011. Recovery of alumina and alkali in Bayer red mud by the formation of andradite-grossular hydrogarnet in hydrothermal process. *Journal of Hazardous Materials* 189: 827–835.

Zhang, L., Gao, Y., Xu, Y. and Liu, J., 2016. Different performances and mechanisms of phosphate adsorption onto metal oxides and metal hydroxides: a comparative study. *Journal of Chemical Technology & Biotechnology* 91: 1232–1239.

Zhao, F., Zou, Y., Lv, X., Liang, H., Jia, Q. and Ning, W., 2015. Synthesis of $CoFe_2O_4$−zeolite materials and application to the adsorption of gallium and indium. *Journal of Chemical & Engineering Data* 60: 1338−1344.

Zheng, F. and Gesser, H.D., 1996. Recovery of Ga from coal fly ash. *Hydrometallurgy* 41: 187–200.

Zhong, L., Zhang, Y. and Zhang, Y., 2009. Extraction of alumina and sodium oxide from red mud by a mild hydro-chemical process. *Journal of Hazardous Materials* 172: 1629–1634.

Zhou, Y.F. and Haynes, R.J., 2012. A comparison of water treatment sludge and red mud as adsorbents of As and Se in aqueous solution and their capacity for desorption and regeneration. *Water, Air, & Soil Pollution* 223: 5563–5573.

Zhou, Z., Hu, D., Ren, W., Zhao, Y., Jiang, L.M. and Wang, L., 2015. Effect of humic substances on phosphorus removal by struvite precipitation. *Chemosphere* 141: 94–99.

Zhu, D.Q., Chun, T.J., Pan, J. and He, Z., 2012. Recovery of iron from high-iron red mud by reduction roasting with adding sodium salt. *Journal of Iron and Steel Research, International* 19: 1–5.

Zimmermann, Y.S., Niewersch, C., Lenz, M., Kül, Z.Z., Corvini, P.F., Schäffer, A. and Wintegs, T., 2014. Recycling of indium from CIGS photovoltaic cells: potential of combining acid-resistant nanofiltration with liquid-liquid extraction. *Environmental and Science Technology* 48: 13412–13418.

Abbreviations

ALIEP	Acidic leaching ion exchange process
BRDA	Bauxite residue disposal area
CEC	Cation exchange capacity
CR	Control
CRM	Critical raw material
D2EHPA	Di-(2-ethylhexyl)phosphoric acid
df	Degrees of freedom
DOE	Design of experiments
EC	Electrical conductivity
EDS	Energy-dispersive X-ray spectroscopy
EU	European Union
FT-IR	Fourier transform infrared
GR	Gypsum amended bauxite residue
ICP-AES	Inductively coupled plasma atomic emission spectroscopy
ICP-OES	Inductively coupled plasma optical emission spectrometer/spectrometry
LLE	Liquid–liquid extraction
O/A	Organic to acidic
PGM	Platinum group metal
PR	Callery mix
PVDF	Polyvinyl difluoride
PZCpH	Point of zero charge
REE	Rare earth element
SEM	Scanning electron microscopy
SR	Super phosphate
SSA	Specific surface area
UC	Untreated coarse
UF	Untreated fine
UFR	Untreated co-disposed
USGS	US Geological Survey
XRD	X-ray diffraction
XRF	X-ray fluorescence

AN GHNÍOMHAIREACHT UM CHAOMHNÚ COMHSHAOIL
Tá an Ghníomhaireacht um Chaomhnú Comhshaoil (GCC) freagrach as an gcomhshaol a chaomhnú agus a fheabhsú mar shócmhainn luachmhar do mhuintir na hÉireann. Táimid tiomanta do dhaoine agus don chomhshaol a chosaint ó éifeachtaí díobhálacha na radaíochta agus an truaillithe.

Is féidir obair na Gníomhaireachta a roinnt ina trí phríomhréimse:

Rialú: *Déanaimid córais éifeachtacha rialaithe agus comhlíonta comhshaoil a chur i bhfeidhm chun torthaí maithe comhshaoil a sholáthar agus chun díriú orthu siúd nach gcloíonn leis na córais sin.*

Eolas: *Soláthraímid sonraí, faisnéis agus measúnú comhshaoil atá ar ardchaighdeán, spriocdhírithe agus tráthúil chun bonn eolais a chur faoin gcinnteoireacht ar gach leibhéal.*

Tacaíocht: *Bímid ag saothrú i gcomhar le grúpaí eile chun tacú le comhshaol atá glan, táirgiúil agus cosanta go maith, agus le hiompar a chuirfidh le comhshaol inbhuanaithe.*

Ár bhFreagrachtaí

Ceadúnú
Déanaimid na gníomhaíochtaí seo a leanas a rialú ionas nach ndéanann siad dochar do shláinte an phobail ná don chomhshaol:
- saoráidí dramhaíola *(m.sh. láithreáin líonta talún, loisceoirí, stáisiúin aistrithe dramhaíola)*;
- gníomhaíochtaí tionsclaíocha ar scála mór *(m.sh. déantúsaíocht cógaisíochta, déantúsaíocht stroighne, stáisiúin chumhachta)*;
- an diantalmhaíocht *(m.sh. muca, éanlaith)*;
- úsáid shrianta agus scaoileadh rialaithe Orgánach Géinmhodhnaithe *(OGM)*;
- foinsí radaíochta ianúcháin *(m.sh. trealamh x-gha agus radaiteiripe, foinsí tionsclaíocha)*;
- áiseanna móra stórála peitril;
- scardadh dramhuisce;
- gníomhaíochtaí dumpála ar farraige.

Forfheidhmiú Náisiúnta i leith Cúrsaí Comhshaoil
- Clár náisiúnta iniúchtaí agus cigireachtaí a dhéanamh gach bliain ar shaoráidí a bhfuil ceadúnas ón nGníomhaireacht acu.
- Maoirseacht a dhéanamh ar fhreagrachtaí cosanta comhshaoil na n-údarás áitiúil.
- Caighdeán an uisce óil, arna sholáthar ag soláthraithe uisce phoiblí, a mhaoirsiú.
- Obair le húdaráis áitiúla agus le gníomhaireachtaí eile chun dul i ngleic le coireanna comhshaoil trí chomhordú a dhéanamh ar líonra forfheidhmiúcháin náisiúnta, trí dhíriú ar chiontóirí, agus trí mhaoirsiú a dhéanamh ar leasúchán.
- Cur i bhfeidhm rialachán ar nós na Rialachán um Dhramhthrealamh Leictreach agus Leictreonach (DTLL), um Shrian ar Shubstaintí Guaiseacha agus na Rialachán um rialú ar shubstaintí a ídíonn an ciseal ózóin.
- An dlí a chur orthu siúd a bhriseann dlí an chomhshaoil agus a dhéanann dochar don chomhshaol.

Bainistíocht Uisce
- Monatóireacht agus tuairisciú a dhéanamh ar cháilíocht aibhneacha, lochanna, uiscí idirchriosacha agus cósta na hÉireann, agus screamhuiscí; leibhéil uisce agus sruthanna aibhneacha a thomhas.
- Comhordú náisiúnta agus maoirsiú a dhéanamh ar an gCreat-Treoir Uisce.
- Monatóireacht agus tuairisciú a dhéanamh ar Cháilíocht an Uisce Snámha.

Monatóireacht, Anailís agus Tuairisciú ar an gComhshaol
- Monatóireacht a dhéanamh ar cháilíocht an aeir agus Treoir an AE maidir le hAer Glan don Eoraip (CAFÉ) a chur chun feidhme.
- Tuairisciú neamhspleách le cabhrú le cinnteoireacht an rialtais náisiúnta agus na n-údarás áitiúil *(m.sh. tuairisciú tréimhsiúil ar staid Chomhshaol na hÉireann agus Tuarascálacha ar Tháscairí)*.

Rialú Astaíochtaí na nGás Ceaptha Teasa in Éirinn
- Fardail agus réamh-mheastacháin na hÉireann maidir le gáis cheaptha teasa a ullmhú.
- An Treoir maidir le Trádáil Astaíochtaí a chur chun feidhme i gcomhair breis agus 100 de na táirgeoirí dé-ocsaíde carbóin is mó in Éirinn.

Taighde agus Forbairt Comhshaoil
- Taighde comhshaoil a chistiú chun brúnna a shainaithint, bonn eolais a chur faoi bheartais, agus réitigh a sholáthar i réimsí na haeráide, an uisce agus na hinbhuanaitheachta.

Measúnacht Straitéiseach Timpeallachta
- Measúnacht a dhéanamh ar thionchar pleananna agus clár beartaithe ar an gcomhshaol in Éirinn *(m.sh. mórphleananna forbartha)*.

Cosaint Raideolaíoch
- Monatóireacht a dhéanamh ar leibhéil radaíochta, measúnacht a dhéanamh ar nochtadh mhuintir na hÉireann don radaíocht ianúcháin.
- Cabhrú le pleananna náisiúnta a fhorbairt le haghaidh éigeandálaí ag eascairt as taismí núicléacha.
- Monatóireacht a dhéanamh ar fhorbairtí thar lear a bhaineann le saoráidí núicléacha agus leis an tsábháilteacht raideolaíochta.
- Sainseirbhísí cosanta ar an radaíocht a sholáthar, nó maoirsiú a dhéanamh ar sholáthar na seirbhísí sin.

Treoir, Faisnéis Inrochtana agus Oideachas
- Comhairle agus treoir a chur ar fáil d'earnáil na tionsclaíochta agus don phobal maidir le hábhair a bhaineann le caomhnú an chomhshaoil agus leis an gcosaint raideolaíoch.
- Faisnéis thráthúil ar an gcomhshaol ar a bhfuil fáil éasca a chur ar fáil chun rannpháirtíocht an phobail a spreagadh sa chinnteoireacht i ndáil leis an gcomhshaol *(m.sh. Timpeall an Tí, léarscáileanna radóin)*.
- Comhairle a chur ar fáil don Rialtas maidir le hábhair a bhaineann leis an tsábháilteacht raideolaíoch agus le cúrsaí práinnfhreagartha.
- Plean Náisiúnta Bainistíochta Dramhaíola Guaisí a fhorbairt chun dramhaíl ghuaiseach a chosc agus a bhainistiú.

Múscailt Feasachta agus Athrú Iompraíochta
- Feasacht chomhshaoil níos fearr a ghiniúint agus dul i bhfeidhm ar athrú iompraíochta dearfach trí thacú le gnóthais, le pobail agus le teaghlaigh a bheith níos éifeachtúla ar acmhainní.
- Tástáil le haghaidh radóin a chur chun cinn i dtithe agus in ionaid oibre, agus gníomhartha leasúcháin a spreagadh nuair is gá.

Bainistíocht agus struchtúr na Gníomhaireachta um Chaomhnú Comhshaoil
Tá an ghníomhaíocht á bainistiú ag Bord lánaimseartha, ar a bhfuil Ard-Stiúrthóir agus cúigear Stiúrthóirí. Déantar an obair ar fud cúig cinn d'Oifigí:
- An Oifig um Inmharthanacht Comhshaoil
- An Oifig Forfheidhmithe i leith cúrsaí Comhshaoil
- An Oifig um Fianaise is Measúnú
- Oifig um Chosaint Radaíochta agus Monatóireachta Comhshaoil
- An Oifig Cumarsáide agus Seirbhísí Corparáideacha

Tá Coiste Comhairleach ag an nGníomhaireacht le cabhrú léi. Tá dáréag comhaltaí air agus tagann siad le chéile go rialta le plé a dhéanamh ar ábhair imní agus le comhairle a chur ar an mBord.

EPA Research Report 308

Al Source

Authors: Éva Ujaczki, Lisa O'Donoghue, Patricia Cusack, Mark Healy, Teresa Curtin and Ronan Courtney

Identifying Pressures

Bauxite residue is an inevitable secondary product that is generated in the extraction of alumina (aluminium oxide) from bauxite by the Bayer process. The global inventory of bauxite residue has exceeded 4.6 billion tonnes and grows by approximately 120 million tonnes per annum.

The large volumes of stockpiled residue represent an opportunity to investigate the recovery of rare earths and also the use of the residue as a filter for phosphorus in waste water. In addition, residue landfills receive negative press regarding the potential environmental damage if the residue is not managed correctly. Innovative projects such as the Al Source project provide an opportunity to promote more positive aspects, including technology development, waste as a resource and potential economic benefits.

Informing Policy

Rare earth materials have been classified as critical raw materials at the European Union level. The recovery of rare earths from residues helps to secure the supply of essential resources (rare earths are used extensively in modern day electronic products) while also developing a circular economy for such materials.

The Al Source project was directly aligned with *A Resource Opportunity – Waste Management Policy in Ireland*, in which maximum value is sought from wastes by researching their reuse potential as a source of rare earth materials or as a filter medium for removing phosphorus from wastewater.

Developing Solutions

Two utilisation techniques were evaluated for bauxite residue to highlight its reuse value. Rare earth content was determined and a baseline characterisation and composition aspect was created. Extraction techniques were optimised and evaluated for the recovery of gallium (Ga) from bauxite residue, achieving 86 mg of Ga from 1 kg of bauxite residue, corresponding to 71% of the total. Second, a process for recovering phosphorus (P) from agricultural wastewater using bauxite residue was developed. Modified residue can be used to absorb P from wastewaters at up to 2.7 mg P/g bauxite residue. Reuse as a source of rare earth elements or in wastewater treatment facilities may be an appropriate option for bauxite residue.

EPA Research: McCumiskey House, Richiew, Clonskeagh, Dublin 14.

Phone: 01 268 0100
Twitter: @EPAResearchNews
Email: research@epa.ie

www.epa.ie

EPA Research Webpages
www.epa.ie/researchandeducation/research/